Technische Universität München
Fakultät für Mathematik

A coupled system of ordinary and partial differential equations modeling the swelling of mitochondria

Sabine Eisenhofer

Vollständiger Abdruck der von der Fakultät für Mathematik der Technischen Universität München zur Erlangung des akademischen Grades eines

Doktors der Naturwissenschaften (Dr. rer. nat.)

genehmigten Dissertation.

Vorsitzender: Univ.-Prof. Dr. Michael Ulbrich
Prüfer der Dissertation: 1. Univ.-Prof. Dr. Rupert Lasser
2. Univ.-Prof. Dr. Dirk Langemann,
Technische Universität Braunschweig
3. Prof. Dr. Mitsuharu Ôtani,
Waseda University Tokyo / Japan
(schriftliche Beurteilung)

Abstract

Mitochondrial swelling has huge impact to multicellular organisms since it triggers apoptosis, the programmed cell death. In this thesis we present a new mathematical approach to model this phenomenon. As a novelty it includes spatial effects, which are of great importance for the *in vivo* process. Our model considers three mitochondrial subpopulations varying in the degree of swelling. The evolution of these groups is dependent on the present calcium concentration and is described by a system of ODEs, whereas the calcium propagation is modeled by a reaction-diffusion equation taking into account spatial effects. Here we study both the case of non-degenerate and degenerate diffusion and analyze the derived model with respect to existence and long-time behavior of solutions.

Zusammenfassung

Das Schwellen von Mitochondrien hat weitreichende Auswirkungen, denn es führt zum programmierten Zelltod durch Apoptose. In dieser Arbeit stellen wir ein neues Modell vor, welches dieses Phänomen mathematisch beschreibt. Es bezieht erstmals räumliche Effekte mit ein. Unser Modell betrachtet drei Subpopulationen von Mitochondrien, die sich hinsichtlich ihres Schwellgrades unterscheiden. Deren Verhalten ist abhängig von der Calcium-Konzentration und wird durch ein ODE-System beschrieben. Die räumliche Calcium-Ausbreitung hingegen wird mit einer Reaktions-Diffusions-Gleichung modelliert. Hierbei untersuchen wir sowohl nicht-degenerierte als auch degenerierte Diffusion und analysieren das aufgestellte Modell hinsichtliche Existenz und Langzeitverhalten von Lösungen.

Acknowledgment

Contents

Preface

In this thesis a new mathematical model of mitochondrial swelling is presented. It consists of one reaction diffusion equation coupled with a system of three ordinary differential equations. This model is of the form

$$
\begin{aligned}
\partial_t u &= d_1 A(u) + d_2 g(u) N_2 \\
\partial_t N_1 &= -f(u) N_1 \\
\partial_t N_2 &= f(u) N_1 - g(u) N_2 \\
\partial_t N_3 &= g(u) N_2
\end{aligned}
$$

with general boundary conditions

$$
a(x) u + b(x) \partial_\nu u = h(x) \text{ on } \partial\Omega .
$$

As a novelty among mitochondria models it takes into account spatial effects by means of the diffusion operator A. Here we consider both the **non-degenerate** diffusion case

$$
A(u) = \Delta u
$$

and the **degenerate** case

$$
A(u) = \Delta(|u|^{m-2} u)
$$

with $m > 2$. In order to handle the more challenging case of degenerate diffusion the theory of **maximal monotone operators** is introduced.

The present approach is capable of modeling the *in vitro* as well as the *in vivo* case. They vary with respect to the initial and boundary conditions dependent on the choice of the domain to be either the test tube or the whole cell.

In the following chapters we will point out why our model as one of few biomathematical models is challenging enough to yield interesting mathematical results and at the same time simple enough to be of great importance for the understanding of the biological process.

In **CHAPTER 1** we provide all necessary information about the underlying biological mechanism. Here we present the structure of mitochondria, the process causing mitochondrial swelling and its role in cell death. We introduce experimental data, which measure swelling by means of changing light scattering values.

CHAPTER 2 then deals with the mathematical modeling of this phenomenon. It presents existing models and shows the necessity of including spatial effects. Based on the biological background we introduce the model variables and their evolution in time. Here u describes the calcium concentration and by N_1, N_2, N_3 we denote three mitochondrial subpopulations. We develop the new coupled ODE-PDE model and show the biological meaning of different boundary conditions.

The mathematical analysis of the derived model starts in **CHAPTER 3**. Here we consider the non-degenerate case with standard diffusion. At first we take a look at the *in vitro* model with homogeneous Neumann boundary conditions. For this setting we are able to obtain a complete classification of the swelling process and show the robustness of the model. For the *in vivo* case with Robin boundary conditions and the homogeneous Dirichlet problem we can derive similar results regarding existence and convergence of solutions. However, many concepts of the analysis do not apply anymore and hence we can not reproduce all results from the Neumann case. Numerical simulations confirm the mathematical results and explain the experimental data.

The final **CHAPTER 4** studies the case of degenerate diffusion with homogeneous Dirichlet boundary conditions. To this end we introduce the theory of maximal monotone operators, by use of which we can prove the existence of a unique solution. This is done by defining the diffusion operator to be the subdifferential of a convex, lower semicontinuous functional. In order to apply this theory, we have to choose another phase space, for which we can obtain similar convergence results as for the non-degenerate model. However, in analogy to the standard diffusion case with Dirichlet boundary conditions we are not able to achieve a complete classification of the whole swelling process.

CHAPTER 1

Biological background

The subject of this thesis is the mathematical modeling of a biological process, the swelling of mitochondria as it is graphically depicted in Figure 1.1. Mitochondria are often termed the cell's powerhouse due to their main function as energy supplier for almost all eukaryotic cells. In this thesis we will become acquainted with another process that is highly regulated by mitochondria, namely cell death.
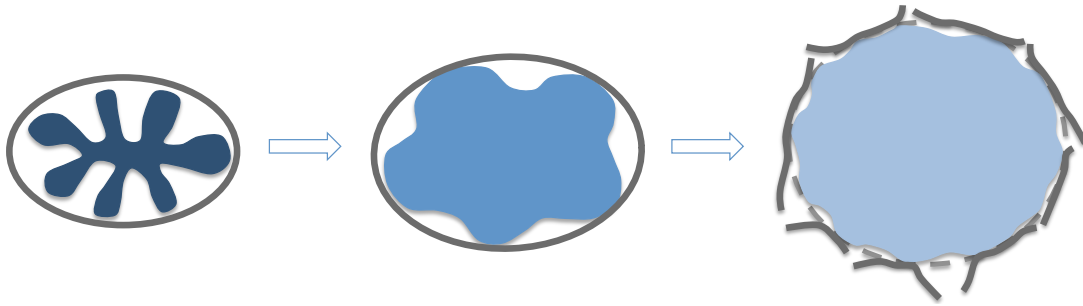
Figure 1.1 – The process of mitochondrial swelling: Extension of the inner membrane until it hits the outer membrane

The mitochondrion

The number of mitochondria in a cell varies widely related to the specific energy consumption, from one single organelle up to several thousands in muscle cells or neurons. For the experiments mostly liver mitochondria are used, which come up to 22 % of the cell volume [1]. It is known that mitochondria within cells are not distributed randomly but are divided into three main regions. This feature will be interesting for the *in vivo* model to be described in Section 2.3. There, Figure 2.5 shows the organization of an eukaryotic cell, restricted to the cell compartments which are of interest for our purpose.

Structure

Figure 1.2 depicts the mitochondrial structure, which will now be described in detail. The function of all occurring mitochondrial components will be explained, where the colors corresponds to the those from the diagram.

▶ One significant attribute of mitochondria is the enclosing double membrane, namely the inner (IM) and outer membrane (OM). A specific characteristic of the IM is the peculiar way of folded appearance, which compartmentalizes it into numerous cristae. Since most of the important chemical reactions of mitochondria take place at its surface area, in doing so the potential working surface can be maximized. To that effect, mitochondria with higher energy demand exhibit more cristae and vice versa. In liver mitochondria, for instance, the surface of the IM exceeds that of the OM five times over [1].
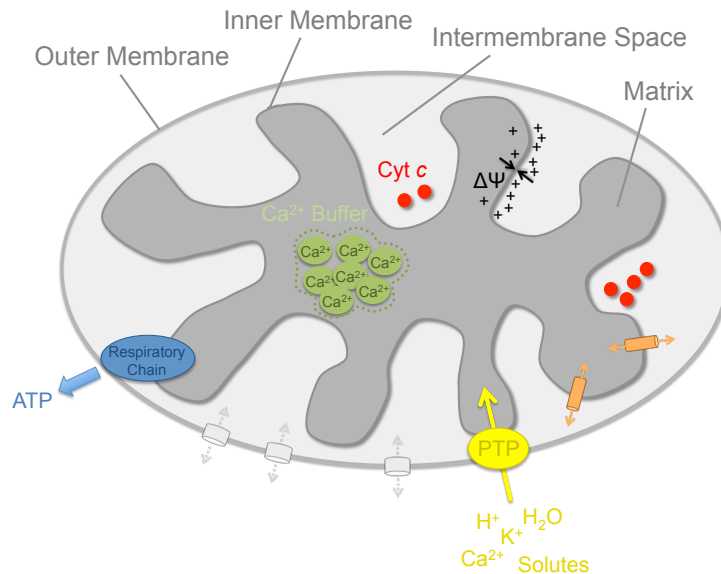
Figure 1.2 – Schematic description of the mitochondrial structure

As can be seen in the picture, the two membranes build up two compartments. These are the intermembrane space (IMS) and the matrix, each one with specialized functions to be presented below. The major difference between the mitochondrial membranes are different permeabilities.

▶ The OM contains several protein channels, which allow for the exchange of molecules and ions up to a certain size [1]. According to this, the concentration of small molecules like ions and sugar in the IMS is nearly identical to that of the cytoplasm, whereas large molecules like proteins occur in much less amounts [34].

▶ By contrast, the IM is nearly impermeable to almost all molecules and so special membrane transporters are needed. These transporters include the calcium uniporter and several other ion exchange fluxes, see e.g. [43]. As it is written in [33], the calcium uniporter plays a major role in intracellular Ca^{2+} signaling. Mitochondrial calcium uptake has controversial impacts on the mitochondrial as well as the cellular function. These are described in [16] and include control of the energy production rate or initiation of cell death. The latter, fatal property will be the topic of this thesis.

▶ Furthermore, mitochondria possess the ability to store a huge amount of calcium inside the matrix, the so-called Ca^{2+} buffer [39]. This calcium storage turns out to be of great importance for the mathematical modeling as it has some accelerating effect to mitochondrial swelling.

▶▶ For the maintenance of cellular respiration it is crucial to create an electrochemical as well as concentration gradient at the IM by pumping protons from the matrix to the IMS [1]. Due to the impermeability of the IM, this leads to a proton gradient which is termed $\Delta\Psi$. The power of this gradient is utilized by the reflux of H^+ into the matrix through turbine-like channels. This flux produces energy which is then spent for the synthesis of ATP.

▶ During this process, electrons are transported by the small protein Cytochrome c (Cyt c). However, it also has an entirely different function. Under normal conditions, Cyt c can not pass the OM. But if the OM is damaged or perforated by some reason, Cyt c is released from the IMS to the cytoplasm. This event is critical in cell death, since now apoptosis is inevitably triggered [25].

▶ As it was first mentioned in [27], there is also another way ions and solutes can enter the impermeable IM. Under pathological conditions, for example high Ca^{2+} concentrations, it happens that a special pore in the IM, the so-called permeability transition pore (PTP) opens. The PTP is formed connecting both membranes and has this name since pore opening makes the IM permeable. Later we will learn more about this pore and the serious consequences of its opening.

Apoptosis

Apoptosis is one of the most important types of programmed cell death. This phenomenon, first mentioned in a publication from 1972, can be described as a kind of "suicide program" of single cells, which have become ectopic or meaningless to the organism. Additionally, mutated or damaged cells use this mechanism to "sacrifice" themselves for the collective good and prevent further deteriorations [23].
The metamorphose of pollywogs to frogs or the degeneration of skins between fingers and toes while human embryonic development are famous examples of this sort of cell death.

The following information are taken from [23] and [34]. Apoptosis plays a crucial role in the maintenance of tissue homeostasis. At this, balance between an increasing cell population by proliferation and its decrease by cell death is required. The following data give an impression of the process dimension: without tissue homeostatis, an 80-year-old person would end up with two tons of bone marrow and lymph nodes together with a 16 km long gut. Apoptosis can be exogenously induced but it is enforced by the affected cell itself as a part of its metabolism.

In contrast to another fundamental cell death mechanism, namely necrosis, apoptosis underlies strong control procedures and assures the intactness of neighboring tissues. As opposed to it, necrosis effects cell swelling with subsequent destruction of the plasma membrane. This leads to local inflammations because released cytoplasm and organelles have to be removed by macrophages.

Pathways

Apoptosis can be elicited by several molecular pathways. The most essential ones, referred to as extrinsic and intrinsic pathways are displayed in Figure 1.3 and will be presented here. These information can be found in [8], [34].
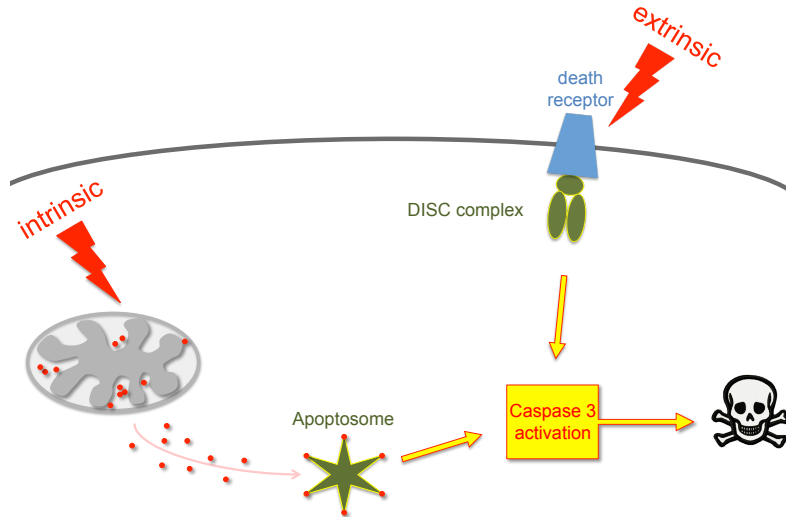
Figure 1.3 – Extrinsic and intrinsic pathways to caspase activation culminating in apoptosis

Extrinsic pathway: On the right hand side a schematical description of the extrinsic, also known as death receptor pathway, is given. At this juncture, the activation of death receptors at the cell surface assembles the death-inducing signaling complex (DISC). This complex in turn mobilizes several enzymes termed caspases which in the end cleave the effector caspase 3. Once these enzymes are formed, apoptosis is inexorably triggered.

Intrinsic pathway: In this work we focus on the intrinsic, also called mitochondrial pathway. Here apoptosis results from intracellular events, where mitochondria play an important role as can be seen on the left hand side of Figure 1.3. Mitochondrial stress is induced by several intracellular signals including high increase of the Ca^{2+} concentration within the cytoplasm, reactive oxygen species, DNA damage, toxins or chemotherapy. It affects the mitochondrial membrane permeability and finally leads to the release of, among others, Cyt c, a common proapoptotic factor. A detailed description of the permeabilization process will be given in the next paragraph.
Cyt c binds to a special gene and thus elicits the formation of the so-called apoptosome complex . Due to its structure and effect, this complex is often termed the "wheel of death". The lethal function of the apoptosome is characterized by activation of caspase 3. At this stage the extrinsic and intrinsic pathways coincide and in both cases cell death by apoptosis is irreversibly initiated.

Mechanism: The activation of caspase 3, also called execution pathway, results in controlled cell destruction including cell shrinkage and DNA fragmentation. In the end the cell is fragmented into small apoptotic bodies, which in turn are digested by

phagocytes. This ensures the clean and tidy removal of apoptotic cells from tissues and with that avoids the problems occurring at necrotic cell death, for instance inflammation.

Mitochondrial permeability transition (MPT)

In the past, mitochondria were only perceived as the cell's powerhouse without any further role in the cell mechanism. Therefore it was very astonishing when it came to light that they also play a decisive role in the control of cell death. In the following we will point out the underlying mechanistic details of this important detection in conformity with [34].

As it was described before, the IM is usually nearly impermeable to all ions. However, this impermeability is not an enduring attribute. Under certain conditions the membrane can be permeabilized to solutes up to a certain size. This IM permeabilization is triggered by multiple factors, one of those being the topic of this thesis, the Ca^{2+}-induced mitochondrial permeability transition (MPT).

Permeability transition pore (PTP)

High loads of Ca^{2+} within the cytoplasm effectuate the permanent opening of the PTP introduced in the description of mitochondria. Consequently, due to the concentration gradient between IMS and matrix, positively charged ions like Ca^{2+} and H^+ are forced into the IMS. This equalization in charge and concentration immediately causes a collapse of the existing membrane potential $\Delta\Psi$. In turn this leads to an increase of the inner membrane permeability and with it to an osmotically driven influx of water and other solutes [12], [28].
As a natural result, the matrix starts to swell and the IM extends further and further until it hits the OM [7]. Due to the surface area of the IM largely exceeding that of the OM, the outer one gets even more permeable and in the end it ruptures. These occurrences can be visualized via an electron microscope as it is shown in Figure 1.4.
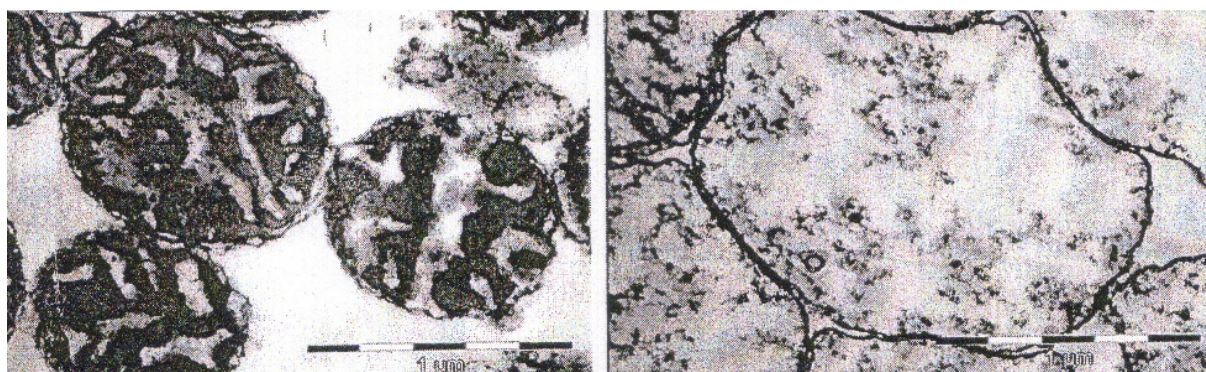
Figure 1.4 – Electron microscopy picture of unswollen (left) and swollen (right) mitochondria, picture taken at the Institute of Toxicology, Helmholtz Zentrum München

This OM permeabilization denotes a point of no return, since it enables the irreversible release of soluble proteins from the IMS. This is a critical event in cell death, because

several proapoptotic factor including Cyt c are set free in this process. That means, once the OM of a sufficient amount of mitochondria is damaged, apoptosis is triggered and the cell will end up in death.

As it is e.g. shown in [41], the rate of PTP activation is dependent on the actual Ca^{2+} load with higher calcium concentrations leading to faster pore opening. Also the experimental data (see Figure 1.5) clearly reveal a positive dependence of the swelling mechanism to increasing concentrations.

Ca^{2+} release

At the beginning we introduced the ability of mitochondria to store calcium inside the matrix. These Ca^{2+} buffers control the calcium homeostasis of the cell and contain large amounts of bounded calcium. If MPT is induced, the total matrix content of calcium is released containing the original buffer amount and the additionally assimilated Ca^{2+} [34].

For that reason, the remaining intact mitochondria are now confronted with an even higher load of Ca^{2+}. In fact, this leads to even faster pore opening and thus to an acceleration of the whole process. This mechanism is often termed "positive feedback" and, as it turns out, is of major importance for the mathematical modeling.

Pharmaceutical background

Apoptosis is also of great interest for the pathophysiological research. It is recognized that this kind of programmed cell death contributes to many diseases in two oppositional ways, which are described in detail in [23], [34]. On the one hand too much apoptosis is involved at (neuro-)degenerative diseases, Parkinson, Alzheimer and AIDS, whereas on the other hand cancer and hemolytic anemia can be associated with too little of it.

Hence, it is not surprising that one of the most promising pharmacological strategies on cancer research is the therapeutic control of MPT. Triggering mitochondrial membrane permeabilization on cancer cells could be an excellent possibility to initiate apoptosis or at least overcome chemotherapeutic resistancies.
In contrast to initiating apoptosis on virulent cells, pharmacological interventions can also be used to inhibit cell death as it is done, for instance, at ischemia/reperfusion injury. In this context, the main goal is to stabilize mitochondrial membranes to protect them from permeabilization.

Experimental procedure

For reasons further elaborated above, MPT induces osmotical swelling of the mitochondrial matrix and with that causes an alteration of the molecular composition. This modification can be quantified by the resulting change of the optical density. We work closely together with the research group of Hans Zischka from the Institute of Molecular Toxicology and Pharmacology at the Helmholtz Zentrum München. They performed all the experiments and provided the light scattering data.

Taking a look at Figure 1.4, it becomes obvious that a population of intact mitochondria

is a very heterogenous one. Light is deflected at the highly folded inner membranes to a great extent, which means we measure high light scattering values. Opposed to it, the more mitochondria are swollen, the more homogenous the population gets, which in turn leads to lower values. Like that mitochondrial swelling is measured indirectly by decreasing light scattering values. In agreement with findings reported in [3] and [41], we have determined this relation to be linear by use of free flow electrophoresis, a technique to partition mitochondria that have undergone MPT [58].

The effects of MPT are measured by use of an absorbance reader, that yields optical density data according to the curves displayed in Figure 1.5. Here the swelling curves depict the mean value of four independent light scattering measurements. For that, a microplate with 4×24 repositories is filled with identical mitochondrial amounts each. Afterwards these are treated with 24 substances, for example different Ca^{2+} concentrations, in order to obtain four independent measurements of similar mixtures. The absorbance reader then quantifies the corresponding light scattering data at a wavelength of 540 nm.
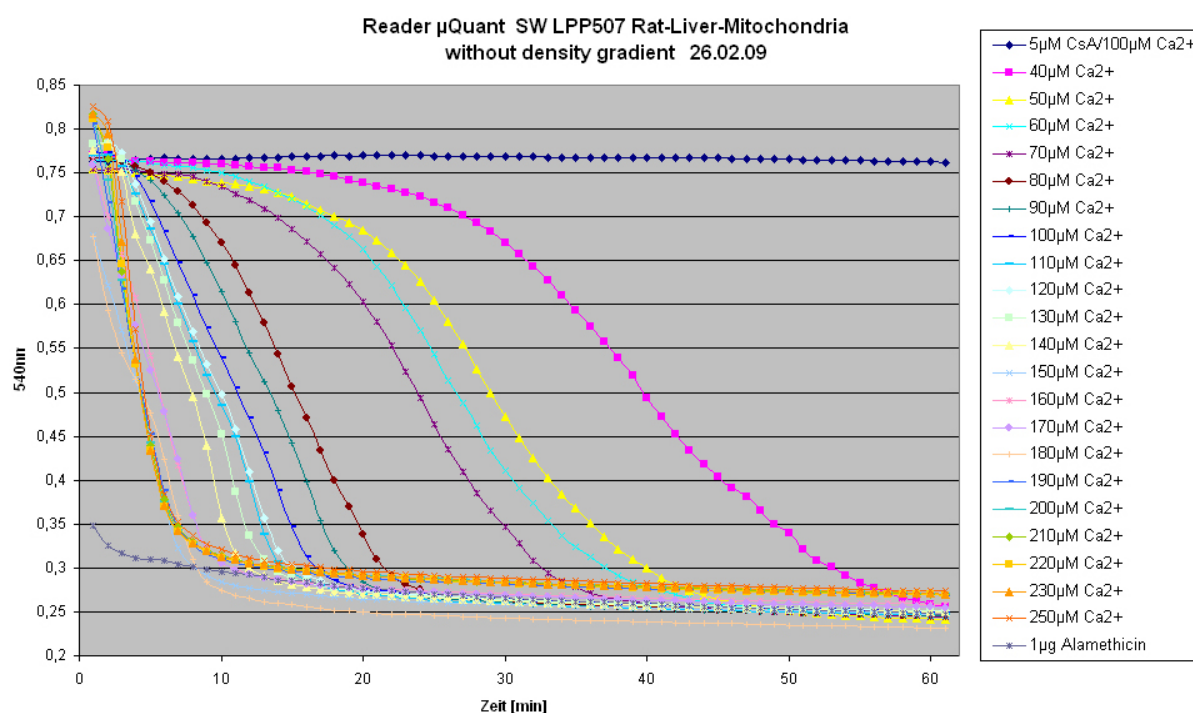
Figure 1.5 – Experimental data of mitochondrial swelling represented by the decrease of optical density

These experimental data show that the more Ca^{2+} is added, the faster the whole swelling proceeds. Starting from time ranges of about one hour, at very high concentrations swelling is completed after less than 10 minutes. The swelling curve appearance is similar for each Ca^{2+} concentration, with an initial lag phase followed by a steep decrease of optical density. This initial phase of moderate decay can be explained by the duration of calcium uptake and the time it needs until the permeabilization process is initiated.

However, there is a one minute time lag between the substance addition on all repositories and the start of the measurement. Indeed, one has to keep in mind that at high Ca^{2+} concentrations the swelling proceeds very fast and thus one missing minute implies a high loss of information. This fact poses problems for the mathematical modeling and with that, the faster swelling proceeds the worse the approximation of mitochondrial incidents gets.

The required mitochondria are extracted from rat liver, isolated from debris and nuclei by multiple centrifugations and resuspended in an isolation buffer. The intactness of the organelles prepared like this is tested by measuring the respiration activity in form of oxygen consumption. On intact mitochondria, osmotic swelling is induced using the "standard swelling buffer" consisting of 10 mM MOPS-Tris, pH 7.4, 200 mM sucrose, 5 mM succinate, 1 mM Pi, 10 μM EGTA and 2 μM rotenone [58].

In our experiments, the common MPT inducer Ca^{2+} is used. As reported in [30] and [42], there are many indicators that calcium plays a main role in several forms of apoptosis, even when MPT is initiated by other substances. This fact traces back to the huge amount of stored calcium in the endoplasmic reticulum, which is then released and targets the mitochondrial membrane permeability. Hence it is really important to obtain a deep understanding of the calcium induced swelling mechanism.

CHAPTER 2

Mathematical modeling of mitochondrial swelling

The process of mitochondrial swelling induced by MPT is known for more than 30 years. However, many important issues concerning the MPT have still remained unanswered or controversial. It is for instance a matter of continuous debate which components exactly build up the PTP [5], [26]. For that reason mathematical modeling is of great importance. It provides the possibility to verify and predict properties of the underlying biological mechanism that possibly can not be obtained from the experiments directly.

2.1 Existing models

The following overview is adapted from our publication [22].

In order to improve the understanding of the kinetics and the complex interdependences of the MPT process, modeling of the MPT pore function has only started recently with two conceptually different approaches.

Microscale

One is mainly oriented on a detailed biochemical and biophysical description of mitochondrial molecular processes such as mitochondrial respiration or ion exchanges [43], [50]. For each of these processes an equation is created, which are then combined in a system of nonlinear ordinary differential equations including a number of variables, e.g. the amount of Ca^{2+} inside the matrix, the pH-value or the membrane potential $\Delta\Psi$.

The specific advantage of this approach is that it can reproduce the three states of the pore: closed, flickering or permanently open. However, this model does not display the time course of pore opening and lacks a major feature, the irreversible volume increase. Hence it is inadequate for simulating mitochondrial swelling. Furthermore, this kind of model only considers the processes for single mitochondria, whereas the experiments are made with huge mitochondrial populations where the resulting data always represent a mean value.

Macroscale

The other modeling approach aims to directly represent mitochondrial swelling. In contrast to the microscale models, it considers a population of mitochondria and studies the total volume increase. It focuses on the basic kinetic processes and hence is mathematically and numerically comparatively easier to handle. It consists of only one [36] or two [3] equations and concentrates on the increase of the number of swollen mitochondria, largely ignoring the details of the underlying biochemical mechanism. Despite these simplifications, this approach can produce a more accurate picture of the mitochondrial volume increase, which can be directly compared with the experimental data.

First order kinetics

To our knowledge, Massari [36] created the first model of this kind assuming first order kinetics. A great advantage of this model is that it can be solved explicitly due to its low mathematical complexity. A drawback of this model is that it fails to account for the initial lag phase in mitochondrial swelling displayed in Figure 1.5. In agreement with the observations mentioned in [3] and [36], we have observed that the Massari model especially fits the end, the "tail" of the swelling curves, but misses their starting phase. The reason for this is the assumption in the derivation of the model, according to which the logarithm of the mitochondrial volume changes linearly during the swelling process. In fact, we showed that for our experimental data this linearity only occurs once most of the actual swelling is done.

Several steps of calcium uptake

Baranov et al. [3] then presented an elaborate model, which provides a good simulation of the swelling on a longer time interval. It consists of two ODEs, one for the amount of calcium and one for the ratio of swollen mitochondria. The authors take into consideration that the Ca^{2+} uptake by mitochondria occurs in several steps with different reaction rates. However, their simulations concentrate on the middle part of the experimental swelling curves, and unfortunately do not explain the above mentioned "tail". The change of the parameters is tested and discussed in dependence of various inducers and inhibitors, but the variation of parameter values with increasing amount of added Ca^{2+} was not examined.

Second order kinetics

Due to the above mentioned disadvantages of the existing models, our aim was to develop a mathematical model that is capable of simulating the whole swelling process. The derived model is based on the known major properties of the process, which allows us to analyze the parameter values and obtain a classification of different swelling inducers or mitochondria from different tissues. In the following we will briefly present this model, which can be found in [22].

Based on experiments we assume that three subpopulations of mitochondria with different corresponding volumes exist: unswollen, swelling and mitochondria that have completely finished swelling. The first and the last group have constant mean volumes, depending

only on their source and the medium. The mean volume of swelling mitochondria additionally depends on the characteristics of the swelling process, which could be influenced e.g. by properties and concentrations of the added substances. Onset and time course of swelling typically vary between mitochondria from different tissues, caused e.g. by different sensitivities to inducers [4], [11].

The dynamical behavior of the total volume of the mitochondrial population, i.e. the subsumed volume of all subpopulations corresponds to the light scattering data obtained from the experiments. As noted before, we have determined the relation of volume increase and optical density decrease to be linear.

Model description The model is based on the observation that mitochondria vary concerning their sensitivity for swelling induction by stimuli like Ca^{2+} as it was described by our collaboration partner in [58]. We model the time progress of swelling with two equations for two variables X and V.

Here $X(t)$ denotes the fraction of mitochondria that are swollen or have started swelling at time t and hence $0 \leq X(t) \leq 1$. $V(t)$ describes the average volume of the mitochondrial population at time t. Since we assume that all mitochondria are intact prior to calcium addition, it holds $X(0) = 0$.

Let X_p be the ratio of swollen mitochondria after the whole swelling is done. During the extraction and isolation from living mitochondria, it happens that some mitochondria are destructed and hence can not react to swelling inducers. This is why it holds $0 < X_p \leq 1$ and in particular we assume $X_p = 0.9$ corresponding to 10 % loss in accordance with experimental observations. By V_0 and V_p we denote the volume of unswollen and completely swollen mitochondria, respectively. These parameter values are chosen in agreement with [43] and we take $V_0 = 1.2$ and $V_p = 1.7$ with unit [ml/mg protein].

The permeability transition process can be described via the initial value problem

$$\boxed{\begin{aligned} \frac{d}{dt}X(t) &= (aX(t) + b) \cdot (X_p - X(t)) \\ X(0) &= 0 \,, \end{aligned}}$$

where $a \geq$ and $b > 0$ are biological parameters.

Here a describes the positive feedback induced by stored calcium additionally being released when mitochondria get completely swollen. The value $a = 0$ corresponds to the case of no feedback and we are in the situation of the linear kinetics model described earlier. However, it turns out that for an appropriate simulation of the whole swelling process a is always positive, and thus we confirmed the existence of such an accelerating effect mathematically. Parameter b is a background swelling coefficient, i.e. it represents the swelling rate which is induced by the starting stimulus, in our case the addition of Ca^{2+}.

This second order ODE can be solved explicitly by separation of variables, which yields

$$X(t) = X_p \cdot \left(1 - \frac{X_p + \frac{b}{a}}{X_p + \frac{b}{a} \cdot \exp\left((aX_p + b) \cdot t\right)}\right) \,.$$

This representation shows that $X(t)$ is monotone increasing with one inflection point and that $\lim_{t \to \infty} X(t) = X_p$. The solution is also robust in the sense that the rate of convergence is exponential.

We split up the mitochondrial volume $V(t)$ into three different subpopulations V_1, V_2 and V_3. With the delay term $\tau > 0$ denoting the average swelling time of a single mitochondrion, we have

$$V_1(t) = (1 - X(t)) \cdot V_0 \tag{2.1}$$

       Mitochondria that did not yet start swelling at time t

$$V_2(t) = (X(t) - X(t - \tau)) \cdot k V_p, \quad 0 < k < 1 \tag{2.2}$$

       Mitochondria that have started swelling after $t - \tau$ and hence are not fully swollen

       at time t; they only come up to a fixed percentage k of the final volume

$$V_3(t) = X(t - \tau) \cdot V_p \tag{2.3}$$

       Mitochondria that finished swelling completely until $t = t - \tau$

By setting

$$X(t) := 0 \quad \text{for } t < 0,$$

we obtain the volume equation

$$\boxed{V(t) = (1 - X(t)) \cdot V_0 + (X(t) - X(t - \tau)) \cdot k V_p + X(t - \tau) \cdot V_p.} \tag{2.4}$$

The parameter k determines the average swelling volume of mitochondria that are in the swelling process. Naturally, k can not be arbitrarily close to 0, it has a lower bound depending on the experimental setting.

Assuming the average volume to be kV_p necessarily leads to a small break of the curve at $t = \tau$. This results from the fact that the right-hand side derivative of $X(t)$ at $t = 0$ is $\lim_{t \to 0^+} X'(t) = b X_p$ and hence $\lim_{t \to \tau^+} V'(t) - \lim_{t \to \tau^-} V'(t) = b X_p V_p (1 - k) > 0$. Nevertheless, the size of the break tends to 0 as $b \to 0$. As most of our experiments showed rather low and almost invariant values for b, we could largely eliminate the break.

Results

(i) *Parameter estimation:*

     Figure 2.1 shows the experimental data and the rescaled simulated volume curves for various Ca^{2+} concentrations. Here the four parameters a, b, τ and k are estimated by means of least squares minimization using the Nelder-Mead simplex method [35]. Like that we found an accurate fit of the volume curves and the measurement for the total time range of swelling. Moreover, the model parameters change in a well-determined way, consistent with the corresponding Ca^{2+} concentrations.

     As already mentioned, the background swelling parameter b shows no clear correlation with the amount of added calcium over a wide range and always remains around a value of 0.021. Therefore it is possible to fix this parameter in order to reduce the complexity of minimization.
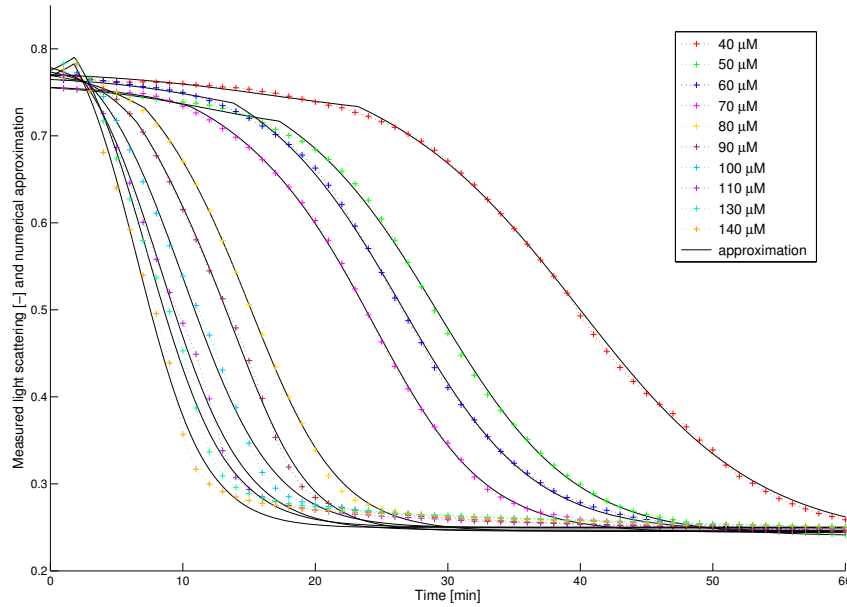
Figure 2.1 – Swelling curves at different Ca^{2+} concentrations compared to the corresponding numerical approximation assuming second order kinetics

The feedback parameter a is estimated to be always positive, i.e. we indeed have an accelerating effect. Furthermore, by assuming second order kinetics, we are now able to appropriately describe the initial lag phase as well as the "tail" of the swelling curve. We determined a linear increase of a with increasing Ca^{2+} concentrations.

The average swelling time τ decreases exponentially with increasing amount of added calcium. This behavior is probably governed by signal transfer processes: a high amount of extra-mitochondrial Ca^{2+} results in a faster arrival of calcium ions inside the mitochondria and hence in a faster initiation of MPT.

Parameter k represents the mean value of mitochondria during their swelling process. Higher values of k thus indicate a faster volume increase in the beginning of the swelling compared to the end, e.g. a less convex / more concave swelling curve of single mitochondria. For our data, k was estimated to be around 0.75 with a very slow exponential increase dependent on the added calcium concentration.

Example
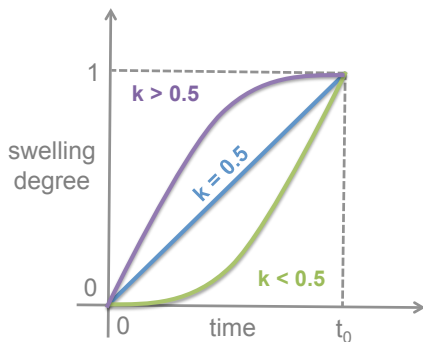
In contrast to the population volume between V_0 and V_p, for simplicity we take a look at single mitochondria with a swelling degree between 0 and 1. Then $k = 0.5$ corresponds to linear swelling curves. Higher values of k lead to faster than linear swelling, whereas lower values represent a slower volume increase. We studied the influence of single swelling curves to the total mitochondrial volume in [21].

(ii) *Curve progression:*

The shape of the resulting volume curves highly depends on the choice of parameter k as it represents the swelling progression of single mitochondria. As was shown for example in [4] or [41], at high Ca^{2+} concentrations mitochondria may go through a short phase of initial shrinking before the actual swelling begins, i.e. we have a slow increase of optical density in the very beginning. Obviously, a value of k with $kV_p < V_0$ means that mitochondria first shrink, thus loose from the initial volume V_0, and then a fast swelling follows to reach the final volume V_p. However, $kV_p > V_0$ does not exclude initial shrinking, but indicates a domination of partly swollen mitochondria over shrunk ones.

Furthermore, for very high values of k we observe a different curve progression, which has a two-phase behavior consisting of two inflection points.

(iii) *Other organs, different inducers:*

We tested the model with mitochondria from other organs and also different inducers of MPT. Figure 2.2 presents the comparison of the swelling curves obtained by treating liver and kidney mitochondria with the same amount of Ca^{2+}.
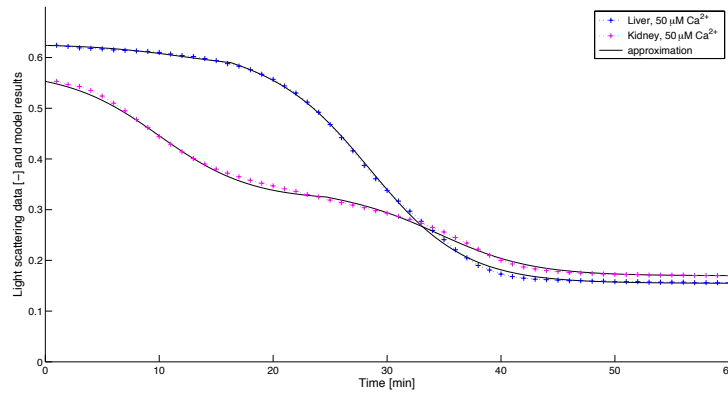
Figure 2.2 – Different curve progressions of liver and kidney mitochondria exposed to the same amount of Ca^{2+}

It is obvious that the swelling curves have completely different curve progressions, but nevertheless our model produces very accurate results. As mentioned before, the two-phase behavior of the kidney swelling curve can be simulated by high values of parameter k. The optimal parameter values are given as follows:

Liver mitochondria	$50\mu M$ Ca^{2+} :	$\tau = 16.28$	$a = 0.25$	$b = 0.012$	$k = 0.74$
Kidney mitochondria	$50\mu M$ Ca^{2+} :	$\tau = 24.65$	$a = 0.25$	$b = 0.019$	$k = 0.89$.

Hence the difference results from differing values of τ and k, while the optimal values for a and b are almost identical. This refers to varying Ca^{2+} uptake and corresponding swelling times, but similar feedback mechanisms in the two organs.

We also made a comparison of liver mitochondria with swelling induced by 50 μM Ca^{2+} and 20 μM Hg^{2+}. This gave the following optimal parameters:

Liver mitochondria	$20\mu M$ Hg^{2+} :	$\tau = 16.54$	$a = 0.055$	$b = 0.041$	$k = 0.70$.

Here all parameters in comparison with liver mitochondria exposed to Ca^{2+} are almost the same, except for the feedback rate a. This definitely makes sense, since we take a look at identical mitochondria, which by default should have the same swelling time and speed. We learned that the mechanism of positive feedback is connected to calcium and since we now induce swelling by mercury, this effect can not appear to the same extent anymore. However, it is not completely zero, because if a sufficiently high amount of mitochondria is swollen, then the stored Ca^{2+} itself can induce swelling, even if it was induced by Hg^{2+}.

In summary, the developed model of mitochondrial swelling is capable to describe the experimental data accurately and over the whole time range. Furthermore it is not only used to reproduce given data, but we are now also able to classify mitochondria and inducers by the corresponding parameter values. If we think for example of the swelling curves for liver and kidney mitochondria, then from the data itself it is not possible to deduce what causes these different curve shapes. But by means of parameter τ we can state that kidney mitochondria have a longer average swelling time.

2.2 Spatial effects

Coming from an ODE model, it is natural to think about the necessity of including spatial effects by means of taking into account partial differential equations.

2.2.1 Motivation

In our previous work mentioned above, we introduced a model which is only focussed on the time evolution. That means we do not take into account local effects and only work with mean values over the whole domain. In other words, the three volume components described in (2.1) - (2.3) can be written as weighted integrals

$$V_1(t) = \quad V_0 \int_\Omega N_1(x,t)\,dx$$

$$V_2(t) = kV_p \int_\Omega N_2(x,t)\,dx$$

$$V_3(t) = \quad V_p \int_\Omega N_3(x,t)\,dx$$

where N_1, N_2 and N_3 denote the density of unswollen, swelling and completely swollen mitochondria. The evolution of these densities depends on the local Ca^{2+} concentration, which is denoted by $u(x,t)$. The added amount of calcium as inducer of mitochondrial swelling is hence given by the initial data $u_0(x)$.

Remark
Here the question appears how a density $N(x)$ of mitochondria on the domain Ω is defined. Mitochondria are a discrete quantity, which has to be translated into a continuous density. Here we present the easiest way to obtain such a density function:

First we define a lattice Γ of points covering Ω. Then for every point $x_i \in \Gamma$ and fixed radius $\varepsilon > 0$ we draw a circle $B_\varepsilon(x_i)$ and count the number n_i of mitochondria within this circle. We set $N(x_i) = n_i$, then interpolation yields a continuous function $N(x)$ for every $x \in \Omega$. In order to derive a density, we have to divide N by the size of Ω.

We assume we are given a test tube with purified mitochondria. If there were no spatial effects, then it should make no difference how the same amount of calcium is added. That is, as long as the integral $\int_\Omega u_0(x)\,dx$ is equal, the resulting mitochondrial volume

$$V(t) = V_1(t) + V_2(t) + V_3(t)$$

should be the same. Figure 2.3 depicts different possibilities to add the same Ca^{2+} amount.

(a) highly localized   (b) "normally distributed"   (c) uniformly distributed
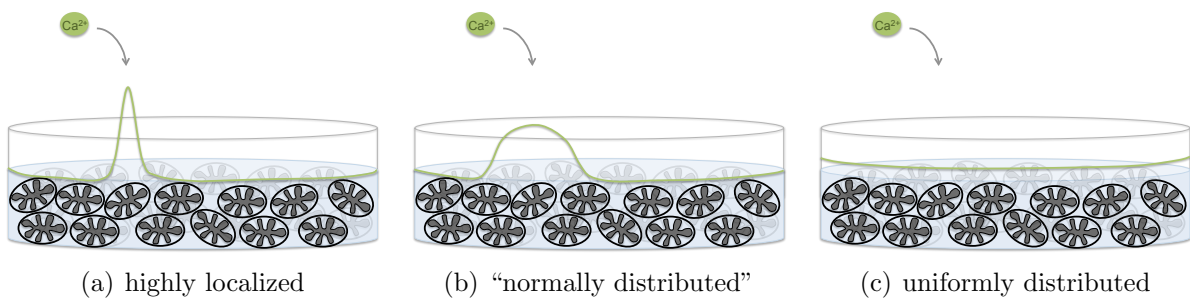
Figure 2.3 – Addition of a fixed calcium amount in varying distribution

The following experiment reveals that different distributions indeed have an influence to the volume outcome. Here three settings with the same total calcium amount are considered:

(i) Volume ratio 1:4

The volume ratio of added Ca^{2+} compared to the volume of the total (unswollen) mitochondrial population is 1:4, i.e. the calcium source is near to being uniformly distributed. This setting is the standard setting for the experimental data displayed in Figure 1.5.

(ii) Volume ratio 1:100 mixed

Here the calcium appears in a much more concentrated form, in order to obtain the same calcium amount in a much smaller volume. After addition to the mitochondria the whole content is mixed, which again leads to a fast calcium dispersion.

(iii) Volume ratio 1:100

Calcium is added in a high concentration with ratio 1:100, but this time no mixing takes place. That means we are in the highly localized case.

The following Figure 2.4 shows the results of these experiments.
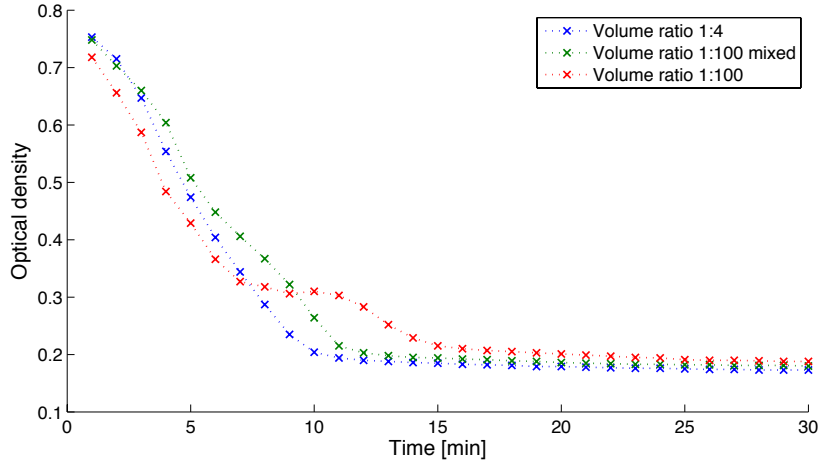
Figure 2.4 – Experimental data resulting from different volume ratios of Ca^{2+} and mitochondria

Here it becomes obvious that the swelling curves and with that the volume increase function $V(t)$ highly depend on the initial calcium distribution. Mixing the test tube content of mitochondria and added calcium, leads to a faster dispersion of the initially highly localized Ca^{2+} source and hence we soon arrive at the nearly uniformly distributed case. This explains why the blue and the green curve show almost the same progression.

However, if we do not mix and wait until calcium is distributed by diffusion, the resulting red curve shows a completely different shape. In the beginning the swelling proceeds faster due to locally very high calcium concentrations, but at the same time several mitochondria remain untreated. Hence, in contrast to the other cases, it takes some time until all of them are reached, which explains the slower second phase of swelling.

With that the necessity of taking into account spatial effects is motivated and in the following we will focus on this topic. That means we are now interested in the local behavior of the densities $N_1(x,t)$, $N_2(x,t)$ and $N_3(x,t)$ in dependence on the calcium concentration $u(x,t)$ instead of only taking a look at the mean values of them.

In order to develop a mathematical model, we have to consider two spatial effects that directly influence the process of mitochondrial swelling:

On the one hand the extent of mitochondrial damage due to calcium is highly dependent on the position of the particular mitochondrion. If the mitochondrion is located near to the Ca^{2+} source, it is exposed to a higher dose compared to mitochondria residing further away and consequently it will be damaged to a higher degree. By diffusion, the locally high calcium dose is diminished and the remaining mitochondria are confronted with a lower concentration.

On the other hand, at a high amount of swollen mitochondria the effect of the positive feedback gets relevant and here the residual mitochondria are confronted with a higher calcium load. Due to the positive feedback mechanism and the natural diffusion, we have some kind of spreading calcium wave e.g. reported in [29], which however is neglected in the existing models. Experiments of our collaboration partner confirmed that not all

mitochondria are damaged to the same degree which implies that they do not react homogeneously [58].

This explains why the distribution of the added Ca^{2+} amount indeed leads to different swelling dynamics. Hence it is important to include the calcium evolution into the model and introduce spatial effects by means of calcium diffusion. This leads to a partial differential equation model.

Remark

The mathematical model to be developed on the following pages does not aim to give a quantitative description of the experimental data as we obtained from our ODE model described earlier. The given data only have mean value character and hence from them we can not deduce more than mean value information. However, our aim now is to qualitatively understand the underlying biological mechanism on the basis of local effects and in particular make the transfer to the processes taking place *in vivo*. Up to now we do not have data of the process in a living cell and thus our model can help to understand the swelling of mitochondria for the biologically and especially pharmacologically more relevant case.

2.2.2 *In vitro* swelling

The experimental procedure introduced in Chapter 1 describes the set up for *in vitro* swelling. Here living mitochondria are extracted from organs and then swelling is artificially triggered within a test tube by addition of MPT inducing substances like Ca^{2+}. Naturally calcium can not leave the test tube and we look at a process taking place in a closed system without any disturbance from the outside. The test tube contains a huge amount of purified mitochondria, which rest in a kind of sugar solution that prevents mitochondria from dying immediately. In this solution the mitochondria are uniformly and "densely" distributed. Furthermore they are either intact or have been destructed while extraction, but in any case at the beginning there are no swelling or completely swollen mitochondria in the test tube.

The initial distribution of calcium describes how it is added to the mitochondria. The experimental data are obtained by assessing a calcium to mitochondria ratio of 1:4, i.e. 20 % of the test tube content then is Ca^{2+}. If one imagines the dissolving of ink in a glass of water, adding ink in a ratio of 1:4 leads to an almost immediate uniform distribution. Therefore, in this case the effects of spatial dependencies are small, since all mitochondria are exposed to the almost same calcium amount simultaneously. Hence the positive feedback only occurs when a large part of the mitochondria is already completely swollen and with that the accelerating effect only happens once most of the swelling is finished.

As we will see in the numerical simulations, the experimental data are best reproduced by assuming highly dissolved initial calcium concentrations, whereas more located initial data lead to completely different curve shapes. Hence, one really has to be aware of the influence of the experimental design on the swelling curve outcome. In order to obtain comparable results, one has to pay attention to what degree of localization the swelling inducer is added.

2.2.3 *In vivo* swelling

Here the swelling process is examined in a living organism, where we do not have a controlled environment as we had in the test tube. We take a look at the whole cell and analyze the effects of high Ca^{2+} concentrations to the mitochondria residing inside the cell. In contrast to the *in vitro* case, here calcium is not artificially added, but rather several biochemical processes in the organism lead to an increase of intracellular Ca^{2+}.

Remark

Ca^{2+} plays an important role in the communication of cells, not only in regard of inducing apoptosis by mitochondrial swelling. As it is e.g. described in [6], calcium acts as a "second messenger", i.e. it is a chemical substance that translates extracellular signals into intracellular ones. This signal transduction by means of calcium ions is also involved in the activation of muscle contraction, cell division or gene expression. Even for mitochondria, the main physiological role of Ca^{2+} uptake is control of the ATP production rate. Only the dose decides whether more energy is produced or the cell dies via apoptosis [45].

Mitochondrial distribution

It is known that mitochondria within cells are not distributed randomly but reside in three main regions. As it was noted in [38], mitochondria reside around the nucleus, in a neighboring group and near the cell membrane. In liver cells, the total mitochondrial population comes up to 22 % and the endoplasmic reticulum to 15 % of the cell volume [1]. Figure 2.5 shows the organization of an eukaryotic cell, restricted to the cell compartments which are of interest for our purpose.
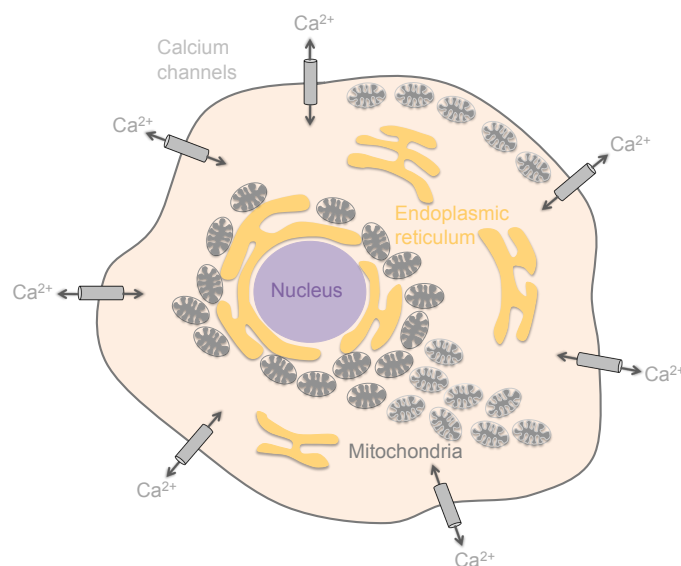
Figure 2.5 – Schematic diagram of a cell with focus on the mitochondrial distribution

The endoplasmic reticulum is the main calcium storage inside a cell and plays a big role in the cellular Ca^{2+} homeostasis [45]. Another important feature are the calcium channels, which allow for an ion exchange between the cell and the extracellular regime.

It is not clear whether all mitochondria in a cell react in the same way, or if e.g. mitochondria located around the nucleus are less sensitive to calcium than mitochondria residing near the cell membrane. At the moment this is not biologically clarified yet, but as we will see, we can introduce such kind of properties into our mathematical model by assuming space dependencies of the mitochondrial behavior.

Now it would be interesting to see if a given amount of calcium is sufficient to induce swelling for all mitochondria or if the process only attacks mitochondria from a specific region. At this the Ca^{2+} source plays a major role.

Increase of intracellular Ca^{2+}

There are two mechanisms that lead to calcium increase inside the cell (see e.g. [45], [46]), which both may lead to apoptosis, as it is depicted in Figure 2.6.

- *Internal:* Ca^{2+} release from endoplasmic reticulum (ER)

  Due to external stimuli, Ca^{2+} is released from the endoplasmic reticulum. When ER stress is triggered by e.g. the exposure to toxins or under pathophysiological conditions like ischemia or viral infections [48], this ER store is depleted and the released Ca^{2+} causes apoptotic events [15].
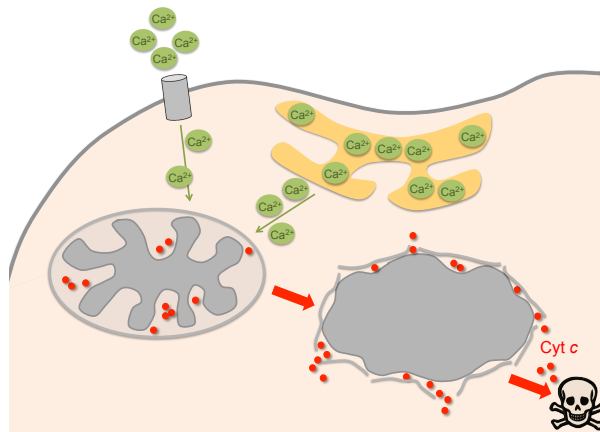
Figure 2.6 – Calcium triggers apoptosis either intra- or extracellular

- *External:* Ca^{2+} influx from extracellular milieu

  The cell membrane itself is impermeable to ions and with that also to Ca^{2+}. However, there are transport systems that enable the calcium flux over the membrane. These are ion channels for the influx, whereas the efflux is is controlled by Na^+/Ca^{2+} exchangers and ATP-dependent Ca^{2+} pumps. As we noted before, calcium acts as a second messenger and hence it is of major importance to maintain a constant cytosolic Ca^{2+} concentration, since a small change may cause severe cellular responses. For that reason there exists an enormous concentration gradient between cytosolic (100nM) and extracellular (1mM) calcium, which is to be maintained actively by use of energy [45].

If apoptosis now is induced by Ca^{2+} as an extracellular signal, it is exposed to the cell in form of a directed calcium flow, that enters the cell via the ion channels in the membrane [6].

For our model this increase of cytosolic Ca^{2+} signifies the start of the swelling process. It represents the initial calcium concentration by setting

$$u_0(x) := C_{in} + u_{peak}(x)\,,$$

where C_{in} denotes the constant cytosolic concentration and $u_{peak}(x)$ describes the local increase. Here we assume this peak to be a singular event and model the resulting events effectuated from this calcium pulse.

A remarkable effect compared to the *in vitro* case is, that for both possibilities of intracellular calcium increase the calcium source is very localized and by no means we have a uniformly distributed initial concentration.

The cell membrane

As described earlier, Ca^{2+} can enter or leave the cell across the plasma membrane via a non-symmetric transport system consisting of channels and pumps. Here the radius and the location of these passage ways are not fixed and dependent on the present need of concentration gradient stabilization.

Since we do not have detailed biological information, for the mathematical modeling we assume that the total channel size over the whole membrane stays constant. Hence scaling down the radius implies a larger number of channels and passing to the limit as we did in Figure 2.7, leads to an all-over permeable "limit membrane".
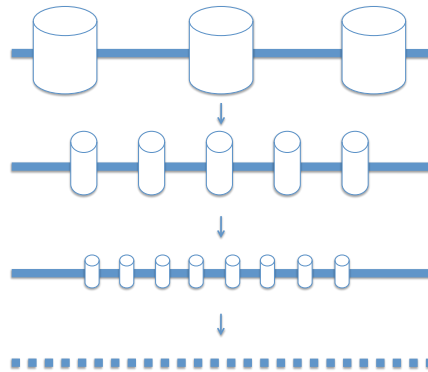
Figure 2.7 – Passing to the limit of the ion channel radius

By simplicity, in the following we will consider the *in vivo* model with this limit membrane.

Remark
In order to avoid this limiting process, we can introduce two regions Γ_1 and Γ_2 with $\Gamma_1 \cap \Gamma_2 = \emptyset$, where Γ_1 contains the channels and Γ_2 the closed parts of the membrane. Then by definition, on Γ_2 calcium can not leave or enter the cell, which implies a different behavior on these two regions.

This poses difficulties for the mathematical analysis since we have to handle these two regions separately. However, it is not clear how to define the size of these subsets in a biological correct way and hence we can not obtain a better description of the biological reality.

Summary

The previous observations make clear why it is really necessary to take into account spatial effects for the *in vivo* modeling of mitochondrial swelling. Briefly summarized, there are three main factors that differ a lot from the *in vitro* case:

- Mitochondria are not uniformly distributed.

- The inducing Ca^{2+} source is very localized.

- The cell is not a closed system.

2.3   The mitochondria model

In the following the biological description of the mitochondrial swelling process is translated into the mathematical language. We already indicated before that for the *in vitro* model we choose the domain Ω to be the test tube, whereas the *in vivo* model considers Ω as the whole cell.

The variables

The model variables were already introduced before and are described in the following way:

$$
\begin{aligned}
u(x,t): &\quad \text{Ca}^{2+} \text{ concentration} \\
N_1(x,t): &\quad \text{density of unswollen mitochondria} \\
N_2(x,t): &\quad \text{density of mitochondria in the swelling process} \\
N_3(x,t): &\quad \text{density of completely swollen mitochondria}
\end{aligned}
$$

Here the transition of intact mitochondria over swelling to completely swollen ones proceeds in dependence on the local calcium concentration. At this we can assume that mitochondria in the test tube as well as within cells do not move in any direction and hence the spatial effects are only introduced by the calcium evolution.

Initial conditions

In accordance with previous findings, the initial data

$$
u(x,0) = u_0(x), \quad N_1(x,0) = N_{1,0}(x), \quad N_2(x,0) = N_{2,0}(x), \quad N_3(x,0) = N_{3,0}(x)
$$

are defined by the type of experiment.

Here the quantities N_i, $i = 1, 2, 3$ are to be interpreted in the density sense described

earlier when we scale $\frac{1}{|\Omega|} N_i(x, t)$.

We assume that they initially take only the values 0 or 1, where $N_{i,0}(x) = 0$ corresponds to "no mitochondrion at point x" and a value of 1 means "mitochondrion at point x".

in vitro: Initially the test tube contains densely distributed mitochondria and the "swelling buffer" described in Chapter 1. It does not contain any calcium, hence we have

$$u_0(x) = u_{peak}(x) \geq 0, \quad N_{1,0}(x) \equiv 1, \quad N_{2,0}(x) \equiv 0, \quad N_{3,0}(x) \equiv 0. \qquad (2.5)$$

Here u_{peak} describes the artificially added Ca^{2+} that induces the swelling process.

in vivo: Mitochondria reside in three main regions, i.e.

$$u_0(x) = C_{in} + u_{peak}(x) \geq 0, \quad N_{1,0}(x) \in \{0, 1\}, \quad N_{2,0}(x) \equiv 0, \quad N_{3,0}(x) \equiv 0,$$

where $C_{in} \geq 0$ denotes the intracellular Ca^{2+} concentration at normal conditions. u_{peak} is the calcium pulse coming either from outside the cell or the endoplasmic reticulum.

Note that for both cases in the beginning there are no swelling mitochondria or those that have already finished swelling.

Remark
For the mathematical analysis we allow for more general initial conditions.

Boundary conditions

The spatial effects only trace back to spreading Ca^{2+}, hence we only need to impose boundary conditions for the variable $u(x, t)$:

in vitro: Calcium can not cross the boundary $\partial\Omega$, i.e. the test tube wall and hence we have homogenous Neumann boundary conditions

$$\partial_\nu u(x, t) = 0 \quad \text{for } x \in \partial\Omega.$$

Mathematically we will also treat the case of homogenous Dirichlet boundary conditions

$$u(x, t) = 0 \quad \text{for } x \in \partial\Omega.$$

Biologically, this kind of boundary condition appears if we put some chemical material on the wall that binds calcium ions and hence removes it as a swelling inducer.

in vivo: As we demonstrated in Figure 2.7, we assume the boundary to be the permeable "limit membrane". Here calcium can enter or leave the cell over this membrane. The concentration gradient between the cell and the extracellular regime needs always be maintained, hence we assume inhomogeneous Robin boundary conditions

$$-\partial_\nu u(x, t) = a(x)\big(u(x, t) - \beta\, C_{ext}\big) \quad \text{for } x \in \partial\Omega.$$

Here $C_{ext} \geq 0$ denotes the extracellular, constant calcium concentration and $\beta \geq 0$ represents the concentration gradient.

That means e.g. for the constants reported in [45], we have $C_{in} = 100$ nM $= 10^{-7}$ M and $C_{ext} = 1$ mM $= 10^{-3}$ M and hence the concentration gradient is of order 10^{-4} and we take $\beta = 10^{-4}$.

Remark

1) In general the extracellular calcium concentration is not constant, however due to its largeness compared to the cell size, single calcium peaks are dissolved very fast.

2) By the choice of the function $a(x)$ we can distinguish between different parts of the membrane. The previously mentioned case $\partial\Omega = \Gamma_1 \cup \Gamma_2$ hence could be realized by setting $a(x) = 0$ for $x \in \Gamma_2$ representing the closed parts of the membrane. This leads to zero flux on Γ_2 and concentration-dependent flux on Γ_1, just as we described the situation for the original membrane. However, for the mathematical analysis we need to assume $a(x) \geq a_0 > 0$.

3) By the choice of a we can switch between Dirichlet and Neumann type boundary conditions. If a is very small, the flux over the boundary is also very small and in the limit case $a \to 0$ we have homogeneous Neumann boundary conditions. On the other hand, for high values of a the solution soon approaches $u = \beta\, C_{ext}$ on the boundary, i.e. we can expect a behavior similar to non-homogeneous Dirichlet boundary conditions.

Coupled ODE-PDE model

Now we are finally prepared to introduce the new model. As we noted before, only the calcium concentration u evolves in time and space, and hence its behavior is described by a partial differential equation. Mitochondria do not move and thus the evolution of the mitochondrial subpopulations N_1, N_2 and N_3 is modeled by a system of ordinary differential equations that are dependent on the current state of $u(x,t)$. These ODEs depend on the space variable x in terms of a parameter. This leads to the following coupled ODE-PDE system determined by the model functions f and g and the diffusion operator A:

$$
\boxed{
\begin{aligned}
\partial_t u &= d_1 A(u) + d_2 g(u) N_2 \\
\partial_t N_1 &= -f(u) N_1 \\
\partial_t N_2 &= f(u) N_1 - g(u) N_2 \\
\partial_t N_3 &= g(u) N_2
\end{aligned}
}
$$

with diffusion constant $d_1 \geq 0$ and feedback parameter $d_2 \geq 0$. The boundary conditions vary for the type of the model and can be generally formulated as

$$a\, u + b\, \partial_\nu u = h \text{ on } \partial\Omega$$

with functions a, b and h defined on the boundary. Furthermore we have initial conditions

$$u(x,0) = u_0(x)\,, \quad N_1(x,0) = N_{1,0}(x)\,, \quad N_2(x,0) = N_{2,0}(x)\,, \quad N_3(x,0) = N_{3,0}(x)$$

with the specific functions depending on the model type as described earlier.

This model is solved on the phase space H, which has to be suitable defined for every type of problem. According to that, the initial data have to be taken from an appropriate space dependent on the diffusion operator A. For the ODE components we can always assume

$$N_{i,0} \in L^\infty(\Omega) \quad \text{for } i = 1, 2, 3 \,.$$

In the following we will explain all model components in detail.

Diffusion operator A

The operator A denotes the diffusion operator responsible for the calcium spreading, i.e. the calcium evolution is described by a reaction-diffusion equation with a positive production term as we will see later on.

In this thesis we will study both to the case of non-degenerate and degenerate diffusion. The non-degenerate diffusion model considers the standard Laplacian

$$\boxed{A(u) = \Delta u \,,}$$

whereas the degenerate case is described by the nonlinear operator

$$\boxed{A(u) = \Delta(|u|^{m-2}u) \,.}$$

with $m > 2$.

The biological reason to consider also the mathematically more complicate case of degeneracy is connected to the propagation speed of calcium. The standard Laplace operator is an appropriate and well-studied tool to model the diffusion process, however it has one disadvantage, namely its infinite speed of propagation. That means, starting from compactly supported initial data, the solution u get immediately positive on the whole domain, i.e. it reaches any corner in arbitrary small time. This effect is not consistent with biological observations and hence we want to get rid of this effect by choosing degenerate diffusion with finite propagation speed. This effect will be described in more detail in Section 4.1.

Model function f

The process of mitochondrial permeability transition is dependent on the calcium concentration. If the local concentration of Ca^{2+} is sufficiently high, the transition pores open and mitochondrial swelling is initiated. This incident is mathematically described by the transition of mitochondria from N_1 to N_2. The corresponding transition function $f(u)$ is zero up to a certain threshold C^- displaying the concentration which is needed to start the whole process. Whenever this Ca^{2+} threshold is reached, the local transition at this point from N_1 to N_3 over N_2 is inevitably triggered. It is written e.g. in [41] that this process is calcium-dependent with higher concentrations leading to faster pore opening. Hence the function $f(u)$ is increasing in u.

The transfer from unswollen to swelling mitochondria is related to pore opening, hence we also postulate that there is some saturation rate f^* displaying the maximal transition rate. This is biologically explained by a bounded speed of pore opening with increasing calcium concentrations. This saturation with respect to calcium also becomes obvious in the experimental data displayed in Figure 1.5, where we see that with increasing Ca^{2+} concentrations the swelling process is speeded up, but at very high concentrations we do not observe changes in the swelling curves appearance any more.

Figure 2.8 (a) displays the type of function we used for the numerical simulations.

Remark

The initiation threshold of f is crucial for the whole swelling procedure. Dependent on the amount and location of added calcium, it can happen that in the beginning the local concentration was enough to induce swelling in this region, but after some time due to diffusion the threshold C^- is not reached anymore. Thus we only have partial swelling and after the whole process there are still intact mitochondria left. Nevertheless, the are no mitochondria in the intermediate state N_2.

(a) Model function f (b) Model function g
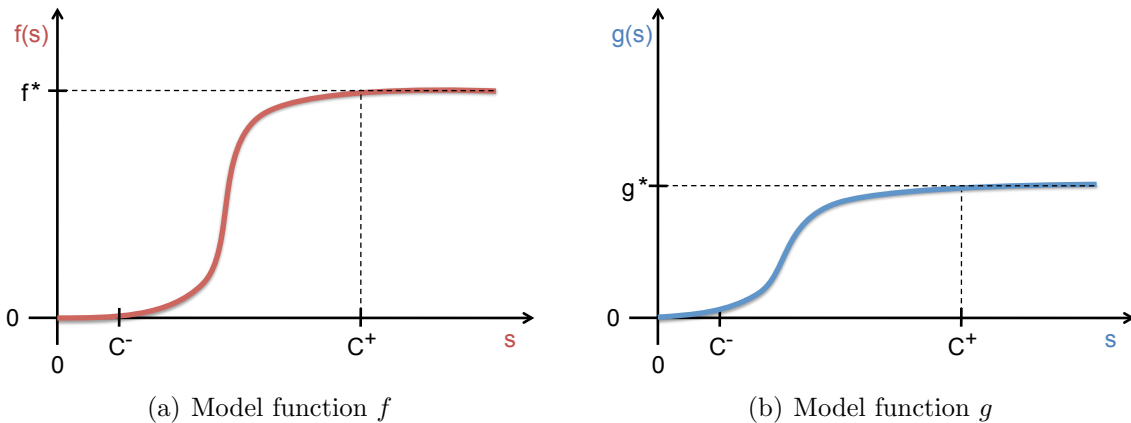
Figure 2.8 – Graphical description of the model functions we used for the numerical simulation

Model function g

The change of the population N_2 consists of mitochondria entering the swelling process (coming from N_1) and mitochondria getting completely swollen (leaving to N_3). The transition of N_2 to N_3 is modeled by the transition function $g(u)$. In contrast to the function f here we have no initiation threshold and this transition can not be avoided (as we will see later: $u(x,t) > 0 \ \forall x \ \forall t$ except for the homogenous Dirichlet case). This property is based on the biological mechanism of swelling. The permeabilization of the inner membrane due to pore opening leads to an osmotically driven influx of water and other solutes into the mitochondrial matrix and induces swelling. This process itself is independent of the present calcium concentration. Due to a limited pore size, this effect also has its restrictions and thus we have saturation at level g^*. By simplicity we assume that the point of saturation C^+ is the same for f and g as can be seen in Figure 2.8 (b), where we depict a typical function g used in the simulations.

However, biologically it is not clear if there are other influences of calcium to this second transition, e.g. by the opening of additional pores. To include such possibilities, for the simulations we assume g to be increasing with saturation at level g^* for $u \geq C^+$.

The third population N_3 of completely swollen mitochondria grows continuously due to the unstoppable transition from N_2 to N_3. All mitochondria that started to swell will be completely swollen in the end.

Remark

1) For the mathematical analysis we allow for more general transition functions f and g. The corresponding assumptions are formulated in Conditions 1 and 2. Note that in particular f and g (up to a small interval) not even have to be monotone.

2) In the present model we assume that mitochondria only differ with respect to their location and with that in the moment when they are hit by the calcium wave.

If we take a look at the whole cell, then it is not clear if all mitochondria react in the same way or if mitochondria residing in different groups have different sensitivities to calcium. At the moment this is not biologically clarified yet, however we can introduce such kind of properties into our model by assuming space dependence $f(x, u)$ and $g(x, u)$.

Calcium evolution

The model consists of spatial developments in terms of diffusing calcium. In addition to the (linear or non-linear) diffusion term, the equation for the calcium concentration contains a production term dependent on N_2, which is justified by the following:

In our earlier ODE approach of modeling mitochondrial swelling [22] it turned out that it is essential to include the positive feedback mechanism. This accelerating effect is induced by stored Ca^{2+} inside the mitochondria, which is additionally released once the mitochondrion gets completely swollen. Due to a fixed amount of stored calcium, we assume that the additional released calcium is proportional to the newly completely swollen mitochondria, i.e. the mitochondria leaving N_2 and entering N_3. Here the feedback parameter d_2 describes the amount of stored calcium.

In contrast to the previous model, now the action of the positive feedback is contained directly by providing additional calcium. As we will see later on, this additional term is always non-negative and hence it is interesting to take a look at the long-time behavior of the solution.

Model analysis

In the following we will analyze the derived model mathematically. Here we take a look at more general initial data and allow for a larger class of model functions. All mathematical results apply for the biological relevant cases $\Omega \subset \mathbb{R}^n$ with $n = 2$ or $n = 3$.

Chapter 3 deals with the non-degenerate model based on the standard Laplacian. Here we study both the dynamics *in vitro* and *in vivo* and verify the mathematical results by numerical simulations.

Chapter 4 then treats the more complicated case of degenerate diffusion. In order to handle it mathematically, we have to assume homogeneous Dirichlet boundary conditions.

Conclusion

To our knowledge, there are no mathematical models taking into account the whole cell and the non-uniform mitochondrial distribution yet. At the moment we do not have experimental data since it is a very complicated task to monitor the processes taking place in a living cell without being too disruptive.

However, biologically this is the relevant case and it is definitely worth to study these spatial dependencies mathematically as well as experimentally. With mathematics we can formulate postulates, which then can be tested biologically by specially designed experiments. This will lead to new insights into the interaction of calcium and mitochondria inside cells.

CHAPTER 3

Non-degenerate mitochondria model

In this Chapter we study the developed mathematical model of mitochondrial swelling with the standard diffusion operator $A = \Delta$. In the following sections we examine the influence of different boundary conditions and show the results for the *in vitro* and the *in vivo* model.

3.1   Neumann boundary conditions

As we have elaborated earlier, homogeneous Neumann boundary conditions apply to test tube experiments and hence we are now analyzing the ***in vitro* model**

$$
\begin{align}
\partial_t u &= d_1 \Delta u + d_2 g(u) N_2 \tag{3.1}\\
\partial_t N_1 &= -f(u) N_1 \tag{3.2}\\
\partial_t N_2 &= f(u) N_1 - g(u) N_2 \tag{3.3}\\
\partial_t N_3 &= g(u) N_2 \tag{3.4}
\end{align}
$$

with boundary condition

$$
\partial_\nu u = 0 \quad \text{on } \partial\Omega \tag{3.5}
$$

and initial values

$$
u(x,0) = u_0(x), \quad N_1(x,0) = N_{1,0}(x), \quad N_2(x,0) = N_{2,0}(x), \quad N_3(x,0) = N_{3,0}(x) \, .
$$

Remark
We already characterized the initial functions in (2.5), however the mathematical analysis can be applied to a more general setting.

3.1.1   Existence and uniqueness of global solutions

The coupled ODE-PDE model (3.1) - (3.5) describing the *in vitro* swelling process shall now be analyzed mathematically. At first we want to show the well-posedness of the model. For that purpose we introduce some assumptions to the model functions f and g.

Condition 1
For the model functions $f : \mathbb{R} \to \mathbb{R}$ and $g : \mathbb{R} \to \mathbb{R}$ it holds:

(i) Non-negativity:

$$f(s) \geq 0 \quad \forall s \in \mathbb{R}$$
$$g(s) \geq 0 \quad \forall s \in \mathbb{R}$$

(ii) Boundedness:

$$f(s) \leq f^* < \infty \quad \forall s \in \mathbb{R}$$
$$g(s) \leq g^* < \infty \quad \forall s \in \mathbb{R}$$

with $f^*, g^* > 0$.

(iii) Lipschitz continuity:

$$|f(s_1) - f(s_2)| \leq L_f |s_1 - s_2| \quad \forall s_1, s_2 \in \mathbb{R}$$
$$|g(s_1) - g(s_2)| \leq L_g |s_1 - s_2| \quad \forall s_1, s_2 \in \mathbb{R}$$

with $L_f, L_g \geq 0$.

Remark
Property (iii) implies bounded derivatives $|f'(s)| \leq L_f$ and $|g'(s)| \leq L_g$ for all $s \in \mathbb{R}$.

One remarkable characteristic of the model is the following:

If we only take a look at the ODE part and define the total mitochondrial population

$$\overline{N}(x,t) := N_1(x,t) + N_2(x,t) + N_3(x,t),$$

then adding the three equations (3.2) + (3.3) + (3.4), we obtain $\partial_t \overline{N} = 0$. This implies

$$\overline{N}(x,t) = \overline{N}(x) = N_{1,0}(x) + N_{2,0}(x) + N_{3,0}(x) \qquad \forall t \geq 0 \quad \forall x \in \Omega, \qquad (3.6)$$

i.e. the total population $\overline{N}$ does not change and is given by the sum of the initial data. In particular we have

$$\|\overline{N}\|_{L^\infty(\Omega)} \leq \|N_{1,0}\|_{L^\infty(\Omega)} + \|N_{2,0}\|_{L^\infty(\Omega)} + \|N_{3,0}\|_{L^\infty(\Omega)} < \infty$$

for initial data from $L^\infty(\Omega)$.

The first aim is to study the model in terms of existence and uniqueness of the solution (u, N_1, N_2, N_3). Here we consider the phase space $H = L^2(\Omega)$.

Theorem 1
Let $\Omega \subset \mathbb{R}^n$ be bounded. Under the assumptions of Condition 1 it holds:
For all initial data $u_0 \in L^2(\Omega)$, $N_{1,0} \in L^\infty(\Omega)$, $N_{2,0} \in L^\infty(\Omega)$ and $N_{3,0} \in L^\infty(\Omega)$ with

$$\|N_{1,0}\|_{L^\infty(\Omega)} + \|N_{2,0}\|_{L^\infty(\Omega)} \neq 0, \qquad (3.7)$$

the system (3.1) - (3.5) *possesses a unique global solution* (u, N_1, N_2, N_3) *satisfying*

$$u \in C([0, T]; L^2(\Omega))$$
$$\sqrt{t}\, \partial_t u \in L^2(0, T; L^2(\Omega))$$
$$\sqrt{t}\, \Delta u \in L^2(0, T; L^2(\Omega))$$
$$N_i \in L^\infty(0, T; L^\infty(\Omega)), \quad i = 1, 2, 3\,,$$

for all $T > 0$.

Remark
The additional assumption (3.7) first comes into play in the proof of global existence. However, this condition is not very restrictive, since from

$$\|N_{1,0}\|_{L^\infty(\Omega)} + \|N_{2,0}\|_{L^\infty(\Omega)} = 0$$

it follows

$$N_{1,0}(x) \equiv 0 \quad \text{and} \quad N_{2,0}(x) \equiv 0$$

which leads to the trivial solution $N_1(x, t) \equiv 0$, $N_2(x, t) \equiv 0$, $N_3(x, t) \equiv N_{3,0}(x)$ for all $x \in \Omega$ and the model is reduced to the standard heat equation with homogeneous Neumann boundary conditions.

Proof

1.) Local solution

At first we proof existence and uniqueness of a local solution.

In the following we only take a look at equations (3.1) - (3.3). From the conservation law (3.6) we know that the solution N_3 is then given by the identity

$$\boxed{N_3(x, t) = \overline{N}(x) - N_1(x, t) - N_2(x, t)\,.} \tag{3.8}$$

We work in the Banach space

$$X := C([0, T]; L^2(\Omega)) \text{ with } \|u\|_X = \max_{0 \le t \le T} \|u(t)\|_{L^2(\Omega)}$$

and define the mapping

$$\mathcal{B} : u \in X \mapsto N^u := \begin{pmatrix} N_1^u \\ N_2^u \end{pmatrix} \mapsto \hat{u} = \mathcal{B}(u)$$

in the following way: By N_i^u we denote the solution of the corresponding ODE with respect to a fixed u, i.e. the vector N^u solves the pure ODE system

$$\partial_t N^u = \begin{pmatrix} -f(u)N_1^u \\ f(u)N_1^u - g(u)N_2^u \end{pmatrix} =: F(N^u) \tag{3.9}$$

$$N^u(x, 0) = \begin{pmatrix} N_{1,0}(x) \\ N_{2,0}(x) \end{pmatrix}. \tag{3.10}$$

This solution dependent on fixed u is now substituted into the PDE (3.1), which means we are looking for the solution $\hat{u}$ of the pure PDE problem

$$
\begin{aligned}
\partial_t \hat{u} &= d_1 \Delta \hat{u} + d_2 g(\hat{u}) N_2^u \\
\hat{u}(x,0) &= u_0(x) \\
\partial_\nu \hat{u}\big|_{\partial\Omega} &= 0 \,.
\end{aligned}
\tag{3.11}
$$

The outline of the proof is the following:

   (i) Show that the ODE system possesses a unique solution N^u for fixed u

   (ii) Show that the PDE corresponding to the solution N^u possesses a unique solution $\hat{u}$

   (iii) Show that the mapping $\mathcal{B}$ possesses a unique fixed-point with $\mathcal{B}(u) = u$.

Step (i): Consider the mapping $u \mapsto N^u$

For every $u \in X$ by Condition 1 (ii) we have $f(u) \le f^*$ and $g(u) \le g^*$. We now take a look at the ODE system (3.9), (3.10) and search for the unique solution of this ODE in the product Banach space

$$
Y := L^2(\Omega) \times L^2(\Omega) \,.
$$

Obviously it holds $F : Y \to Y$. In order to apply the Piccard-Lindelöf theorem we need Lipschitz-continuity of F:

$$
\|F(A) - F(B)\|_Y \overset{!}{\le} L_F \|A - B\|_Y \quad \forall A, B \in Y \text{ with } A = (A_1, A_2), B = (B_1, B_2)
$$

$$
\begin{aligned}
\|F(A) - F(B)\|_Y^2 &= \| - f(u)(A_1 - B_1)\|_{L^2(\Omega)}^2 + \|f(u)(A_1 - B_1) - g(u)(A_2 - B_2)\|_{L^2(\Omega)}^2 \\
&\le |f(u)|^2 \|A_1 - B_1\|_{L^2(\Omega)}^2 + 2|f(u)|^2 \|A_1 - B_1\|_{L^2(\Omega)}^2 + 2|g(u)|^2 \|A_2 - B_2\|_{L^2(\Omega)}^2 \\
&\le \underbrace{\max\left(3 f^{*2}, 2 g^{*2}\right)}_{=: L_F{}^2 \text{ with } L_F > 0} \|A - B\|_Y^2
\end{aligned}
$$

Thus it follows:

> For every $u \in X$ there exists a unique solution $N^u = \begin{pmatrix} N_1^u \\ N_2^u \end{pmatrix} \in C([0, \infty], Y) \,.$ (3.12)

Our aim now is to obtain upper bounds in $L^\infty(\Omega)$.

Remark
For general initial data $N_{1,0}(x)$, $N_{2,0}(x)$ we do not have any information about the sign of $N_1^u(x,t)$ and $N_2^u(x,t)$.

For that reason we define for $i = 1, 2$

$$\mathcal{T}^+(x) := \{t \in [0, \infty) : N_i^u(x, t) > 0\} = \bigcup_{j \in J} \mathcal{T}_j^+(x)$$

$$\mathcal{T}^-(x) := \{t \in [0, \infty) : N_i^u(x, t) < 0\} = \bigcup_{k \in K} \mathcal{T}_k^-(x)$$

$$\mathcal{T}^0(x) := \{t \in [0, \infty) : N_i^u(x, t) = 0\} = \bigcup_{l \in L} p_l(x) \cup \mathcal{T}_z(x)$$

where $\mathcal{T}_j^+(x)$, $\mathcal{T}_k^-(x)$ and $\mathcal{T}_z(x)$ are connected intervals and the point $p_l(x)$ is the location of the lth zero.
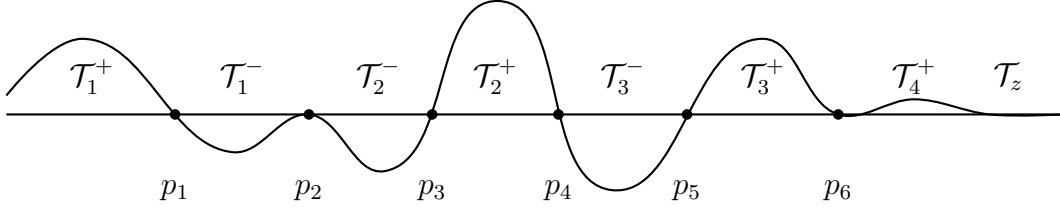
Like that we have the following partition of the time interval $[0, \infty)$ for fixed $x \in \Omega$:

$$[0, \infty) = \mathcal{T}^+(x) \, \dot\cup \, \mathcal{T}^-(x) \, \dot\cup \, \mathcal{T}^0(x) \,.$$

We are now looking at the equations point-wise. For N_1^u it holds

$$\partial_t N_1^u(x, t) = -f(u(x, t)) N_1^u(x, t)$$

and that relation immediately implies that if $N_1^u(x, t)$ attains zero at time $t = t_1$, then $N_1^u(x, t) \equiv 0$ for all $t \geq t_1$, i.e. for N_1^u the partition is either given by

$$[0, \infty) = \mathcal{T}^+(x) \, \dot\cup \, \mathcal{T}_z(x) \quad \text{or} \quad [0, \infty) = \mathcal{T}^-(x) \, \dot\cup \, \mathcal{T}_z(x) \,. \tag{3.13}$$

So we only have to consider the cases $N_1^u(x, t) > 0$ for $t \in \mathcal{T}^+(x)$ or $N_1^u(x, t) < 0$ for $t \in \mathcal{T}^-(x)$. For both cases, N_1^u satisfies

$$\partial_t |N_1^u(x, t)| = -f(u(x, t)) |N_1^u(x, t)|$$

with $f(u(x, t)) \geq 0$ by Condition 1 (i). Hence it easily follows for all $x \in \Omega$ with Gronwall's inequality

$$|N_1^u(x, t)| \leq |N_{1,0}(x)| e^{-f(u(x,t))t} \leq |N_{1,0}(x)|$$
$$\leq \|N_{1,0}\|_{L^\infty(\Omega)} \quad \forall t \in \mathcal{T}^+(x) \text{ or } \forall t \in \mathcal{T}^-(x) \,.$$

For $t \in \mathcal{T}_z(x)$ we clearly have

$$|N_1^u(x, t)| = 0 \leq \|N_{1,0}\|_{L^\infty(\Omega)}$$

and all together by (3.13) we obtain the L^∞ bound

$$\boxed{\|N_1^u(t)\|_{L^\infty(\Omega)} \leq \|N_{1,0}\|_{L^\infty(\Omega)} =: C_1 < \infty \quad \forall t \geq 0 \,.} \tag{3.14}$$

An analogous result can be achieved for N_2^u. However, in that case the partition of $[0, \infty)$ can not be simplified as before. For fixed $x \in \Omega$ we have to distinguish between different cases.

Case 1: $N_{2,0}(x) \neq 0$, i.e. $p_1(x) \neq 0$

   a) $N_2^u(x, t) > 0$ on the interval $[0, p_1(x))$, i.e. $[0, p_1(x)) = \mathcal{T}_1^+(x)$

       In that case due to the non-negativity of g, the boundedness of f and (3.14), it holds

$$\partial_t N_2^u(x, t) = f(u(x, t)) N_1^u(x, t) - g(u(x, t)) N_2^u(x, t)$$
$$\leq f^* \|N_{1,0}\|_{L^\infty(\Omega)} \quad \forall t \in \mathcal{T}_1^+(x) \,.$$

       Hence we easily get by integration $\int_0^t ds$

$$N_2^u(x, t) \leq N_{2,0}(x) + t f^* \|N_{1,0}\|_{L^\infty(\Omega)}$$
$$\leq \|N_{2,0}\|_{L^\infty(\Omega)} + t f^* \|N_{1,0}\|_{L^\infty(\Omega)} \quad \forall t \in \mathcal{T}_1^+(x) \,.$$

   b) $N_2^u(x, t) < 0$ on the interval $[0, p_1(x))$, i.e. $[0, p_1(x)) = \mathcal{T}_1^-(x)$

       In contrary to the previous case we have

$$\partial_t N_2^u(x, t) \geq -f(u(x, t)) |N_1^u(x, t)| - g(u(x, t)) N_2^u(x, t)$$
$$\geq -f^* \|N_{1,0}\|_{L^\infty(\Omega)} \quad \forall t \in \mathcal{T}_1^-(x) \,,$$

       which implies

$$N_2^u(x, t) \geq -|N_2(x, 0)| - t f^* \|N_{1,0}\|_{L^\infty(\Omega)}$$
$$\geq -\|N_{2,0}\|_{L^\infty(\Omega)} - t f^* \|N_{1,0}\|_{L^\infty(\Omega)} \quad \forall t \in \mathcal{T}_1^-(x) \,.$$

In summary for *Case 1* we obtain

$$|N_2^u(x, t)| \leq \|N_{2,0}\|_{L^\infty(\Omega)} + t f^* \|N_{1,0}\|_{L^\infty(\Omega)} \quad \forall x \in \Omega \quad \forall t \in [0, p_1(x)) \,.$$

Case 2: $N_{2,0}(x) = 0$, i.e. $p_1(x) = 0$

   a) $N_2^u(x, t) > 0$ on the interval $(p_1(x), p_2(x))$, i.e. $(p_1(x), p_2(x)) = \mathcal{T}_1^+(x)$

       In analogy to *Case 1* but with $N_2^u(x, 0) = N_2^u(x, p_1(x)) = 0$ we obtain by integration $\int_{p_1(x)}^t ds$

$$N_2^u(x, t) \leq (t - p_1(x)) f^* \|N_{1,0}\|_{L^\infty(\Omega)}$$
$$\leq \|N_{2,0}\|_{L^\infty(\Omega)} + t f^* \|N_{1,0}\|_{L^\infty(\Omega)} \quad \forall t \in \mathcal{T}_1^+(x) \,.$$

   b) $N_2^u(x, t) < 0$ on the interval $(p_1(x), p_2(x))$, i.e. $(p_1(x), p_2(x)) = \mathcal{T}_1^-(x)$

       The same statements yield

$$|N_2^u(x, t)| \leq \|N_{2,0}\|_{L^\infty(\Omega)} + t f^* \|N_{1,0}\|_{L^\infty(\Omega)} \quad \forall t \in \mathcal{T}_1^-(x) \,.$$

With that for the first interval $\mathcal{T}_1^{\pm}(x)$ we achieved the desired estimate in both cases. Our aim now is to make the transition to the whole time interval $t \geq 0$. It obviously holds

$$|N_2^u(x,t)| = 0 \leq \|N_{2,0}\|_{L^\infty(\Omega)} + t f^* \|N_{1,0}\|_{L^\infty(\Omega)} \quad \forall t \in \mathcal{T}_z(x) \text{ and } \forall t \in \bigcup_{l \in L} p_l(x) \,.$$

By repeating the arguments of *Case 2* to the remaining intervals $[p_l(x), p_{l+1}(x))$ using $t - p_l(x) \leq t \; \forall t \in [p_l(x), p_{l+1}(x))$ and $N_2^u(x, p_l(x)) = 0$, with the partition of $[0, \infty)$ we finally obtain

$$\boxed{\|N_2^u(t)\|_{L^\infty(\Omega)} \leq \|N_{2,0}\|_{L^\infty(\Omega)} + t f^* \|N_{1,0}\|_{L^\infty(\Omega)} =: C_2(t) \quad \forall t \geq 0 \,.} \tag{3.15}$$

Step (ii): Consider the mapping $N^u \mapsto \hat{u}$

Now we are given the solutions N_1^u and N_2^u for fixed u and take a look at the solution of the corresponding PDE. That means we are focussing on the problem

$$\begin{aligned} \partial_t \hat{u} &= d_1 \Delta \hat{u} + d_2 g(\hat{u}) N_2^u \\ \hat{u}(x, 0) &= u_0(x) \\ \partial_\nu \hat{u}\big|_{\partial\Omega} &= 0 \,. \end{aligned} \tag{3.16}$$

In Condition 1 (iii) we require the function g to be Lipschitz continuous on $\mathbb{R}$. That can be easily expanded to Lipschitz continuity on $L^2(\Omega)$:

$$\begin{aligned} \|g(v_1) - g(v_2)\|_{L^2(\Omega)}^2 &= \int_\Omega |g(v_1(x)) - g(v_2(x))|^2 \, dx \leq L_g^2 \int_\Omega |v_1(x) - v_2(x)|^2 \, dx \\ &= L_g^2 \|v_1 - v_2\|_{L^2(\Omega)}^2 \,. \end{aligned}$$

From that and the properties of the solution N_2^u we are indeed dealing with a parabolic equation with Lipschitz type perturbation. Problems of this type are treated e.g. in [2], [13] or in a more abstract way in [9], [40]. There the existence and uniqueness of a solution $\hat{u}$ is shown and it is proved that the solution satisfies

$$\boxed{\begin{aligned} \hat{u} &\in C([0, T]; L^2(\Omega)) \\ \sqrt{t}\, \partial_t \hat{u} &\in L^2(0, T; L^2(\Omega)) \\ \sqrt{t}\, \Delta \hat{u} &\in L^2(0, T; L^2(\Omega)) \,. \end{aligned}} \tag{3.17}$$

The standard technique to show this kind of properties is introduced in Chapter 4 in the proof of Theorem 26.

By the property of the solution $\hat{u} \in X$ it follows $\mathcal{B} : X \to X$.

Step (iii): Consider the mapping $u \mapsto \mathcal{B}(u)$

This mapping maps u to the solution $\hat{u}$ of the PDE problem (3.16), which is dependent on the argument u via the term N_2^u. Our aim now is to find the specific solution $\hat{u} = u$ of (3.16) corresponding to N_2^u. That means we are searching for the fixed point

$$\mathcal{B}(u) = \hat{u} \overset{!}{=} u \,.$$

If we can show that this fixed point exists and is unique, then we can find the unique solution of the original problem (3.1) - (3.5) and the proof is finished. This is done by the famous contraction mapping theorem, which means we have to show the following:

$\exists\, T_0 > 0$ sufficiently small and $\exists\, \alpha \in (0,1)$ such that the mapping

$$\mathcal{B} : C([0,T_0]; L^2(\Omega)) =: X_0 \to X_0$$

is a contraction, i.e.

$$\|\mathcal{B}(u_1) - \mathcal{B}(u_2)\|_{X_0} \le \alpha \|u_1 - u_2\|_{X_0} \quad \forall u_1, u_2 \in X_0\,.$$

For that we calculate the difference between two solutions of the ODE problem (3.9), (3.10) and the PDE problem (3.16) corresponding to different fixed $u_1,\, u_2 \in X$:

① $\delta N_1 := N_1^{u_1} - N_1^{u_2}$, where

$$\begin{aligned}
\partial_t N_1^{u_1} &= -f(u_1) N_1^{u_1} & N_1^{u_1}(x,0) &= N_{1,0}(x) \\
\partial_t N_1^{u_2} &= -f(u_2) N_1^{u_2} & N_1^{u_2}(x,0) &= N_{1,0}(x)\,.
\end{aligned}$$

This yields $\delta N_1(x,0) = 0$ and

$$\begin{aligned}
\partial_t \delta N_1 &= -f(u_1) N_1^{u_1} + f(u_2) N_1^{u_2} \\
&= -f(u_1) N_1^{u_1} + f(u_1) N_1^{u_2} - f(u_1) N_1^{u_2} + f(u_2) N_1^{u_2} \\
&= -f(u_1) \delta N_1 + \big(f(u_2) - f(u_1)\big) N_1^{u_2}\,.
\end{aligned}$$

Multiplication by δN_1, integration over $\int_\Omega dx$ and using the Lipschitz continuity of f leads to

$$\int_\Omega \partial_t \delta N_1 \, \delta N_1 \, dx = -\int_\Omega f(u_1) |\delta N_1|^2 \, dx + \int_\Omega \big(f(u_2) - f(u_1)\big) N_1^{u_2} \delta N_1 \, dx$$

$$\Rightarrow \quad \frac{1}{2}\frac{d}{dt}\|\delta N_1\|_{L^2(\Omega)}^2 \le -\int_\Omega f(u_1) |\delta N_1|^2 \, dx + L_f \int_\Omega |u_2 - u_1| |N_1^{u_2}| |\delta N_1| \, dx\,.$$

With $\delta u := u_1 - u_2$, the non-negativity of f and the L^∞-estimate (3.14) it follows

$$\frac{1}{2}\frac{d}{dt}\|\delta N_1(t)\|_{L^2(\Omega)}^2 \le L_f C_1 \int_\Omega |\delta u(x,t)| |\delta N_1(x,t)| \, dx\,.$$

and by Hölder's inequality we obtain

$$\frac{d}{dt}\|\delta N_1(t)\|_{L^2(\Omega)} \|\delta N_1(t)\|_{L^2(\Omega)} \le L_f C_1 \|\delta u(t)\|_{L^2(\Omega)} \|\delta N_1(t)\|_{L^2(\Omega)}$$

$$\Rightarrow \quad \frac{d}{dt}\|\delta N_1(t)\|_{L^2(\Omega)} \le L_f C_1 \|\delta u(t)\|_{L^2(\Omega)}\,.$$

Integrating over $\int_0^t ds$ and using the fact $\delta N_1(0) = 0$, we are led to the final result

$$\boxed{\|\delta N_1(t)\|_{L^2(\Omega)} \le L_f C_1 \int_0^t \|\delta u(s)\|_{L^2(\Omega)} \, ds \quad \forall t \in [0,T]\,.} \tag{3.18}$$

② $\delta N_2 := N_2^{u_1} - N_2^{u_2}$, where $N_2^{u_1}$, $N_2^{u_2}$ solve

$$\partial_t N_2^{u_1} = f(u_1)N_1^{u_1} - g(u_1)N_2^{u_1} \qquad\qquad N_2^{u_1}(x,0) = N_{2,0}(x)$$
$$\partial_t N_2^{u_2} = f(u_2)N_1^{u_2} - g(u_2)N_2^{u_2} \qquad\qquad N_2^{u_2}(x,0) = N_{2,0}(x)\,.$$

Again we have $\delta N_2(x,0) = 0$ and

$$\partial_t \delta N_2 = f(u_1)N_1^{u_1} - f(u_2)N_1^{u_2} - g(u_1)N_2^{u_1} + g(u_2)N_2^{u_2}$$
$$= f(u_1)\delta N_1 + \big(f(u_1) - f(u_2)\big)N_1^{u_2} - g(u_1)\delta N_2 + \big(g(u_2) - g(u_1)\big)N_2^{u_2}\,.$$

Multiplying by δN_2 and integrating over $\int_\Omega dx$ using the boundedness of f and the non-negativity of g together with the Lipschitz continuity, we get

$$\frac{1}{2}\frac{d}{dt}\|\delta N_2\|^2_{L^2(\Omega)} \le f^* \int_\Omega |\delta N_1||\delta N_2|\,dx + L_f \int_\Omega |\delta u||N_1^{u_2}||\delta N_2|\,dx$$
$$+ L_g \int_\Omega |\delta u||N_2^{u_2}||\delta N_2|\,dx\,.$$

We are looking for local solutions and the existence of a time T_0 sufficiently small to assure contraction. Hence without loss of generality we can assume $t \le T \le 1$. Then by (3.15) we have the estimate

$$\|N_2^u(t)\|_{L^\infty(\Omega)} \le C_2(t) \le C_2(1) = \|N_{2,0}\|_{L^\infty(\Omega)} + f^*\|N_{1,0}\|_{L^\infty(\Omega)} =: C_2 < \infty\,. \qquad (3.19)$$

Application of Hölder's inequality, canceling out $\|\delta N_2(t)\|_{L^2(\Omega)}$ and using estimate (3.14) together with the previous result, we get

$$\frac{d}{dt}\|\delta N_2(t)\|_{L^2(\Omega)} \le f^*\|\delta N_1(t)\|_{L^2(\Omega)} + \underbrace{(L_f C_1 + L_g C_2)}_{=:C_{1,2}}\|\delta u(t)\|_{L^2(\Omega)}\,.$$

By substituting estimate (3.18), integrating over $\int_0^t ds$ and using $\delta N_2(0) = 0$ we obtain

$$\|\delta N_2(t)\|_{L^2(\Omega)} \le f^* L_f C_1 \int_0^t \int_0^s \|\delta u(\tau)\|_{L^2(\Omega)}\,d\tau\,ds + C_{1,2}\int_0^t \|\delta u(s)\|_{L^2(\Omega)}\,ds\,.$$

Due to the fact $t \in [0,T]$ with $T \le 1$ the double integral is estimated by

$$\int_0^t \int_0^s \|\delta u(\tau)\|_{L^2(\Omega)}\,d\tau\,ds \le \int_0^t \int_0^t \|\delta u(\tau)\|_{L^2(\Omega)}\,d\tau\,ds \le \int_0^t \|\delta u(s)\|_{L^2(\Omega)}\,ds\,.$$

This finally gives

$$\boxed{\|\delta N_2(t)\|_{L^2(\Omega)} \le \underbrace{(f^* L_f C_1 + C_{1,2})}_{=:C_3}\int_0^t \|\delta u(s)\|_{L^2(\Omega)}\,ds \quad \forall t \in [0,T]\,.} \qquad (3.20)$$

③ $\delta\hat{u} := \hat{u}_1 - \hat{u}_2 = \mathcal{B}(u_1) - \mathcal{B}(u_2)$, where $\hat{u}_1$, $\hat{u}_2$ are solutions of

$$\partial_t \hat{u}_1 = d_1\Delta\hat{u}_1 + d_2 g(\hat{u}_1)N_2^{u_1} \qquad \hat{u}_1(x,0) = u_0(x) \qquad \partial_\nu\hat{u}_1\big|_{\partial\Omega} = 0$$
$$\partial_t \hat{u}_2 = d_1\Delta\hat{u}_2 + d_2 g(\hat{u}_2)N_2^{u_2} \qquad \hat{u}_2(x,0) = u_0(x) \qquad \partial_\nu\hat{u}_2\big|_{\partial\Omega} = 0\,.$$

Remark

Our goal was to show that the mapping $\mathcal{B} : X_0 \to X_0$ is a contraction for an appropriate choice of the time interval $[0, T_0]$. By the definition of δu and $\delta \hat{u}$, $\mathcal{B}$ is a contraction if

$$\max_{0 \leq t \leq T_0} \|\delta \hat{u}(t)\|_{L^2(\Omega)} \leq \alpha \max_{0 \leq t \leq T_0} \|\delta u(t)\|_{L^2(\Omega)}, \quad 0 < \alpha < 1 \,.$$

It holds $\delta \hat{u}(x, 0) = 0$ and

$$\partial_t \delta \hat{u} = d_1 \Delta \delta \hat{u} + d_2 g(\hat{u}_1) N_2^{u_1} - d_2 g(\hat{u}_2) N_2^{u_2}$$
$$= d_1 \Delta \delta \hat{u} + d_2 g(\hat{u}_1) \delta N_2 + d_2 \big(g(\hat{u}_1) - g(\hat{u}_2) \big) N_2^{u_2} \,.$$

As before, multiplication by $\delta \hat{u}$, integration over $\int_\Omega dx$, application of Hölder's inequality and making use of estimate (3.19), $T \leq 1$ and the properties of g together with the Neumann boundary condition gives

$$\frac{1}{2} \frac{d}{dt} \|\delta \hat{u}(t)\|^2_{L^2(\Omega)} + d_1 \|\nabla \delta \hat{u}(t)\|^2_{L^2(\Omega)} \leq d_2 g^* \|\delta N_2(t)\|_{L^2(\Omega)} \|\delta \hat{u}(t)\|_{L^2(\Omega)} + d_2 L_g C_2 \|\delta \hat{u}(t)\|^2_{L^2(\Omega)}$$

$$\Rightarrow \quad \frac{d}{dt} \|\delta \hat{u}(t)\|_{L^2(\Omega)} \leq d_2 g^* \|\delta N_2(t)\|_{L^2(\Omega)} + d_2 L_g C_2 \|\delta \hat{u}(t)\|_{L^2(\Omega)} \,.$$

Substituting the previous result (3.20) and taking $\int_0^t ds$ with $\delta \hat{u}(0) = 0$, we have

$$\|\delta \hat{u}(t)\|_{L^2(\Omega)} \leq d_2 g^* C_3 \int_0^t \int_0^s \|\delta u(\tau)\|_{L^2(\Omega)} \, d\tau \, ds + d_2 L_g C_2 \int_0^t \|\delta \hat{u}(s)\|_{L^2(\Omega)} \, ds \,.$$

With the same argument as before, the double integral can be cancelled and we can further estimate by using Gronwall's inequality

$$\|\delta \hat{u}(t)\|_{L^2(\Omega)} \leq d_2 g^* C_3 \, T \max_{0 \leq t \leq T} \|\delta u(t)\|_{L^2(\Omega)} + d_2 L_g C_2 \int_0^t \|\delta \hat{u}(s)\|_{L^2(\Omega)} \, ds$$

$$\Rightarrow \quad \|\delta \hat{u}(t)\|_{L^2(\Omega)} \leq d_2 g^* C_3 \, T \|\delta u\|_X e^{d_2 L_g C_2 T} \quad \forall t \in [0, T] \,.$$

$$\Rightarrow \quad \|\delta \hat{u}\|_X \leq \underbrace{d_2 g^* C_3 \, T e^{d_2 L_g C_2 T}}_{=: \, C_4(T) > 0} \|\delta u\|_X \,.$$

From that it follows

$$\mathcal{B} \text{ is a contraction } \Leftrightarrow \exists T_0 > 0 \text{ such that } C_4(T_0) < 1 \,.$$

This is indeed the case since for $T \to 0$ we have $C_4(T) \to 0$, whence follows the existence of $T_0 = T_0 \big(\|N_{1,0}\|_{L^\infty(\Omega)}, \|N_{2,0}\|_{L^\infty(\Omega)} \big)$ with the required properties. Thus we showed

$$\mathcal{B} \text{ is a contraction on the space } X_0 = C([0, T_0], L^2(\Omega)) \,.$$

Now the contraction mapping theorem can be applied to $\mathcal{B}$ and yields

$$\boxed{\exists! \, u \in X_0 : \mathcal{B}(u) = u \,.}$$

As noted before, the unique fixed-point u is exactly the solution of the original problem and thus we have the existence and uniqueness of the local solution u. This solution satisfies (3.17) with $T = T_0$.

Furthermore the uniqueness of N_1 and N_2 in $[0, T_0]$ follows from (3.18) and (3.20) immediately, since by the uniqueness of u we have $\delta u = 0$. The conservation identity (3.8) provides the unique solution N_3. For $t \in [0, T_0]$ with $T_0 \leq 1$, estimates (3.14) and (3.19) induce

$$\left.\begin{array}{ll} \|N_1(t)\|_{L^\infty(\Omega)} \leq C_1 < \infty & \Rightarrow \quad \|N_1\|_{L^\infty(0,T_0;L^\infty(\Omega))} < \infty \\ \|N_2(t)\|_{L^\infty(\Omega)} \leq C_2 < \infty & \Rightarrow \quad \|N_2\|_{L^\infty(0,T_0;L^\infty(\Omega))} < \infty \end{array}\right\} \Rightarrow \|N_3\|_{L^\infty(0,T_0;L^\infty(\Omega))} < \infty\,.$$

This completes the proof of local existence and uniqueness.

$$\square\,\textbf{1.)}$$

2.) Global solution

Our next aim is to show that this local solution exists globally in time, i.e. not only on the time interval $[0, T_0]$ but on any bounded interval $[0, T]$ for all $T > 0$.

For that we come back to the definition of the function $C_4(T)$ determining the time T_0 such that $C_4(T_0) < 1$. For simplification this function can be further estimated by the definition of the appearing constants C_2 and C_3 and the fact $T_0 \leq 1$. Here we define

$$\begin{array}{lll} s := \|N_{1,0}\|_{L^\infty(\Omega)} + \|N_{2,0}\|_{L^\infty(\Omega)} & & > 0 \text{ by (3.7)} \\ a_1 := 2d_2 g^* \max\left(L_f + L_g f^* + L_f f^*, L_g\right) & & > 0 \\ a_2 := 2d_2 L_g \max\left(1, f^*\right) & & > 0 \end{array}$$

and it follows

$$C_4(T_0) \leq a_1 s\, T_0 e^{a_2 s T_0} \leq a_1 s\, T_0 e^{a_2 s} \overset{!}{<} 1\,,$$

i.e. then there exists $0 < \xi < 1$ such that

$$a_1 s\, T_0 e^{a_2 s} = \xi \quad \Leftrightarrow \quad T_0 = \frac{\xi}{a_1 s e^{a_2 s}} =: H(s) \geq 0\,. \tag{3.21}$$

More precisely, the function $H(s)$ is strictly monotonically decreasing due to

$$\tfrac{d}{ds} H(s) = -\xi \frac{a_1 e^{a_2 s} + a_1 a_2 s e^{a_2 s}}{(a_1 s e^{a_2 s})^2} < 0\,.$$

Up to this point, we obtained the existence of a unique solution (u, N_1, N_2, N_3) satisfying the properties of Theorem 1 on the time interval $[0, T_0]$. Thus we can define new initial conditions

$$u_0(x) = u(x, T_0)\,, \quad N_{1,0}(x) = N_1(x, T_0)\,, \quad N_{2,0}(x) = N_2(x, T_0)\,, \quad N_{3,0}(x) = N_3(x, T_0)$$

which satisfy

$$\|N_1(x, T_0)\|_{L^\infty(\Omega)} + \|N_2(x, T_0)\|_{L^\infty(\Omega)} \leq C_{T_0} < \infty\,.$$

Relation (3.21) implies that we have the existence of a positive time $T_0 > 0$ as long as s is bounded by some constant. This is the case here, whence follows the existence of a time T_1 such that the problem (3.1) - (3.4) with the new initial conditions possesses a unique local solution on $[T_0, T_1]$. With that we can extend the solution to the bigger interval $[0, T_1]$.

Hence, in order to assure the existence of the unique global solution, it suffices to show that

$$\sup_{0 \leq t \leq T} \left(\|N_1(t)\|_{L^\infty(\Omega)} + \|N_2(t)\|_{L^\infty(\Omega)} \right) \leq C_T < \infty$$

for any bounded intervall $[0, T]$, where the constant C_T is dependent on the time T. If we can show the boundedness of this expression, we can stepwise extend the existence interval of the local solution to any interval $[0, T]$ for all $T > 0$, which means that the solution exists globally in time.

In fact, proceeding in exactly the same way as in Step (i) of the local existence proof to show (3.14) and (3.15), we obtain the following estimates:

$$\|N_1(t)\|_{L^\infty(\Omega)} \leq \|N_{1,0}\|_{L^\infty(\Omega)} \qquad \text{for all } t \geq 0$$
$$\|N_2(t)\|_{L^\infty(\Omega)} \leq \|N_{2,0}\|_{L^\infty(\Omega)} + t f^* \|N_{1,0}\|_{L^\infty(\Omega)} \quad \text{for all } t \geq 0 \,.$$

This yields the desired result

$$\sup_{0 \leq t \leq T} \left(\|N_1(t)\|_{L^\infty(\Omega)} + \|N_2(t)\|_{L^\infty(\Omega)} \right) \leq \|N_{2,0}\|_{L^\infty(\Omega)} + (1 + T f^*) \|N_{1,0}\|_{L^\infty(\Omega)} =: C_T < \infty$$

which implies that the unique local solution can be continued globally.

$$\square \, \mathbf{2.)}$$

Theorem 2
Let all assumptions of Theorem 1 hold and in addition assume that

$$u_0 \geq 0, \quad N_{1,0} \geq 0, \quad N_{2,0} \geq 0, \quad N_{3,0} \geq 0 \,.$$

Then the solution (u, N_1, N_2, N_3) preserves non-negativity. Furthermore N_1, N_2 and N_3 are uniformly bounded in $\Omega \times [0, \infty)$.

Proof

1.) Non-negativity

The property of preserving non-negativity starting from non-negative initial values is proved with the standard technique to show that the negative part of the solution is zero. For a general function v the positive and negative part is defined by

$$v^+ := \max(v, 0) \geq 0, \quad v^- := \max(-v, 0) \geq 0 \quad \text{and with that} \quad v = v^+ - v^- \,.$$

That means for the preservation of non-negativity we have to show

$$v^-(\cdot, 0) \equiv 0 \quad \Rightarrow \quad v^-(\cdot, t) \equiv 0 \quad \forall t \geq 0 \,.$$

In order to apply this concept to functions from Sobolev spaces, we need the following lemma of Stampacchia.

Lemma 3 (Stampacchia)
Let $\Omega \subset \mathbb{R}^n$ be bounded, $v \in W^{1,p}(\Omega)$, $1 \le p \le \infty$. Then it holds $v^+, v^- \in W^{1,p}(\Omega)$ and

$$\nabla v^+(x) = \begin{cases} \nabla v(x) & \text{for } x \in \{x \in \Omega : v(x) > 0\} \\ 0 & \text{else} \end{cases}$$

$$\nabla v^-(x) = \begin{cases} -\nabla v(x) & \text{for } x \in \{x \in \Omega : v(x) < 0\} \\ 0 & \text{else} \end{cases}$$

in the sense of distributions.

A proof of this lemma can be found in [32].

Remark
An analogous result is not true for higher Sobolev spaces $W^{k,p}$ with $k > 1$.

For the integral over Ω it follows immediately

$$\int_\Omega v^+(x)v^-(x)\, dx = 0 \quad \text{and} \quad \int_\Omega \nabla u^+(x)\nabla u^-(x)\, dx = 0\,.$$

① $N_1(t) \ge 0$

By assumption we have $N_{1,0}(x) \ge 0$ and consequently $N_1^-(0) \equiv 0$. Multiplying (3.2)

$$\partial_t N_1 = -f(u)N_1$$

by N_1^-, using $N_1 = N_1^+ - N_1^-$ and integrating over $\int_\Omega dx$, we get with Condition 1 (i)

$$\frac{1}{2}\frac{d}{dt}\|N_1^-(t)\|_{L^2(\Omega)}^2 = -\int_\Omega f(u(t))|N_1^-(t)|^2\, dx \le 0\,,$$

which gives

$$\|N_1^-(t)\|_{L^2(\Omega)}^2 \le \|N_1^-(0)\|_{L^2(\Omega)}^2 = 0\,.$$

This implies $\|N_1^-(t)\|_{L^2(\Omega)} = 0 \ \forall t > 0$, i.e.

$$N_1^-(t) \equiv 0 \quad \forall t \ge 0 \quad \Leftrightarrow \quad N_1(t) \ge 0 \quad \forall t \ge 0\,.$$

② $N_2(t) \ge 0$

We have $N_2^-(0) \equiv 0$, $N_2 = N_2^+ - N_2^-$ and by the previous result $N_1 = N_1^+$. Multiplying the equation (3.3)

$$\partial_t N_2 = f(u)N_1 - g(u)N_2$$

by the negative part N_2^- and taking $\int_\Omega dx$, we have with Condition 1 (i)

$$\frac{1}{2}\frac{d}{dt}\|N_2^-(t)\|_{L^2(\Omega)}^2 = -\int_\Omega f(u(t))N_1^+(t)N_2^-(t)\, dx - \int_\Omega g(u(t))|N_2^-(t)|^2\, dx \le 0\,.$$

As before we obtain

$$N_2^-(t) \equiv 0 \quad \forall t \geq 0 \quad \Leftrightarrow \quad N_2(t) \geq 0 \quad \forall t \geq 0 \,.$$

③ $N_3(t) \geq 0$

With the same arguments making use of the result $N_2 = N_2^+$ we get

$$N_3^-(t) \equiv 0 \quad \forall t \geq 0 \quad \Leftrightarrow \quad N_3(t) \geq 0 \quad \forall t \geq 0 \,.$$

④ $u(t) \geq 0$

Multiplication of (3.1) by u^- and integration over $\int_\Omega dx$ yields

$$-\frac{1}{2}\frac{d}{dt}\|u^-(t)\|_{L^2(\Omega)}^2 = d_1 \int_\Omega \Delta u(t) u^-(t)\, dx + d_2 \int_\Omega g(u(t)) N_2(t) u^-(t)\, dx \,.$$

It holds due to Stampacchia's lemma

$$\int_\Omega \Delta u(t) u^-(t)\, dx = \int_{\partial\Omega} \nabla u(t) u^-(t)\, \vec{n}\, dS - \int_\Omega \nabla u(t) \nabla u^-(t)\, dx = \|\nabla u^-(t)\|_{L^2(\Omega)}^2 \quad (3.22)$$

and by using the fact $N_2 = N_2^+$, we obtain

$$\frac{1}{2}\frac{d}{dt}\|u^-(t)\|_{L^2(\Omega)}^2 = -d_1\|\nabla u^-(t)\|_{L^2(\Omega)}^2 - d_2 \int_\Omega g(u(t)) N_2^+(t) u^-(t)\, dx \leq 0 \,.$$

This implies in analogy to the cases before

$$u^-(t) \equiv 0 \quad \forall t \geq 0 \quad \Leftrightarrow \quad u(t) \geq 0 \quad \forall t \geq 0 \,.$$

<div align="right">□ 1.)</div>

2.) Uniform boundedness of (N_1, N_2, N_3)

From the conservation law

$$N_1(x,t) + N_2(x,t) + N_3(x,t) = N_{1,0}(x) + N_{2,0}(x) + N_{3,0}(x) = \overline{N}(x) \in L^\infty(\Omega) \quad (3.23)$$

for $x \in \Omega$, and the proved non-negativity of the ODE parts N_1, N_2 and N_3 it follows immediately

$$\boxed{0 \leq N_i(x,t) \leq \|\overline{N}\|_{L^\infty(\Omega)} \quad \forall t \geq 0\,, \forall x \in \Omega\,,\ i = 1,2,3\,.} \quad (3.24)$$

<div align="right">□ 2.)</div>

3.1.2 Asymptotic behavior of solutions

Now the longtime behavior of the solution (u, N_1, N_2, N_3) is studied. This behavior is highly dependent on the special structure of the model functions f and g.

Proposition 4

Let all assumptions of Theorems 1 and 2 hold and in addition assume $u_0 \not\equiv 0$.

Then the unique solution u is strictly positive for $t > 0$ and becomes bounded by below:

$$\exists\, t_0 > 0 \ \text{and} \ \exists\, \varrho > 0 : \quad u(x, t) \geq \varrho > 0 \quad \forall t \geq t_0 \quad \forall x \in \Omega.$$

Proof

The solution u fulfills the PDE problem

$$\partial_t u = d_1 \Delta u + d_2 g(u) N_2$$
$$u(x, 0) = u_0(x)$$
$$\partial_\nu u\big|_{\partial\Omega} = 0\,.$$

For the proof we introduce a subsolution $\underline{u}$ and show the relation

$$u(x, t) \geq \underline{u}(x, t) \geq \varrho > 0\,.$$

First we show that the subsolution $\underline{u}$ is given by the solution of the following auxiliary problem

$$\partial_t \underline{u} = d_1 \Delta \underline{u}$$
$$\underline{u}(x, 0) = u_0(x)$$
$$\partial_\nu \underline{u}\big|_{\partial\Omega} = 0\,.$$

By Condition 1 and Theorem 2 we have $g(u) \geq 0$, $N_2 \geq 0$. Thus it holds

$$\underbrace{\partial_t \underline{u} - d_1 \Delta \underline{u}}_{=\,0} - \underbrace{g(\underline{u})N_2}_{\geq\,0} \leq \underbrace{\partial_t u - d_1 \Delta u - g(u)N_2}_{=\,0}$$
$$\underline{u}(x, 0) = u(x, 0)$$
$$\partial_\nu \underline{u}\big|_{\partial\Omega} = \partial_\nu u\big|_{\partial\Omega}\,.$$

From the comparison principle it follows

$$\underline{u}(x, t) \leq u(x, t) \quad \forall (x, t) \in \Omega_T := \Omega \times (0, T]\,.$$

By $\partial\Omega_T$ we denote the parabolic boundary $\partial\Omega_T = (\{0\} \times \overline{\Omega}) \cup ([0, T] \times \partial\Omega)$.

The next step is to show that $\underline{u} > 0$. For that we consider the constant function $\underline{\underline{u}} \equiv 0$, which is a subsolution of the auxiliary problem due to the initial condition $\underline{u}(x, \overline{0}) = 0$. Thus we have

$$\underline{\underline{u}}(x, t) \leq \underline{u}(x, t) \quad \forall (x, t) \in \Omega_T\,.$$

We assume that there exists $y_0 := (x_0, t_0) \in \Omega_T \backslash \partial \Omega_T$ such that

$$\underline{\underline{u}}(y_0) = \underline{u}(y_0) \,.$$

That means there is an inner point y_0 at which the function $\underline{\underline{u}}$ attains its maximum. By the strong parabolic maximum principle this implies

$$\underline{\underline{u}} \equiv \underline{u} \text{ in } \overline{\Omega}_T \; \lightning$$

which is a contradiction to $\underline{u}(0) = u_0(x) \not\equiv 0 = \underline{\underline{u}}(0)$.
It follows: There is no inner point y_0 such that $\underline{\underline{u}}(y_0) = \underline{u}(y_0) = 0 \Rightarrow \underline{u} > 0$ in $\Omega_T \backslash \partial \Omega_T$.

Furthermore we can also show that $\underline{u}$ is positive on the boundary for all $t > 0$, i.e. on $\partial \Omega_T \backslash (\{0\} \times \Omega)$. We assume that there exists $y_1 := (x_1, t_1)$ with $x_1 \in \partial \Omega$ and $t_1 > 0$ such that

$$\underline{u}(y_1) = 0 \,.$$

Then by the properties of $\underline{u}$, Hopf's maximum principle (see e.g. [44], [56]) implies

$$\partial_\nu \underline{u}(y_1) \neq 0 \; \lightning$$

which is a contradiction to the homogeneous Neumann boundary condition $\partial_\nu \underline{u}(y_1) = 0$.
It follows: There is no point y_1 on the boundary with $\underline{u}(y_1) = 0 \Rightarrow \underline{u} > 0$ in $\partial \Omega_T \backslash (\{0\} \times \Omega)$.

All together it follows:

$$u(x, t) \geq \underline{u}(x, t) > 0 \text{ in } \Omega_T \,,$$

which means that u is proceeding instantaneously with infinite spreading speed.

It remains to show that u in fact is bounded below by some positive constant.
From $u(x, t) > 0 \; \forall (x, t) \in \Omega_T$ it follows

$$\exists\, t_0 > 0 \text{ and } \varrho > 0 \text{ such that } \min_{x \in \Omega} u(x, t_0) \geq \varrho > 0 \,.$$

We define the constant function $\underline{u}_\varrho \equiv \varrho$. Then by the choice of t_0 it holds

$$\partial_t \underline{u}_\varrho - d_1 \Delta \underline{u}_\varrho = \partial_t \underline{u} - d_1 \Delta \underline{u}$$
$$\underline{u}_\varrho(x, t_0) \leq \underline{u}(x, t_0)$$
$$\partial_\nu \underline{u}_\varrho \big|_{\partial \Omega} = \partial_\nu \underline{u} \big|_{\partial \Omega} \,.$$

Again applying the comparison principle we obtain

$$\underline{u}(x, t) \geq \underline{u}_\varrho \equiv \varrho \qquad \forall t \geq t_0 \quad \forall x \in \Omega \,.$$

Taking everything together yields the desired result

$$u(x, t) \geq \varrho > 0 \qquad \forall t \geq t_0 \quad \forall x \in \Omega \,.$$

<div align="right">□</div>

This result is now used to obtain information about the type of convergence as time goes to infinity. For that we need additional assumptions on the functions f and g.

Condition 2

Let the model functions $f : \mathbb{R} \to \mathbb{R}$ and $g : \mathbb{R} \to \mathbb{R}$ fulfill Condition 1. In addition we assume that there exist constants $C^- \geq 0$, $m_1 > 0$, $m_2 > 0$, $\delta > 0$ and $\varrho_0 > 0$ such that the following assertions hold:

(i) Starting threshold:

$$f(s) = 0 \quad \forall s \leq C^-$$
$$g(s) = 0 \quad \forall s \leq 0$$

(ii) Smoothness in $[C^-, C^- + \delta]$:

$$m_1(s - C^-) \leq f'(s) \leq m_2(s - C^-) \quad \forall s \in [C^-, C^- + \delta]$$

(iii) Lower bounds:

$$f(s) \geq f(C^- + \delta) > 0 \quad \forall s \geq C^- + \delta$$
$$g(s) \geq g(\varrho_0) > 0 \qquad \forall s \geq \varrho_0 > 0$$

(iv) Monotonicity in $[0, \varrho_0]$:

$$g'(s) > 0 \quad \forall s \in [0, \varrho_0]$$

In order to show several convergence results we need the following statement:

Proposition 5

Let $y(t)$ and $a(t)$ be non-negative functions with $y \in C^1([t_0, t_1])$ and $a \in C([t_0, t_1])$ for $0 \leq t_0 < t_1 \leq \infty$. If the inequality

$$\frac{d}{dt}y(t) + \gamma y(t) \leq a(t) \tag{3.25}$$

is satisfied with $\gamma \geq 0$, then for $t_0 \leq t \leq t_1$ it holds

$$y(t) \leq y(t_0)e^{-\gamma(t-t_0)} + \int_{t_0}^{t} a(s)e^{-\gamma(t-s)} \, ds \, .$$

Depending on the properties of $a(t)$, we can deduce further estimates:

(i) $a(t) \equiv C$ in $[t_0, t_1]$:

$$y(t) \leq y(t_0) + \frac{C}{\gamma}$$

(ii) $\int_{0}^{\infty} a(t) \, dt < \infty$:

$$y(t) \leq y(t_0)e^{-\gamma(t-t_0)} + \int_{t_0}^{\infty} a(t) \, dt$$

which implies $y(t) \xrightarrow{t \to \infty} 0$.

Proof

Multiplying (3.25) by $e^{\gamma t}$ yields

$$\frac{d}{dt}y(t)e^{\gamma t} + \gamma y(t)e^{\gamma t} = \frac{d}{dt}\left(y(t)e^{\gamma t}\right) \leq a(t)e^{\gamma t}$$

and by integration over $\int_{t_0}^t ds$ and multiplication with $e^{-\gamma t}$ we obtain

$$y(t) \leq y(t_0)e^{-\gamma(t-t_0)} + \int_{t_0}^t a(s)e^{-\gamma(t-s)}\,ds\,. \qquad (3.26)$$

In the first case (i) we can further estimate

$$\leq y(t_0)e^{-\gamma(t-t_0)} + \frac{C}{\gamma}\left(1 - e^{-\gamma(t-t_0)}\right)$$

$$\leq y(t_0) + \frac{C}{\gamma}\,.$$

In the second case (ii) the basic estimate (3.26) yields

$$y(t) \leq y(t_0)e^{-\gamma(t-t_0)} + \int_{t_0}^t a(s)\,ds \xrightarrow{t\to\infty} \int_{t_0}^{\infty} a(s)\,ds$$

for all $t_0 \geq 0$. From the assumption $\int_0^{\infty} a(t)\,dt < \infty$ it follows $\int_{t_0}^{\infty} a(s)\,ds \to 0$ for t_0 sufficiently large which implies $y(t) \xrightarrow{t\to\infty} 0$.

$\square$

The next theorem gives information about the strong convergence of the solution.

Theorem 6

Let Condition 2 hold. Under the assumptions of Theorem 2 we have the following strong convergence results:

$$
\begin{aligned}
N_1(x,t) &\xrightarrow{t\to\infty} N_1^{\infty}(x) \geq 0 & &\text{in } L^p(\Omega), \quad 1 \leq p < \infty \\
N_2(x,t) &\xrightarrow{t\to\infty} N_2^{\infty}(x) \equiv 0 & &\text{in } L^p(\Omega), \quad 1 \leq p < \infty \\
N_3(x,t) &\xrightarrow{t\to\infty} N_3^{\infty}(x) \leq \|\overline{N}\|_{L^{\infty}(\Omega)} & &\text{in } L^p(\Omega), \quad 1 \leq p < \infty \\
u(x,t) &\xrightarrow{t\to\infty} u^{\infty}(x) \equiv C & &\text{in } L^2(\Omega)\,.
\end{aligned}
$$

Proof

① $N_1(x,t) \to N_1^{\infty}(x)$

From the model equation (3.2), Condition 1 (i) and the non-negativity result it holds in the point-wise sense

$$\partial_t N_1(x,t) = -f\bigl(u(x,t)\bigr)N_1(x,t) \leq 0 \quad \forall t \geq 0 \quad \forall x \in \Omega\,.$$

Thus the sequence is non-increasing and bounded below by 0 which yields the convergence

$$N_1(x,t) \xrightarrow{t \to \infty} N_1^\infty(x) \geq 0 \quad \forall x \in \Omega \,.$$

From (3.24) we know $\sup_{x \in \Omega} N_1(x,t) \leq \|\overline{N}\|_{L^\infty(\Omega)} \; \forall t \geq 0$. Since $N_1(x,t)$ is non-increasing in t it follows

$$\sup_{x \in \Omega} N_1^\infty(x) \leq \sup_{x \in \Omega} N_1(x,t) \leq \|\overline{N}\|_{L^\infty(\Omega)} \,. \tag{3.27}$$

Furthermore we have

$$N_1(x,t) = |N_1(x,t)| \leq \overline{N}(x) \text{ where } \int_\Omega |\overline{N}(x)| \, dx \leq |\Omega| \|\overline{N}\|_{L^\infty(\Omega)} < \infty \,.$$

Thus the Lebesgue dominated convergence theorem can be applied and yields

$$\lim_{t \to \infty} \int_\Omega |N_1(x,t) - N_1^\infty(x)| \, dx = 0 \,,$$

i.e. we have strong convergence in $L^1(\Omega)$ to the unique limit $N_1^\infty(x)$. This result can be adapted to $L^p(\Omega)$, $1 \leq p < \infty$. We note

$$\int_\Omega |N_1(x,t) - N_1^\infty(x)|^p \, dx = \int_\Omega |N_1(x,t) - N_1^\infty(x)|^{p-1} |N_1(x,t) - N_1^\infty(x)| \, dx$$

$$\leq \sup_{x \in \Omega} |N_1(x,t) - N_1^\infty(x)|^{p-1} \int_\Omega |N_1(x,t) - N_1^\infty(x)| \, dx \,.$$

Applying Minkowski's inequality, we get

$$\leq 2^{p-2} \left(\sup_{x \in \Omega} |N_1(x,t)|^{p-1} + \sup_{x \in \Omega} |N_1^\infty(x)|^{p-1} \right) \int_\Omega |N_1(x,t) - N_1^\infty(x)| \, dx$$

$$\overset{(3.27)}{\leq} 2^{p-1} \underbrace{\|\overline{N}\|_{L^\infty(\Omega)}^{p-1}}_{< \infty} \underbrace{\int_\Omega |N_1(x,t) - N_1^\infty(x)| \, dx}_{\longrightarrow 0} \xrightarrow{t \to \infty} 0 \,.$$

This finally yields

$$\boxed{N_1(x,t) \xrightarrow{t \to \infty} N_1^\infty(x) \quad \text{strongly in } L^p(\Omega), \quad 1 \leq p < \infty \,.}$$

② $N_3(x,t) \to N_3^\infty(x)$

For $N_3(x,t)$ the model equation (3.4) gives

$$\partial_t N_3(x,t) = g\big(u(x,t)\big) N_2(x,t) \geq 0 \quad \forall t \geq 0 \quad \forall x \in \Omega \,.$$

Since $N_3(x,t)$ is bounded above by $\|\overline{N}\|_{L^\infty(\Omega)}$, the monotonicity yields almost everywhere convergence

$$N_3(x,t) \xrightarrow{t \to \infty} N_3^\infty(x) \leq \|\overline{N}\|_{L^\infty(\Omega)} \text{ for a.e. } x \in \Omega \,.$$

Analogously to ①, $|N_3(x, t)|$ is dominated by $\overline{N}(x)$ and $\sup_{x \in \Omega} N_3(x, t) \le \sup_{x \in \Omega} N_3^\infty(x) \le \|\overline{N}\|_{L^\infty(\Omega)}$. Thus we have the same convergence result

$$\boxed{N_3(x, t) \xrightarrow{t \to \infty} N_3^\infty(x) \quad \text{strongly in } L^p(\Omega), \quad 1 \le p < \infty.}$$

③ $N_2(x, t) \to N_2^\infty(x)$

Using (3.6) we obtain the almost everywhere convergence

$$
\begin{array}{ccccc}
N_2(x, t) & = & \overline{N}(x) & - \quad N_1(x, t) & - \quad N_3(x, t) \\
& & \downarrow t \to \infty & \downarrow t \to \infty & \downarrow t \to \infty \\
& & \overline{N}(x) & - \quad N_1^\infty(x) & - \quad N_3^\infty(x) \quad =: \quad N_2^\infty(x)
\end{array}
$$

and the convergence in $L^p(\Omega)$ follows immediately:

$$\int_\Omega |N_2(x, t) - N_2^\infty(x)|^p \, dx = \int_\Omega |N_1^\infty(x) - N_1(x, t) + N_3^\infty(x) - N_3(x, t)|^p \, dx$$

$$\le 2^{p-1} \Big(\underbrace{\int_\Omega |N_1(x, t) - N_1^\infty(x)|^p \, dx}_{\longrightarrow 0} + \underbrace{\int_\Omega |N_3(x, t) - N_3^\infty(x)|^p \, dx}_{\longrightarrow 0} \Big) \xrightarrow{t \to \infty} 0.$$

Thus we have

$$\boxed{N_2(x, t) \xrightarrow{t \to \infty} N_2^\infty(x) \quad \text{strongly in } L^p(\Omega), \quad 1 \le p < \infty.} \tag{3.28}$$

④ $u(x, t) \to u^\infty(x)$

In order to show the convergence properties of u we take a look at the eigenvalue problem

$$
\begin{aligned}
-\Delta \varphi_j(x) &= \lambda_j \varphi_j(x), \qquad x \in \Omega \\
\partial_\nu \varphi_j\big|_{\partial\Omega} &= 0.
\end{aligned}
\tag{3.29}
$$

It is well known that this eigenvalue problem with Neumann boundary conditions has the following properties:

(i) For the first eigenvalue and the corresponding eigenfunction it holds:

$$\lambda_1 = 0 \quad \text{and} \quad \varphi_1(x) \equiv C_\varphi.$$

(ii) The remaining eigenvalues satisfy

$$\lambda_2 > 0 \quad \text{and} \quad \lambda_i \to \infty \ \text{ as } \ i \to \infty$$

and the set of eigenfunctions $\{\varphi_i\}_{i \in \mathbb{N}}$, $\|\varphi_j\|_{L^2(\Omega)} = 1$ forms a complete orthonormal system in $L^2(\Omega)$.

Remark

We denote by $\lambda(\Omega) := |\Omega|$ the Lebesgue measure of the domain Ω.

From the normalizing condition $\|\varphi_1\|_{L^2(\Omega)} = 1$ it follows

$$\varphi_1 = C_\varphi = \lambda(\Omega)^{-1/2}. \tag{3.30}$$

The function $u(t) \in L^2(\Omega)$ can be projected onto the space spanned by eigenfunctions:

$$u(x,t) = \sum_{j=1}^{\infty} a_j(t)\varphi_j(x).$$

For the convergence result we work with the following orthogonal decomposition

$$\boxed{u(x,t) = a_1(t)\varphi_1(x) + \varphi^\perp(x,t)} \tag{3.31}$$

where the orthogonal complement $\varphi^\perp$ of $a_1(t)\varphi_1(x)$ is given by $\varphi^\perp(x,t) = \sum_{j=2}^{\infty} a_j(t)\varphi_j(x)$ due to the orthogonality of the eigenfunctions. By (3.29) $\varphi^\perp(x,t)$ also satisfies the zero Neumann boundary condition

$$\partial_\nu \varphi^\perp\big|_{\partial\Omega} = 0.$$

The Fourier coefficients are calculated by

$$a_j(t) = (u(t), \varphi_j)_{L^2(\Omega)}$$

and thus for the first coefficient $a_1(t)$ it holds

$$a_1(t) = (u(t), C_\varphi)_{L^2(\Omega)} = C_\varphi \int_\Omega u(x,t)\, dx \tag{3.32}$$

$$\frac{d}{dt}a_1(t) = C_\varphi \int_\Omega \partial_t u(x,t)\, dx.$$

Substituting this relation into PDE (3.1) gives

$$\frac{d}{dt}a_1(t) = C_\varphi \underbrace{\int_\Omega d_1 \Delta u(x,t)\, dx}_{=0} + d_2 C_\varphi \int_\Omega \underbrace{g(u(x,t))N_2(x,t)}_{\geq 0}\, dx \geq 0 \tag{3.33}$$

since

$$\int_\Omega d_1 \Delta u(x,t)\, dx = \int_{\partial\Omega} d_1 \nabla u(x,t) \cdot \nu\, dS - \int_\Omega \nabla d_1 \nabla u(x,t)\, dx = d_1 \int_{\partial\Omega} \partial_\nu u(x,t)\, dS = 0.$$

Thus the function $a_1(t)$ is non-decreasing. In order to show convergence, we need to find an upper bound. For that we interpret the previous equation in a different way using the relation $g(u(x,t))N_2(x,t) = \partial_t N_3(x,t)$:

$$\frac{d}{dt}a_1(t) = d_2 C_\varphi \frac{d}{dt}\int_\Omega N_3(x,t)\, dx.$$

Integration of this identity over $\int_0^t ds$ yields the term we have to estimate:

$$a_1(t) = a_1(0) + d_2 C_\varphi \left(\int_\Omega N_3(x,t)\, dx - \int_\Omega N_3(x,0)\, dx \right) .$$

From (3.24) we know that

$$N_3(x,t) = N_3(x,0) + \int_0^t \partial_s N_3(x,s)\, ds = N_{3,0}(x) + \int_0^t g(u(x,s)) N_2(x,s)\, ds \leq \|\overline{N}\|_{L^\infty(\Omega)} \tag{3.34}$$

and since $N_{3,0}(x) \geq 0$ we obtain

$$N_3(x,t) - N_{3,0}(x) \leq \|\overline{N}\|_{L^\infty(\Omega)}$$

$$\Rightarrow \quad \int_\Omega N_3(x,t)\, dx - \int_\Omega N_{3,0}(x)\, dx \leq \lambda(\Omega) \|\overline{N}\|_{L^\infty(\Omega)} < \infty .$$

The constant $a_1(0)$ is given by

$$a_1(0) = (u(0), C_\varphi)_{L^2(\Omega)} = C_\varphi \|u_0\|_{L^1(\Omega)} \leq C_\varphi \lambda(\Omega)^{1/2} \|u_0\|_{L^2(\Omega)} < \infty .$$

All together we obtain

$$a_1(t) \leq C_\varphi \lambda(\Omega)^{1/2} \|u_0\|_{L^2(\Omega)} + d_2 C_\varphi \lambda(\Omega) \|\overline{N}\|_{L^\infty(\Omega)} =: C_{a_1} < \infty ,$$

which yields the existence of the limit $a_1^\infty \leq C_{a_1}$ such that

$$\boxed{a_1(t) \xrightarrow{\ t \to \infty\ } a_1^\infty .} \tag{3.35}$$

In order to show that u converges to a constant function, it is thus sufficient to show that $\varphi^\perp(t,x) \to 0$ as $t \to \infty$ for a.e. $x \in \Omega$.

For this purpose, we need to derive the boundedness of $\|N_2\|_{L^1(0,\infty;L^1(\Omega))}$: From (3.34), Proposition 4 and Condition 2 (iii), (iv) it holds

$$\lambda(\Omega) \|\overline{N}\|_{L^\infty(\Omega)} \geq \int_\Omega \int_0^t g(u(x,s)) N_2(x,s)\, ds\, dx \geq g(\overline{\varrho}) \int_\Omega \int_0^t N_2(x,s)\, ds\, dx ,$$

where $\overline{\varrho} := \min(\varrho, \varrho_0) > 0$.

Permuting the integration order we obtain a non-decreasing sequence

$$F(t) := \int_0^t \|N_2(s)\|_{L^1(\Omega)}\, ds \leq \frac{\lambda(\Omega)}{g(\overline{\varrho})} \|\overline{N}\|_{L^\infty(\Omega)}$$

which is bounded for every $t \geq 0$ and thus converging to $F(\infty) \leq \frac{\lambda(\Omega)}{g(\overline{\varrho})} \|\overline{N}\|_{L^\infty(\Omega)}$:

$$\lim_{t \to \infty} F(t) = \int_0^\infty \|N_2(t)\|_{L^1(\Omega)}\, dt = \|N_2\|_{L^1(0,\infty;L^1(\Omega))} \leq \frac{\lambda(\Omega)}{g(\overline{\varrho})} \|\overline{N}\|_{L^\infty(\Omega)} . \tag{3.36}$$

This estimate also gives a characterization of $N_2^\infty(x)$ since the convergence of the integral over the non-negative integrand $\int_0^\infty \|N_2(t)\|_{L^1(\Omega)}\,dt$ implies the existence of a sequence $\{t_k\}_{k\in\mathbb{N}}$ with $t_k \to \infty$ such that

$$\lim_{k\to\infty} \|N_2(t_k)\|_{L^1(\Omega)} = 0\,.$$

From (3.28) and the uniqueness of the strong limit it follows

$$\lim_{k\to\infty} \int_\Omega N_2(x,t_k)\,dx = \int_\Omega N_2^\infty(x)\,dx = 0 = \int_\Omega 0\,dx\,,$$

i.e. $N_2(x,t) \to 0$ in $L^1(\Omega)$ and by the arguments we used earlier we have

$$\boxed{N_2(x,t) \xrightarrow{\ t\to\infty\ } 0 \quad \text{strongly in } L^p(\Omega), \quad 1 \le p < \infty\,.}$$

Furthermore $\int_\Omega N_2^\infty(x)\,dx = 0$ implies

$$\boxed{N_2^\infty(x) \equiv 0 \ \text{ for a.e. } x \in \Omega\,.}$$

Now we return to the decomposition of u and our aim is to show

$$a_1(t)\varphi_1(x) + \varphi^\perp(x,t) = u(x,t) \xrightarrow{\ t\to\infty\ } u^\infty \equiv a_1^\infty C_\varphi \ \text{ in } L^2(\Omega)\,.$$

For this aim we use the following lemma:

Lemma 7 (Wirtinger's inequality)
Let $v \in H^1(\Omega)$ with zero mean value

$$\int_\Omega v\,dx = 0\,.$$

Then there exists a constant $C_W > 0$ such that the following estimate holds:

$$\|v\|_{L^2(\Omega)} \le C_W \|\nabla v\|_{L^2(\Omega)}\,.$$

A proof of that inequality can be found in [10]. Under some condition we can further estimate:

Corollary 8
Let $v \in H^2(\Omega)$ satisfy the conditions of Lemma 7 and in addition assume

$$\|\nabla v\|_{L^2(\Omega)}^2 = (-\Delta v, v)_{L^2(\Omega)}\,. \tag{3.37}$$

Then it holds with the same constant $C_W > 0$

$$\|v\|_{L^2(\Omega)} \le C_W \|\nabla v\|_{L^2(\Omega)} \le C_W^2 \|\Delta v\|_{L^2(\Omega)}\,.$$

Proof

Due to Cauchy-Schwarz and Wirtinger's inequality it follows immediately

$$(-\Delta v, v)_{L^2(\Omega)} = \|\nabla v\|^2_{L^2(\Omega)} \leq \|\Delta v\|_{L^2(\Omega)} \|v\|_{L^2(\Omega)} \leq C_W \|\Delta v\|_{L^2(\Omega)} \|\nabla v\|_{L^2(\Omega)}$$

and consequently

$$\|\nabla v\|_{L^2(\Omega)} \leq C_W \|\Delta v\|_{L^2(\Omega)}.$$

$\square$

Remark

Condition (3.37) is not very restrictive. If v satisfies homogeneous Dirichlet or Neumann boundary conditions, it follows

$$(-\Delta v, v)_{L^2(\Omega)} = \int_\Omega -\Delta v \, v \, dx = -\underbrace{\int_{\partial\Omega} \nabla v \, v \, \vec{n} \, dS}_{=0} + \int_\Omega \nabla v \, \nabla v \, dx = \|\nabla v\|^2_{L^2(\Omega)}.$$

The orthogonal complement $\varphi^\perp$ fulfills by definition

$$\left(\varphi^\perp(t), \varphi_1\right)_{L^2(\Omega)} = C_\varphi \int_\Omega \varphi^\perp(x, t) = 0$$

and thus Wirtinger's inequality can be applied to $\varphi^\perp(t)$:

$$\|\varphi^\perp(t)\|_{L^2(\Omega)} \leq C_W \|\nabla \varphi^\perp(t)\|_{L^2(\Omega)}.$$

Substitution of the decomposition into the PDE (3.1) gives

$$\partial_t \left(a_1(t)\varphi_1(x) + \varphi^\perp(x, t)\right) = d_1 \Delta \left(a_1(t)\varphi_1(x) + \varphi^\perp(x, t)\right) + d_2 g(u(x,t))N_2(x,t),$$

which leads to

$$\frac{d}{dt}a_1(t)\varphi_1 + \partial_t\varphi^\perp(x,t) = d_1\Delta\varphi^\perp(x,t) + d_2 g(u(x,t))N_2(x,t) \qquad (3.38)$$

due to the fact $\varphi_1(x) \equiv C_\varphi$. Multiplying that equation by $\varphi^\perp$, integrating over $\int_\Omega dx$ and using the orthogonality, we get

$$\frac{d}{dt}a_1(t) \underbrace{\int_\Omega \varphi_1 \, \varphi^\perp(x,t) \, dx}_{=0} + \frac{1}{2}\frac{d}{dt}\|\varphi^\perp(t)\|^2_{L^2(\Omega)}$$

$$= -d_1\|\nabla\varphi^\perp(t)\|^2_{L^2(\Omega)} + d_2\int_\Omega g(u(x,t))N_2(x,t)\varphi^\perp(x,t)\,dx,$$

i.e.

$$\frac{1}{2}\frac{d}{dt}\|\varphi^\perp(t)\|^2_{L^2(\Omega)} + d_1\|\nabla\varphi^\perp(t)\|^2_{L^2(\Omega)} = d_2\int_\Omega g(u(x,t))N_2(x,t)\varphi^\perp(x,t)\,dx. \qquad (3.39)$$

Applying Wirtinger's and Hölder's inequality we have

$$\frac{1}{2}\frac{d}{dt}\|\varphi^\perp(t)\|_{L^2(\Omega)}^2 + \frac{d_1}{C_W{}^2}\|\varphi^\perp(t)\|_{L^2(\Omega)}^2 \leq d_2\|g(u(t))N_2(t)\|_{L^2(\Omega)}\|\varphi^\perp(t)\|_{L^2(\Omega)}$$

and Young's inequality with $\varepsilon = \frac{d_1}{d_2 C_W^2}$ gives

$$\frac{d}{dt}\|\varphi^\perp(t)\|_{L^2(\Omega)}^2 + \underbrace{\frac{d_1}{C_W{}^2}}_{=:\,\gamma\,>\,0}\|\varphi^\perp(t)\|_{L^2(\Omega)}^2 \leq \underbrace{\frac{d_2{}^2 C_W{}^2}{d_1}}_{=:\,C_5\,>\,0}\|g(u(t))N_2(t)\|_{L^2(\Omega)}^2\,. \tag{3.40}$$

Remark

By the term "applying Young's inequality with ε" we mean that we solve the following scenario:

<u>Aim</u>: For a given expression kAB with numbers $k > 0$, $A, B \geq 0$ and a given target constant $C_t > 0$, find a constant $\varepsilon > 0$ such that

$$kAB = k\sqrt{\varepsilon}A\frac{1}{\sqrt{\varepsilon}}B \leq k\left(\frac{\varepsilon}{2}A^2 + \frac{1}{2\varepsilon}B^2\right) \overset{!}{=} C_t A^2 + C_\varepsilon B^2\,.$$

This implies

$$k\frac{\varepsilon}{2} \overset{!}{=} C_t \quad \Leftrightarrow \quad \varepsilon = \frac{2C_t}{k} \quad \Rightarrow \quad C_\varepsilon = \frac{k}{2\varepsilon} = \frac{k^2}{4C_t}\,.$$

Put

$$y(t) := \quad \|\varphi^\perp(t)\|_{L^2(\Omega)}^2$$
$$a(t) := C_5\|g(u(t))N_2(t)\|_{L^2(\Omega)}^2\,,$$

then our aim is to show $y(t) \to 0$ by use of Proposition 5. Here the estimate of $\|N_2\|_{L^1(0,\infty;L^1(\Omega))}$ comes into play: From (3.36) and Condition 1 (ii) it follows

$$\int_0^\infty a(t)\,dt = C_5 \int_0^\infty \int_\Omega |g(u(x,t))N_2(x,t)|^2\,dx\,dt$$
$$\leq g^{*2}\|\overline{N}\|_{L^\infty(\Omega)}C_5 \int_0^\infty \int_\Omega |N_2(x,t)|\,dx\,dt$$
$$= g^{*2}\|\overline{N}\|_{L^\infty(\Omega)}C_5\|N_2\|_{L^1(0,\infty;L^1(\Omega))} \leq C_5\lambda(\Omega)\frac{g^{*2}}{g(\overline{\varrho})}\|\overline{N}\|_{L^\infty(\Omega)}^2 =: C_6 < \infty\,. \tag{3.41}$$

Remark

From that it also follows $\|N_2\|_{L^2(0,\infty;L^2(\Omega))} < \infty$:

By the definition of $\overline{\varrho} > 0$ we know $g(u(x,t)) \geq g(\overline{\varrho}) > 0$ which leads to

$$C_5 g(\overline{\varrho})^2\|N_2\|_{L^2(0,\infty;L^2(\Omega))}^2 \leq \int_0^\infty a(t)\,dt \leq C_6\,.$$

Hence the assumptions of Proposition 5 are fulfilled and we can conclude

$$y(t) = \|\varphi^\perp(t)\|^2_{L^2(\Omega)} \xrightarrow{t\to\infty} 0.$$

This yields

$$\boxed{\varphi^\perp(x,t) \xrightarrow{t\to\infty} 0 \quad \text{strongly in } L^2(\Omega).}$$

Together with the convergence result (3.35) of $a_1(t)$, this gives the almost everywhere convergence result for $u(x,t)$:

$$
\begin{array}{ccccc}
u(x,t) & = & a_1(t)\varphi(x) & + & \varphi^\perp(x,t) \\
 & & \downarrow t\to\infty & & \downarrow t\to\infty \\
 & & a_1^\infty C_\varphi & + & 0 \qquad := u^\infty
\end{array}
$$

and we have

$$\boxed{u(x,t) \xrightarrow{t\to\infty} u^\infty(x) \equiv a_1^\infty C_\varphi \quad \text{strongly in } L^2(\Omega).}$$

This completes the proof.

$\square$

Further estimates

Up to now we have the following convergence results:

$$
\boxed{
\begin{array}{llll}
N_1(x,t) & \xrightarrow{t\to\infty} N_1^\infty(x) & \text{in } L^p(\Omega), & 1 \le p < \infty \\[4pt]
N_2(x,t) & \xrightarrow{t\to\infty} 0 & \text{in } L^p(\Omega), & 1 \le p < \infty \\[4pt]
N_3(x,t) & \xrightarrow{t\to\infty} N_3^\infty(x) & \text{in } L^p(\Omega), & 1 \le p < \infty \\[4pt]
u(x,t) & \xrightarrow{t\to\infty} a_1^\infty C_\varphi & \text{in } L^2(\Omega) \\[4pt]
\varphi^\perp(x,t) & \xrightarrow{t\to\infty} 0 & \text{in } L^2(\Omega)
\end{array}
}
$$

Corollary 9
Under the assumptions of Theorem 6 the following additional facts hold:
We have the convergence

$$\nabla\varphi^\perp(x,t) = \nabla u(x,t) \xrightarrow{t\to\infty} 0 \ \text{in } L^2(\Omega) \tag{3.42}$$

and the following expressions are bounded:

$$
\begin{aligned}
&\sup_{t>0} \ \|u(t)\|_{L^1(\Omega)} < \infty \\
&\sup_{t>0} \ \|u(t)\|_{L^2(\Omega)} < \infty \\
&\sup_{t\ge\delta} \|\nabla u(t)\|_{L^2(\Omega)} < \infty \quad \textit{for } \delta > 0 \\
&\sup_{t>0} \|\varphi^\perp(t)\|_{L^2(\Omega)} < \infty \\
&\int_0^T \|\nabla u(t)\|^2_{L^2(\Omega)} \, dt < \infty.
\end{aligned}
\tag{3.43}
$$

Furthermore the following integrals converge, where (3.45) only holds if we make the additional assumption $u_0 \in H^1(\Omega)$

$$\int_0^\infty \|\nabla\varphi^\perp(t)\|_{L^2(\Omega)}^2 \, dt < \infty \tag{3.44}$$

$$\int_0^\infty \|\Delta\varphi^\perp(t)\|_{L^2(\Omega)}^2 \, dt < \infty \quad \textit{if } u_0 \in H^1(\Omega) \, . \tag{3.45}$$

Proof

The first result is obtained in analogy to the previous case $\varphi^\perp(x,t) \to 0$. For that we use again equation (3.38) in terms of the decomposition of u, multiply by $-\Delta\varphi^\perp$ and integrate over $\int_\Omega dx$. From the zero Neumann boundary condition it follows

$$(-\Delta\varphi^\perp(t), \varphi_1)_{L^2(\Omega)} = (-\Delta\varphi^\perp(t), C_\varphi)_{L^2(\Omega)} = 0$$

and we have

$$\frac{1}{2}\frac{d}{dt}\|\nabla\varphi^\perp(t)\|_{L^2(\Omega)}^2 + d_1\|\Delta\varphi^\perp(t)\|_{L^2(\Omega)}^2 = -d_2 \int_\Omega g(u(x,t))N_2(x,t)\Delta\varphi^\perp(x,t) \, dx$$

$$\leq d_2\|g(u(t))N_2(t)\|_{L^2(\Omega)}\|\Delta\varphi^\perp(t)\|_{L^2(\Omega)} \, . \tag{3.46}$$

Young's inequality with $\varepsilon = \frac{d_1}{d_2}$ yields

$$\frac{d}{dt}\|\nabla\varphi^\perp(t)\|_{L^2(\Omega)}^2 + d_1\|\Delta\varphi^\perp(t)\|_{L^2(\Omega)}^2 \leq \frac{d_2^2}{d_1}\|g(u(t))N_2(t)\|_{L^2(\Omega)}^2 \tag{3.47}$$

and by use of Corollary 8 we get

$$\frac{d}{dt}\|\nabla\varphi^\perp(t)\|_{L^2(\Omega)}^2 + \frac{d_1}{C_W{}^2}\|\nabla\varphi^\perp(t)\|_{L^2(\Omega)}^2 \leq \frac{d_2^2}{d_1}\|g(u(t))N_2(t)\|_{L^2(\Omega)}^2 \, . \tag{3.48}$$

As before, we set

$$y(t) := \|\nabla\varphi^\perp(t)\|_{L^2(\Omega)}^2$$

$$a(t) := \frac{d_2^2}{d_1}\|g(u(t))N_2(t)\|_{L^2(\Omega)}^2 \, .$$

From the differential inequality

$$\frac{d}{dt}y(t) + \gamma y(t) \leq a(t)$$

with the same constant $\gamma = \frac{d_1}{C_W{}^2} > 0$ and the same arguments as in the previous case $\varphi^\perp(x,t) \to 0$, by Proposition 5 it follows

$$y(t) = \|\nabla\varphi^\perp(t)\|_{L^2(\Omega)}^2 \xrightarrow{t\to\infty} 0 \, .$$

This yields

$$\boxed{\nabla\varphi^\perp(x,t) \xrightarrow{t\to\infty} 0 \quad \text{strongly in } L^2(\Omega).}$$

Now we want to analyze the solution u in terms of the supremum norm over the time interval $(0,\infty]$. Integrating the PDE

$$\partial_t u = d_1 \Delta u + d_2 g(u) N_2 \qquad (3.49)$$

over $\int_\Omega dx$, we obtain due to the boundary condition

$$\frac{d}{dt}\|u(t)\|_{L^1(\Omega)} = d_2 \int_\Omega g(u(x,t)) N_2(x,t)\,dx = d_2 \frac{d}{dt}\|N_3(t)\|_{L^1(\Omega)} \geq 0$$

and thus the sequence $\|u(t)\|_{L^1(\Omega)}$ is monotonically increasing. Furthermore it is bounded for every $t > 0$, which is shown by integration over $\int_0^t ds$:

$$\|u(t)\|_{L^1(\Omega)} = \|u_0\|_{L^1(\Omega)} - d_2\|N_{3,0}\|_{L^\infty(\Omega)} + d_2\|N_3(t)\|_{L^1(\Omega)}$$
$$\leq \|u_0\|_{L^1(\Omega)} - d_2\|N_{3,0}\|_{L^\infty(\Omega)} + \lambda(\Omega)\|\overline{N}\|_{L^\infty(\Omega)} =: C_7 < \infty.$$

This yields

$$\boxed{\sup_{t>0}\|u(t)\|_{L^1(\Omega)} \leq C_7.}$$

This result is now used to give an upper bound for $\|u(t)\|_{L^2(\Omega)}$.

Multiplying (3.49) by u and integrating over $\int_\Omega dx$, we obtain

$$\frac{1}{2}\frac{d}{dt}\|u(t)\|_{L^2(\Omega)}^2 + d_1\|\nabla u(t)\|_{L^2(\Omega)}^2 \leq d_2 g^*\|\overline{N}\|_{L^\infty(\Omega)}\|u(t)\|_{L^1(\Omega)}$$
$$\leq d_2 g^*\|\overline{N}\|_{L^\infty(\Omega)} \sup_{t>0}\|u(t)\|_{L^1(\Omega)} =: C_8 < \infty. \qquad (3.50)$$

By the non-negativity of the norm we can deduce $\frac{d}{dt}\|u(t)\|_{L^2(\Omega)} < \infty$. Together with the property $u \in C([0,T];L^2(\Omega))$ and the convergence $\|u(t)\|_{L^2(\Omega)} \to \|u^\infty\|_{L^2(\Omega)}$, this gives

$$\boxed{\sup_{t>0}\|u(t)\|_{L^2(\Omega)} < \infty.}$$

In order to obtain a similar result for ∇u, we first have to show the boundedness of $\int_0^T \|\nabla u(t)\|_{L^2(\Omega)}^2\,dt$. Integrating estimate (3.50) over $\int_0^T dt$, we get

$$\frac{1}{2}\|u(T)\|_{L^2(\Omega)}^2 + d_1\int_0^T \|\nabla u(t)\|_{L^2(\Omega)}^2\,dt \leq \frac{1}{2}\|u_0\|_{L^2(\Omega)}^2 + C_8 T =: C_9,$$

which is a bounded expression due to the initial condition $u_0 \in L^2(\Omega)$ and yields

$$\boxed{\int_0^T \|\nabla u(t)\|_{L^2(\Omega)}^2\,dt \leq \frac{1}{d_1}C_9.} \qquad (3.51)$$

By the orthogonal decomposition (3.31) with $\varphi_1 \equiv C_\varphi$, we know $\nabla \varphi^\perp = \nabla u$ and thus (3.48) also reads with Condition 1 (ii) and (3.24)

$$\frac{d}{dt}\|\nabla u(t)\|_{L^2(\Omega)}^2 + \frac{d_1}{C_W{}^2}\|\nabla u(t)\|_{L^2(\Omega)}^2 \leq \frac{d_2{}^2}{d_1}g^{*2}\|\overline{N}\|_{L^\infty(\Omega)}^2\lambda(\Omega) =: C_{10}\,.$$

Again we set $y(t) := \|\nabla u(t)\|_{L^2(\Omega)}^2$ and apply Proposition 5 with $\gamma = \frac{d_1}{C_W^2}$ and constant right hand side $C = C_{10}$. This gives

$$\|\nabla u(t)\|_{L^2(\Omega)}^2 \leq \|\nabla u(\delta)\|_{L^2(\Omega)}^2 + \frac{C_{10}}{\gamma} \quad \text{for } t \geq \delta\,, \tag{3.52}$$

i.e. for the boundedness we need $\|\nabla u(\delta)\|_{L^2(\Omega)} < \infty$.

At this we know $\delta > 0$ since we only have initial data from $L^2(\Omega)$. However, from estimate (3.51) we can deduce the existence of a time $\delta \in (0, T]$ such that $\|\nabla u(\delta)\|_{L^2(\Omega)} < \infty$ and thus it follows for a suitable constant $C_{11} < \infty$

$$\boxed{\sup_{t \geq \delta}\|\nabla u(t)\|_{L^2(\Omega)} \leq C_{11}\,.} \tag{3.53}$$

Remark

1) Since $\nabla u = \nabla \varphi^\perp$, we also have

$$\sup_{t \geq \delta}\|\nabla \varphi^\perp(t)\|_{L^2(\Omega)} \leq C_{11}\,.$$

2) If we assume $u_0 \in H^1(\Omega)$, then (3.52) also holds for $\delta = 0$, i.e. in that case we have

$$\boxed{\sup_{t > 0}\|\nabla u(t)\|_{L^2(\Omega)} \leq C_{12}} \tag{3.54}$$

with $C_{12} := \left(\|\nabla u_0\|_{L^2(\Omega)}^2 + \frac{C_{10}}{\gamma}\right)^{\frac{1}{2}} < \infty$.

Our next aim is to estimate $\sup_{t>0}\|\varphi^\perp(t)\|_{L^2(\Omega)}$. This is done by use of inequality (3.40), which yields after integration $\int_0^t ds$

$$\|\varphi^\perp(t)\|_{L^2(\Omega)}^2 \leq \|\varphi^\perp(0)\|_{L^2(\Omega)}^2 + C_5 \int_0^t \|g(u(s))N_2(s)\|_{L^2(\Omega)}^2\,ds$$

$$\leq \|\varphi^\perp(0)\|_{L^2(\Omega)}^2 + C_5 \int_0^\infty \|g(u(s))N_2(s)\|_{L^2(\Omega)}^2\,ds\,.$$

From (3.77) we know that the integral is bounded and thus we only need $\varphi^\perp(0) \in L^2(\Omega)$.

This follows from the orthogonal representation of $u_0 \in L^2(\Omega)$

$$u_0 = \sum_{j=1}^{\infty} a_j(0)\varphi_j = \sum_{j=1}^{\infty} (u_0, \varphi_j)_{L^2(\Omega)}\varphi_j$$

$$\Rightarrow \quad \varphi^\perp(0) = \sum_{j=2}^{\infty} (u_0, \varphi_j)_{L^2(\Omega)}\varphi_j = u_0 - (u_0, C_\varphi)_{L^2(\Omega)}C_\varphi$$

$$\Rightarrow \quad \|\varphi^\perp(0)\|_{L^2(\Omega)} \leq \|u_0\|_{L^2(\Omega)} + |(u_0, C_\varphi)_{L^2(\Omega)}| \|C_\varphi\|_{L^2(\Omega)}$$
$$\leq \|u_0\|_{L^2(\Omega)}^2 + \|u_0\|_{L^2(\Omega)} \underbrace{\|C_\varphi\|_{L^2(\Omega)}}_{=1} \|C_\varphi\|_{L^2(\Omega)} = 2\|u_0\|_{L^2(\Omega)} < \infty \,.$$

$$(3.55)$$

In summary this gives

$$\boxed{\sup_{t>0} \|\varphi^\perp(t)\|_{L^2(\Omega)} < \infty \,.}$$

The next estimate is obtained from inequality (3.39). Application of Hölder's, Wirtinger's and Young's inequality with $\varepsilon = \frac{d_1}{d_2 C_W}$ yields

$$\frac{1}{2}\frac{d}{dt}\|\varphi^\perp(t)\|_{L^2(\Omega)}^2 + \frac{d_1}{2}\|\nabla\varphi^\perp(t)\|_{L^2(\Omega)}^2 \leq \frac{d_2{}^2 C_W{}^2}{2d_1}\|g(u(t))N_2(t)\|_{L^2(\Omega)}^2 \,.$$

Integration over $\int_0^t ds$ and omitting the positive term $\|\varphi^\perp(t)\|_{L^2(\Omega)}^2$ gives

$$d_1 \int_0^t \|\nabla\varphi^\perp(s)\|_{L^2(\Omega)}^2 \, ds \leq \|\varphi^\perp(0)\|_{L^2(\Omega)}^2 + \frac{d_2{}^2 C_W{}^2}{d_1} \int_0^t \|g(u(s))N_2(s)\|_{L^2(\Omega)}^2 \, ds \,.$$

This holds true for every $t > 0$, whence follows with (3.77) and (3.55)

$$\int_0^\infty \|\nabla\varphi^\perp(t)\|_{L^2(\Omega)}^2 \, dt \leq \frac{1}{d_1}\|\varphi^\perp(0)\|_{L^2(\Omega)}^2 + \frac{d_2{}^2 C_W{}^2}{d_1{}^2} \int_0^\infty \|g(u(t))N_2(t)\|_{L^2(\Omega)}^2 \, dt$$
$$\leq \frac{2}{d_1}\|u_0\|_{L^2(\Omega)}^2 + \frac{d_2{}^2 C_W{}^2}{d_1{}^2}\lambda(\Omega)\frac{g^{*2}}{g(\overline{\varrho})}\|\overline{N}\|_{L^\infty(\Omega)}^2 =: C_{13} < \infty \,.$$

Thus we have

$$\boxed{\int_0^\infty \|\nabla\varphi^\perp(t)\|_{L^2(\Omega)}^2 \, dt \leq C_{13} \,.}$$

In an analogous way we now want to show the same result for $\Delta\varphi^\perp$. Here we use inequality (3.47) and integrate over $\int_0^t ds$. Again omitting the positive term $\|\nabla\varphi^\perp(t)\|_{L^2(\Omega)}^2$ and passing to the limit $t \to \infty$ we obtain

$$\int_0^\infty \|\Delta\varphi^\perp(t)\|_{L^2(\Omega)}^2 \, dt \leq \frac{1}{d_1}\|\nabla\varphi^\perp(0)\|_{L^2(\Omega)}^2 + \frac{d_2{}^2}{d_1{}^2} \int_0^\infty \|g(u(t))N_2(t)\|_{L^2(\Omega)}^2 \, dt \,.$$

Remark

At this point we explicitly need $\nabla \varphi^{\perp}(0) \in L^2(\Omega)$. For all the observations before it was sufficient to have $\varphi^{\perp}(0) \in L^2(\Omega)$, which follows immediately from $u_0 \in L^2(\Omega)$ as it was shown in (3.55). In order to have $\nabla \varphi^{\perp}(0) \in L^2(\Omega)$, we need to assume $u_0 \in H^1(\Omega)$. By the definition of $\varphi^{\perp}$ it holds

$$\nabla \varphi^{\perp}(0) = \sum_{j=2}^{\infty} (u_0, \varphi_j) \nabla \varphi_j = \nabla u_0 - (u_0, \varphi_1)_{L^2(\Omega)} \nabla \varphi_1 = \nabla u_0 \,.$$

If $u_0 \in H^1(\Omega)$, then we obtain by (3.77)

$$\int_0^{\infty} \|\Delta \varphi^{\perp}(t)\|_{L^2(\Omega)}^2 \, dt \le \frac{1}{d_1} \|\nabla u_0\|_{L^2(\Omega)}^2 + \frac{d_2{}^2}{d_1{}^2} \lambda(\Omega) \frac{g^{*2}}{g(\overline{\varrho})} \|\overline{N}\|_{L^{\infty}(\Omega)}^2 =: C_{14} < \infty \,,$$

$$\boxed{\int_0^{\infty} \|\Delta \varphi^{\perp}(t)\|_{L^2(\Omega)}^2 \, dt \le C_{14} \,.}$$

□

3.1.3 Classification of partial and complete swelling

The mitochondrial swelling process and its extent is dependent on the local calcium dose. If the initial concentration u_0 stays below the initiation threshold C^- at any point $x \in \Omega$, then no swelling will happen and we have $N_i(x,t) \equiv N_{i,0}(x) \; \forall x \in \Omega$, $i = 1, 2, 3$.

Another possible scenario is the so-called "partial swelling". This effect of partial swelling occurs in the experiments and can also be seen in the simulations when the initial calcium concentration lies above C^- at a small region but due to diffusion it does not stay above this threshold for the whole time. This leads to $N_1(x,t) = N_1(x,T_1) \; \forall t \ge T_1$ and $N_3(x,t) = N_3(x,T_2) \; \forall t \ge T_2$.

But if the initial calcium distribution together with the influence of the positive feedback is sufficiently high, then "complete swelling" occurs which means $N_1(x,t) \to 0$ and $N_3(x,t) \to \overline{N}(x)$ for all $x \in \Omega$.

As it was shown before, for both cases it holds $N_2(x,t) \to 0$.

Condition 3

Let the assumption of Conditions 1 and 2 hold. In addition we assume more regularity of the initial data:

$$u_0 \in H^1(\Omega)$$
$$N_{1,0} \in H^1(\Omega)$$
$$N_{2,0} \in H^1(\Omega)$$

A crucial point to distinguish between partial and complete swelling is to check if $f(u)$ stays positive for all times. For that it is necessary to have uniform convergence of $u(x,t)$ to $u^{\infty} \equiv a_1^{\infty} C_{\varphi}$. Up to now we only have strong convergence in $L^2(\Omega)$. So our aim now is to show uniform convergence, which turns out to be an extensive task.

Theorem 10
Under the assumptions of Condition 3, the following additional statements hold:

$$\sup_{t>0} \|\nabla N_1(t)\|_{L^2(\Omega)} < \infty$$

$$\sup_{t>0} \|\nabla N_2(t)\|_{L^2(\Omega)} < \infty$$

$$\sup_{t\geq\tilde{\delta}} \|\Delta\varphi^\perp(t)\|_{L^2(\Omega)} < \infty \quad \text{for } \tilde{\delta} > 0\,.$$

Furthermore we have uniform convergence

$$\|u(t) - u^\infty\|_{L^\infty(\Omega)} \longrightarrow 0 \quad \text{as } t \to \infty\,.$$

Proof

The course of action is to show the implications

$$\sup_{t>0} \|\nabla N_2(t)\|_{L^2(\Omega)} \leq C \;\Rightarrow\; \sup_{t\geq\tilde{\delta}} \|\Delta\varphi^\perp(t)\|_{L^2(\Omega)} \leq C \;\Rightarrow\; \|u(x,t) - u^\infty\|_{C^\alpha(\Omega)} \xrightarrow{t\to\infty} 0$$

for $t \geq \tilde{\delta}$, where $C^\alpha(\Omega)$ denotes the Hölder space $C^{0,\alpha}(\Omega)$, $\alpha \in (0,1]$.

For that we need the following statements:

Lemma 11 ([53])
Let $v \in C^\alpha(\Omega)$. Then there exist positive constants $\theta > 0$ and $C_\theta > 0$ such that

$$\|v\|_{C^\alpha(\Omega)} \leq C_\theta \|\nabla v\|_{L^2(\Omega)}^\theta \|\Delta v\|_{L^2(\Omega)}^{1-\theta}\,.$$

Theorem 12 (Morrey, [52])
Let $\Omega \subset \mathbb{R}^n$ be open with Lipschitz boundary $\partial\Omega \in C^{0,1}$. For $k > l$, $1 \leq p < \infty$ and $0 < \alpha < 1$ satisfying

$$k - \frac{n}{p} \geq l + \alpha$$

we have the continuous imbedding

$$W^{k,p}(\Omega) \hookrightarrow C^{l,\alpha}(\Omega)\,.$$

Lemma 13 ([56])
Let $\Omega \subset \mathbb{R}^n$ be bounded. Then we have the continuous imbeddings

$$C^{l,\beta}(\Omega) \hookrightarrow C^{0,\beta}(\Omega) \hookrightarrow C^{0,\alpha}(\Omega) \hookrightarrow L^\infty(\Omega)$$

for $0 < \alpha < \beta \leq 1$.

Applied to our case, for every space dimension $n \leq 3$ there exists $\alpha \in (0,1]$ such that

$$k \geq \frac{3}{2} + \alpha \;\Rightarrow\; H^k \hookrightarrow C^\alpha(\Omega)\,.$$

For our problem the domain of $-\Delta$ is given by $D(-\Delta) = \{v \in H^2(\Omega) : \partial_\nu v|_{\partial\Omega} = 0\}$ and thus by the previous result with $k = 2$ the solution $u(t)$ as well as the constant function u^∞ lie in $C^\alpha(\Omega)$. So we can apply Lemma 11 to the difference $u(t) - u^\infty$, which yields by Lemma 13 for $t \geq \tilde{\delta}$

$$
\begin{aligned}
\|u(t) - u^\infty\|_{L^\infty(\Omega)} &\leq C\|u(t) - u^\infty\|_{C^\alpha(\Omega)} \leq CC_\theta \|\nabla(u(t) - u^\infty)\|_{L^2(\Omega)}^\theta \|\Delta(u(t) - u^\infty)\|_{L^2(\Omega)}^{1-\theta} \\
&= CC_\theta \|\nabla\varphi^\perp(t)\|_{L^2(\Omega)}^\theta \|\Delta\varphi^\perp(t)\|_{L^2(\Omega)}^{1-\theta} \\
&\leq CC_\theta \sup_{t \geq \tilde{\delta}} \|\Delta\varphi^\perp(t)\|_{L^2(\Omega)}^{1-\theta} \|\nabla\varphi^\perp(t)\|_{L^2(\Omega)}^\theta \,.
\end{aligned}
$$

From (3.42) we know $\|\nabla\varphi^\perp(t)\|_{L^2(\Omega)} \xrightarrow{t\to\infty} 0$ and so we conclude

$$
\boxed{\|u(t) - u^\infty\|_{L^\infty(\Omega)} \xrightarrow{t\to\infty} 0 \ \text{ if } \ \sup_{t \geq \tilde{\delta}} \|\Delta\varphi^\perp(t)\|_{L^2(\Omega)} \leq C \,,}
$$

i.e. in that case we have uniform convergence of $u(x,t)$ to u^∞ for $t \geq \tilde{\delta}$.

Remark
The restriction $t \geq \tilde{\delta} > 0$ does not pose any problems. We are interested in the longtime dynamics, where we study the behavior for $t \to \infty$ and the small initial interval $[0, \tilde{\delta})$ need not be taken into account.

So our aim now is to show that $\|\Delta\varphi^\perp(t)\|_{L^2(\Omega)}$ is bounded for all $t \geq \tilde{\delta}$. For that purpose we introduce the operator $A = -\Delta$, which is well known to be positive and self-adjoint. Thus we can define its square root $A^{\frac{1}{2}}$ which inherits the property of self-adjointness. The norm $\|A^{\frac{1}{2}}v\|_{L^2(\Omega)}$ is then given by

$$
\|A^{\frac{1}{2}}v\|_{L^2(\Omega)}^2 = (A^{\frac{1}{2}}v, A^{\frac{1}{2}}v)_{L^2(\Omega)} = (v, Av)_{L^2(\Omega)} = (\nabla v, \nabla v)_{L^2(\Omega)} = \|\nabla v\|_{L^2(\Omega)}^2 \,.
$$

PDE (3.1) is written in terms of A

$$
\partial_t u + d_1 A u = d_2 g(u) N_2
$$

and the application of $A^{\frac{1}{2}}$ to this equation gives us

$$
\partial_t A^{\frac{1}{2}}u + d_1 A^{\frac{3}{2}}u = d_2 A^{\frac{1}{2}} \left(g(u) N_2\right) \,.
$$

Multiplying by $A^{\frac{3}{2}}u$ and integrating over $\int_\Omega dx$ we obtain due to $A^{\frac{1}{2}}$ being self-adjoint

$$
\frac{1}{2}\frac{d}{dt}\|Au(t)\|_{L^2(\Omega)}^2 + d_1\|A^{\frac{3}{2}}u(t)\|_{L^2(\Omega)}^2 = d_2\left(A^{\frac{1}{2}}\left(g(u(t))N_2(t)\right), A^{\frac{3}{2}}u(t)\right)_{L^2(\Omega)} \,.
$$

This term can be further estimated by Cauchy Schwarz and Young's inequality with $\varepsilon = \frac{d_1}{d_2}$, whence it follows

$$
\frac{1}{2}\frac{d}{dt}\|Au(t)\|_{L^2(\Omega)}^2 + \frac{d_1}{2}\|A^{\frac{3}{2}}u(t)\|_{L^2(\Omega)}^2 \leq \frac{d_2^2}{2d_1}\|A^{\frac{1}{2}}\left(g(u(t))N_2(t)\right)\|_{L^2(\Omega)}^2
$$

and from the norm definition we have

$$\frac{1}{2}\frac{d}{dt}\|\Delta u(t)\|^2_{L^2(\Omega)} + \frac{d_1}{2}\|A^{\frac{3}{2}}u(t)\|^2_{L^2(\Omega)} \leq \frac{d_2^2}{2d_1}\|\nabla\left(g(u(t))N_2(t)\right)\|^2_{L^2(\Omega)}$$

$$\leq \frac{d_2^2}{d_1}\|g'(u(t))\nabla u(t)N_2(t)\|^2_{L^2(\Omega)} + \frac{d_2^2}{d_1}\|g(u(t))\nabla N_2(t)\|^2_{L^2(\Omega)}\,.$$

The term $\|A^{\frac{3}{2}}u\|^2_{L^2(\Omega)}$ can again be estimated by Wirtinger's inequality. From the decomposition of u we know $Au = A\varphi^\perp = -\Delta\varphi^\perp$ and A is mapping from the orthogonal complement to itself:

$$(A\varphi^\perp, \varphi_1)_{L^2(\Omega)} = 0 = C_\varphi \int_\Omega A\varphi^\perp\, dx\,.$$

Thus Wirtinger's inequality can be applied to $A\varphi^\perp$ and yields

$$\|A\varphi^\perp\|_{L^2(\Omega)} \leq C_W\|\nabla\left(A\varphi^\perp\right)\|_{L^2(\Omega)} = C_W\|A^{\frac{1}{2}}\left(A\varphi^\perp\right)\|_{L^2(\Omega)} = C_W\|A^{\frac{3}{2}}\varphi^\perp\|_{L^2(\Omega)}$$

$$= C_W\|A^{\frac{3}{2}}u\|_{L^2(\Omega)}$$

Substituting that relation into the previous inequality with $\Delta u = \Delta\varphi^\perp$, $\nabla u = \nabla\varphi^\perp$ and using the boundedness $g(s) \leq g^*$, $|g'(s)| \leq L_g$ by Condition 1 (i), (iii) and $N_2(t) \leq \|\overline{N}\|_{L^\infty(\Omega)}$, we obtain

$$\frac{d}{dt}\|\Delta\varphi^\perp(t)\|^2_{L^2(\Omega)} + \frac{d_1}{C_W{}^2}\|\Delta\varphi^\perp(t)\|^2_{L^2(\Omega)}$$

$$\leq \frac{2d_2^2}{d_1}L_g^2\|\overline{N}\|^2_{L^\infty(\Omega)}\|\nabla\varphi^\perp(t)\|^2_{L^2(\Omega)} + \frac{2d_2^2}{d_1}g^{*2}\|\nabla N_2(t)\|^2_{L^2(\Omega)}\,.$$

In the following we assume

$$\sup_{t>0}\|\nabla N_2(t)\|_{L^2(\Omega)} \leq C_N < \infty \tag{3.56}$$

and show that under this assumption we have $\sup_{t\geq\tilde{\delta}}\|\Delta\varphi^\perp(t)\|_{L^2(\Omega)} < \infty$.

Remark
It remains to show that this assumption holds true in general.

From (3.53) we know that $\sup_{t\geq\delta}\|\nabla\varphi^\perp(t)\|_{L^2(\Omega)} \leq C_{11}$ and due to Condition 3 even $\sup_{t>0}\|\nabla\varphi^\perp(t)\|_{L^2(\Omega)} \leq C_{12}$ (c.f. Remark, (3.54)). In summary we have

$$\frac{d}{d}y(t) + \gamma y(t) \leq C_{15} =: \frac{2d_2^2}{d_1}L_g^2\|\overline{N}\|^2_{L^\infty(\Omega)}C_{12}^2 + \frac{2d_2^2}{d_1}g^{*2}C_N^2$$

where $y(t) := \|\Delta\varphi^\perp(t)\|^2_{L^2(\Omega)}$ and $\gamma := \frac{d_1}{C_W{}^2}$. Proposition 5 yields by integration $\int_{\underline{t}}^t ds$ with $\underline{t} > 0$

$$\|\Delta\varphi^\perp(t)\|^2_{L^2(\Omega)} \leq \|\Delta\varphi^\perp(\underline{t})\|^2_{L^2(\Omega)} + \frac{C_{15}}{\gamma} \quad \text{for all } t \geq \underline{t}\,. \tag{3.57}$$

Theorem 1 states that the solution u fulfills $\sqrt{t}\,\Delta u \in L^2(0,T;L^2(\Omega))$, i.e. the solution is immediately smoothened. By definition it holds for $\Delta u = \Delta \varphi^\perp$

$$\int_0^T t\|\Delta\varphi^\perp(t)\|^2_{L^2(\Omega)}\,dt < \infty\,,$$

which yields the existence of a time $\underline{t} \in (0,T]$ and a constant $C_{16} < \infty$ such that

$$\underline{t}\|\Delta\varphi^\perp(\underline{t})\|^2_{L^2(\Omega)} \le C_{16} \iff \|\Delta\varphi^\perp(\underline{t}))\|_{L^2(\Omega)} \le \frac{1}{\sqrt{\underline{t}}}C_{16}\,.$$

This expression is bounded if $\underline{t}$ is bounded away from zero, i.e. if $\underline{t} \ge \tilde{\delta} > 0$ for some positive constant $\tilde{\delta} > 0$. Then (3.57) implies

$$\|\Delta\varphi^\perp(t)\|^2_{L^2(\Omega)} \le \frac{1}{\tilde{\delta}}C_{16} + \frac{C_{15}}{\gamma} =: C_{17}^2 < \infty \quad \text{for all } t \ge \underline{t} \ge \tilde{\delta}$$

and consequently

$$\boxed{\sup_{t \ge \tilde{\delta}} \|\Delta\varphi^\perp(t)\|_{L^2(\Omega)} \le C_{17}\,.}$$

In order to show the uniform convergence of $u(t)$ to u^∞, at this point it only remains to show that assumption (3.56) is always satisfied. For that the higher regularity of the initial data under the terms of Condition 3 is crucial.

First we need to show that the same holds for $\nabla N_1(t)$, i.e. $\sup_{t>0}\|\nabla N_1(t)\|_{L^2(\Omega)} < \infty$. Application of the gradient to the model equation (3.2) leads to

$$\partial_t \nabla N_1 = -f'(u)\nabla u\, N_1 - f(u)\nabla N_1$$

and by multiplying with ∇N_1 and integrating over $\int_\Omega dx$ we obtain

$$\frac{1}{2}\frac{d}{dt}\|\nabla N_1(t)\|^2_{L^2(\Omega)} =$$

$$= -\int_\Omega f'(u(x,t))\nabla u(x,t)N_1(x,t)\nabla N_1(x,t)\,dx - \int_\Omega f(u(x,t))|\nabla N_1(x,t)|^2\,dx$$

$$\le \int_\Omega |f'(u(x,t))||\nabla u(x,t)||N_1(x,t)||\nabla N_1(x,t)|\,dx - \int_\Omega f(u(x,t))|\nabla N_1(x,t)|^2\,dx\,.$$

$$(3.58)$$

Remark
Recall the decomposition

$$u(x,t) = a_1(t)C_\varphi + \varphi^\perp(x,t)\,.$$

From previous observations we know $u^\infty = a_1^\infty C_\varphi$ and the function $a_1(t)$ in non-decreasing, i.e.

$$a_1(t)C_\varphi \le u^\infty \quad \text{for all } t \ge 0\,. \tag{3.59}$$

Now Condition 2 (ii) comes into play, which holds for $u \in [C^-, C^- + \delta]$. According to that we define the following subsets of Ω for all $t \geq 0$:

$$\Omega_1(t) := \{x \in \Omega : u(x,t) < C^-\}$$
$$\Omega_2(t) := \{x \in \Omega : u(x,t) \in [C^-, C^- + \delta]\}$$
$$\Omega_3(t) := \{x \in \Omega : u(x,t) > C^- + \delta\}$$

Then for every point of time we have a disjoint partition of Ω:

$$\Omega = \Omega_1(t) \,\dot\cup\, \Omega_2(t) \,\dot\cup\, \Omega_3(t) \quad \forall t \geq 0\,.$$

Our aim now is to estimate the term $|f'(u(x,t))|$ appearing in (3.58) for the regions $\Omega_1(t)$ and $\Omega_2(t)$. From Condition 2 (i) we know that $f(u(x,t))$ is constant zero on $\Omega_1(t)$ and thus it holds

$$|f'(u(x,t))| = 0 \ \text{ on } \Omega_1(t)\,.$$

To obtain an estimate in $\Omega_2(t)$, at this stage we have to distinguish between the two cases

$$\text{I) } u^\infty \leq C^- \quad \text{and} \quad \text{II) } u^\infty > C^-\,.$$

Case I
We first take a look at the case $u^\infty \leq C^-$. On $\Omega_2(t)$ we have by (3.59)

$$0 \leq m_1 \left(u(x,t) - C^-\right) \leq f'\left(u(x,t)\right) \leq m_2 \left(u(x,t) - C^-\right)$$
$$\leq m_2 \left(u^\infty + \varphi^\perp(x,t) - C^-\right) \leq m_2 \varphi^\perp(x,t)$$
$$\Rightarrow |f'(u(x,t))| \leq m_2 |\varphi^\perp(x,t)| \ \text{ on } \Omega_2(t)\,.$$

Substituting these estimates into (3.58), we get

$$\frac{1}{2}\frac{d}{dt}\|\nabla N_1(t)\|^2_{L^2(\Omega)} \leq m_2 \|\overline{N}\|_{L^\infty(\Omega)} \int_{\Omega_2(t)} |\varphi^\perp(x,t)||\nabla u(x,t)||\nabla N_1(x,t)|\,dx$$
$$+ \|\overline{N}\|_{L^\infty(\Omega)} \int_{\Omega_3(t)} |f'(u(x,t))||\nabla u(x,t)||\nabla N_1(x,t)|\,dx - \int_\Omega f(u(x,t))|\nabla N_1(x,t)|^2\,dx\,.$$
$$(3.60)$$

The first integral can be further estimated by use of Hölder's inequality:

$$\int_{\Omega_2(t)} |\varphi^\perp(x,t)||\nabla u(x,t)||\nabla N_1(x,t)|\,dx \leq \|\varphi^\perp(t)\nabla u(t)\nabla N_1(t)\|_{L^1(\Omega)}$$
$$\leq \|\varphi^\perp(t)\nabla u(t)\|_{L^2(\Omega)}\|\nabla N_1(t)\|_{L^2(\Omega)} \leq \|\varphi^\perp(t)\|_{L^4(\Omega)}\|\nabla u(t)\|_{L^4(\Omega)}\|\nabla N_1(t)\|_{L^2(\Omega)}\,.$$

From Theorem 1 we know that $u(t)$ and $\nabla u(t)$ lie in $H^1(\Omega)$ for $t > 0$ and the Sobolev imbedding theorem states $H^1(\Omega) \hookrightarrow L^4(\Omega)$ with constant C_{H^1} since $n \leq 3$. This allows to further estimate

$$\leq C_{H^1}^2 \|\varphi^\perp(t)\|_{H^1(\Omega)}\|\nabla u(t)\|_{H^1(\Omega)}\|\nabla N_1(t)\|_{L^2(\Omega)}$$

and applying Corollary 8 to $\|\varphi^\perp(t)\|_{H^1(\Omega)}$ and $\|\nabla u(t)\|_{H^1(\Omega)} = \|\nabla\varphi^\perp(t)\|_{H^1(\Omega)}$ leads us to

$$\leq C_{H^1}^2 (C_W^2 + 1)\|\nabla\varphi^\perp(t)\|_{L^2(\Omega)}\|\Delta\varphi^\perp(t)\|_{L^2(\Omega)}\|\nabla N_1(t)\|_{L^2(\Omega)}.$$

For the second integral we artificially insert $\frac{\sqrt{f(u(x,t))}}{\sqrt{f(u(x,t))}}$ which is possible since in $\Omega_3(t)$ it holds $u(x,t) > C^- + \delta$ and with that by Condition 2 (iii) we know $f(u(x,t)) > 0$. By Young's inequality we have

$$\int_{\Omega_3(t)} \frac{|f'(u(x,t))|}{\sqrt{f(u(x,t))}}|\nabla u(x,t)|\,\sqrt{f(u(x,t))}\,|\nabla N_1(x,t)|\,dx$$

$$\leq \frac{1}{2}\int_{\Omega_3(t)} \frac{|f'(u(x,t))|^2}{f(u(x,t))}|\nabla u(x,t)|^2\,dx + \frac{1}{2}\int_{\Omega_3(t)} f(u(x,t))|\nabla N_1(x,t)|^2\,dx$$

and due to Conditions 1 (iii) and 2 (iii)

$$\leq \frac{1}{2}\frac{L_f^2}{f(C^- + \delta)}\|\nabla\varphi^\perp(t)\|_{L^2(\Omega)}^2 + \frac{1}{2}\int_\Omega f(u(x,t))|\nabla N_1(x,t)|^2\,dx.$$

Substitution of these findings into (3.60) leads to

$$\frac{1}{2}\frac{d}{dt}\|\nabla N_1(t)\|_{L^2(\Omega)}^2 \leq \underbrace{m_2\|\overline{N}\|_{L^\infty(\Omega)}C_{H^1}^2(C_W^2 + 1)}_{=:C_{18}}\|\nabla\varphi^\perp(t)\|_{L^2(\Omega)}\|\Delta\varphi^\perp(t)\|_{L^2(\Omega)}\|\nabla N_1(t)\|_{L^2(\Omega)}$$

$$+ \underbrace{\|\overline{N}\|_{L^\infty(\Omega)}\frac{1}{2}\frac{L_f^2}{f(C^- + \delta)}}_{=:\frac{C_{19}}{2}}\|\nabla\varphi^\perp(t)\|_{L^2(\Omega)}^2 - \frac{1}{2}\int_\Omega f(u(x,t))|\nabla N_1(x,t)|^2\,dx.$$

The last term can be omitted and we obtain with Young's inequality

$$\frac{d}{dt}\|\nabla N_1(t)\|_{L^2(\Omega)}^2 \leq (C_{18} + C_{19})\|\nabla\varphi^\perp(t)\|_{L^2(\Omega)}^2 + C_{18}\|\Delta\varphi^\perp(t)\|_{L^2(\Omega)}^2\|\nabla N_1(t)\|_{L^2(\Omega)}^2.$$

Integration over $\int_0^t ds$ yields with (3.44) under the assumption of Condition 3

$$\|\nabla N_1(t)\|_{L^2(\Omega)}^2 \leq \underbrace{\|\nabla N_{1,0}\|_{L^2(\Omega)}^2 + (C_{18} + C_{19})\int_0^\infty \|\nabla\varphi^\perp(t)\|_{L^2(\Omega)}^2\,dt}_{\leq C_{20} < \infty}$$

$$+ C_{18}\int_0^t \|\Delta\varphi^\perp(s)\|_{L^2(\Omega)}^2\|\nabla N_1(s)\|_{L^2(\Omega)}^2\,ds.$$

Now Gronwall's inequality can be applied and we finally obtain with (3.45)

$$\|\nabla N_1(t)\|_{L^2(\Omega)}^2 \leq C_{20}\,e^{C_{18}\int_0^\infty \|\Delta\varphi^\perp(t)\|_{L^2(\Omega)}^2\,dt} < \infty \quad \text{for all } t > 0,$$

i.e. for the case $u^\infty \leq C^-$ we achieved

$$\boxed{\sup_{t>0} \|\nabla N_1(t)\|_{L^2(\Omega)} < \infty \,.} \tag{3.61}$$

This result is now used to show that $\nabla N_2(t)$ also stays bounded in $L^2(\Omega)$. For that we apply the gradient to model equation (3.3) and get

$$\partial_t \nabla N_2 = f'(u)\nabla u\, N_1 + f(u)\nabla N_1 - g'(u)\nabla u\, N_2 - g(u)\nabla N_2 \,.$$

Multiplication by ∇N_2 and integration over $\int_\Omega dx$ leads to

$$\frac{1}{2}\frac{d}{dt}\|\nabla N_2(t)\|_{L^2(\Omega)}^2 = \int_\Omega f'(u(x,t))\nabla u(x,t) N_1(x,t) \nabla N_2(x,t)\, dx$$

$$+ \int_\Omega f(u(x,t))\nabla N_1(x,t)\nabla N_2(x,t)\, dx - \int_\Omega g'(u(x,t))\nabla u(x,t) N_2(x,t)\nabla N_2(x,t)\, dx$$

$$- \int_\Omega g(u(x,t))|\nabla N_2(x,t)|^2\, dx \,.$$

Condition 1 (ii), (iii) yields

$$\frac{1}{2}\frac{d}{dt}\|\nabla N_2(t)\|_{L^2(\Omega)}^2 \leq \underbrace{(L_f + L_g)\|\overline{N}\|_{L^\infty(\Omega)}}_{=:C_{21}} \int_\Omega |\nabla u(x,t)||\nabla N_2(x,t)|\, dx$$

$$+ f^* \int_\Omega |\nabla N_1(x,t)||\nabla N_2(x,t)|\, dx - \int_\Omega g(u(x,t))|\nabla N_2(x,t)|^2\, dx \,.$$

Our first aim is to derive the boundedness of $\|\nabla N_2(t)\|_{L^2(\Omega)}$ for the fixed interval $t \in (0, t_0]$. Omitting the last integral and using Hölder's together with Young's inequality, we obtain with (3.54) and (3.61)

$$\frac{d}{dt}\|\nabla N_2(t)\|_{L^2(\Omega)}^2 \leq C_{21}\|\nabla u(t)\|_{L^2(\Omega)}^2 + f^*\|\nabla N_1(t)\|_{L^2(\Omega)}^2 + (C_{21} + f^*)\|\nabla N_2(t)\|_{L^2(\Omega)}^2$$

$$\leq C_{21}\sup_{t>0}\|\nabla u(t)\|_{L^2(\Omega)}^2 + f^*\sup_{t>0}\|\nabla N_1(t)\|_{L^2(\Omega)}^2 + (C_{21} + f^*)\|\nabla N_2(t)\|_{L^2(\Omega)}^2$$

$$\leq C + (C_{21} + f^*)\|\nabla N_2(t)\|_{L^2(\Omega)}^2 \quad \text{with } C < \infty \,.$$

Integration over $\int_0^t ds$ with $0 < t \leq t_0$ yields

$$\|\nabla N_2(t)\|_{L^2(\Omega)}^2 \leq \|\nabla N_{2,0}\|_{L^2(\Omega)}^2 + Ct_0 + (C_{21} + f^*)\int_0^t \|\nabla N_2(s)\|_{L^2(\Omega)}^2\, ds$$

and hence with Gronwall's inequality and Condition 3

$$\|\nabla N_2(t)\|_{L^2(\Omega)}^2 \leq \big(\|\nabla N_{2,0}\|_{L^2(\Omega)}^2 + Ct_0\big)e^{(C_{21}+f^*)t_0} < \infty \quad \text{for all } t \in (0, t_0] \,. \tag{3.62}$$

In particular this implies

$$\|\nabla N_2(t_0)\|_{L^2(\Omega)} < \infty \tag{3.63}$$

and we can proceed to the whole time intervall $t > 0$.

From Proposition 4 we know that for all $x \in \Omega$ it holds $u(x, t) \geq \varrho > 0 \ \forall t \geq t_0$ and consequently Condition 2 (iii), (iv) implies

$$g(u(x, t)) \geq g(\overline{\varrho}) > 0 \quad \forall t \geq t_0$$

with $\overline{\varrho} = \min(\varrho, \varrho_0)$ as defined earlier.

We use this result and apply Young's inequality to the first two integrals with $\varepsilon_1 = \frac{1}{2C_{21}} g(\overline{\varrho})$ and $\varepsilon_2 = \frac{1}{2f^*} g(\overline{\varrho})$. This gives for all $t \geq t_0$

$$\frac{1}{2}\frac{d}{dt}\|\nabla N_2(t)\|^2_{L^2(\Omega)} + \frac{1}{2}g(\overline{\varrho})\|\nabla N_2(t)\|^2_{L^2(\Omega)} \leq \frac{C_{21}^2}{g(\overline{\varrho})}\|\nabla u(t)\|^2_{L^2(\Omega)} + \frac{f^{*2}}{g(\overline{\varrho})}\|\nabla N_1(t)\|^2_{L^2(\Omega)}$$

$$\leq \frac{C_{21}^2}{g(\overline{\varrho})}\sup_{t>0}\|\nabla u(t)\|^2_{L^2(\Omega)} + \frac{f^{*2}}{g(\overline{\varrho})}\sup_{t>0}\|\nabla N_1(t)\|^2_{L^2(\Omega)}$$

$$\leq C_{22} < \infty \quad \text{due to (3.54) and (3.61)}.$$

Hence Proposition 5 can be applied and yields with (3.63)

$$\|\nabla N_2(t)\|^2_{L^2(\Omega)} \leq \|\nabla N_2(t_0)\|^2_{L^2(\Omega)} + \frac{2C_{22}}{g(\varrho)} < \infty \quad \text{for all } t \geq t_0,$$

i.e. together with (3.62) we achieved

$$\boxed{\sup_{t>0}\|\nabla N_2(t)\|_{L^2(\Omega)} < \infty.}$$

That means for the first case I) $u^\infty \leq C^-$ we showed that assumption (3.56) holds for all $t > 0$ and taking it all together we obtain with $C_{23} > 0$ chosen appropriately

$$\sup_{t>0}\|\nabla N_2(t)\|_{L^2(\Omega)} < \infty \ \Rightarrow \ \sup_{t \geq \tilde{\delta}}\|\Delta\varphi^\perp(t)\|_{L^2(\Omega)} \leq C_{23} < \infty.$$

From the previous observations we know

$$\|u(t) - u^\infty\|_{L^\infty(\Omega)} \leq CC_\theta \sup_{t \geq \tilde{\delta}}\|\Delta\varphi^\perp(t)\|^{1-\theta}_{L^2(\Omega)}\|\nabla\varphi^\perp(t)\|^\theta_{L^2(\Omega)} \text{ for all } t \geq \tilde{\delta}$$

and from the boundedness of $\Delta\varphi^\perp(t)$ it follows

$$\|u(t) - u^\infty\|_{L^\infty(\Omega)} \leq CC_\theta C_{23}^{1-\theta}\|\nabla\varphi^\perp(t)\|^\theta_{L^2(\Omega)} \text{ for all } t \geq \tilde{\delta}.$$

With (3.42) we finally obtain

$$\boxed{\|u(t) - u^\infty\|_{L^\infty(\Omega)} \longrightarrow 0 \quad \text{as } t \to \infty}$$

and the uniform convergence of $u(t)$ to the constant function u^∞ is shown.

Case II

Now the same considerations are made in the case $u^\infty > C^-$. Again by Condition 2 (ii) on $\Omega_2(t)$ it holds

$$m_1(u(x,t) - C^-) \leq f'(u(x,t)) \leq m_2(u(x,t) - C^-)$$

and this time we take a look at the lower part and integrate over the interval $[C^-, u(x,t)]$:

$$\int_{C^-}^{u(x,t)} m_1(v - C^-)\, dv \leq \int_{C^-}^{u(x,t)} f'(v)\, dv = f(u(x,t)) - \underbrace{f(C^-)}_{=0}$$

which leads to

$$f(u(x,t)) \geq \frac{1}{2} m_1 \left(u(x,t) - C^- \right)^2 .$$

Due to the condition $u^\infty > C^-$ and the monotonicity of $a_1(t)$, with (3.59) it follows:
For all α with $0 < \alpha < (u^\infty - C^-)$ there exists $T_\alpha > 0$ such that

$$a_1(t)C_\varphi \geq C^- + \alpha \quad \text{for all } t \geq T_\alpha .$$

Substituting that relation into the previous estimate, we obtain with Young's inequality

$$
\begin{aligned}
f(u(x,t)) &\geq \frac{1}{2} m_1 \left(a_1(t)C_\varphi + \varphi^\perp(x,t) - C^- \right)^2 \geq \frac{1}{2} m_1 \left(\alpha + \varphi^\perp(x,t) \right)^2 \\
&\geq \frac{1}{2} m_1 \left(\alpha^2 - 2\alpha|\varphi^\perp(x,t)| + |\varphi^\perp(x,t)|^2 \right) \\
&\geq \frac{1}{2} m_1 \left(\frac{1}{2}\alpha^2 - |\varphi^\perp(x,t)|^2 \right) \qquad\qquad \text{for all } t \geq T_\alpha \text{ and } x \in \Omega_2(t) ,
\end{aligned}
$$

i.e. this estimates holds for f applied to $u(x,t) \in [C^-, C^- + \delta]$. The boundedness of f from below given by Condition 2 (iii) implies

$$f(u(x,t)) \geq f(C^- + \delta) \geq \frac{1}{2} m_1 \left(\frac{1}{2}\alpha^2 - |\varphi^\perp(x,t)|^2 \right) \quad \text{for all } t \geq T_\alpha \text{ and } x \in \Omega_3(t) .$$

We start again with the boundedness of $\nabla N_1(t)$ and go back to (3.58). With the preceding observations and $f(u(x,t)) = 0 = f'(u(x,t))$ in $\Omega_1(t)$ we have for $t \geq T_\alpha$

$$
\begin{aligned}
\frac{1}{2}\frac{d}{dt}\|\nabla N_1(t)\|_{L^2(\Omega)}^2 &\leq L_f \|\overline{N}\|_{L^\infty(\Omega)} \int_{\Omega_2(t)\cup\Omega_3(t)} |\nabla(u(x,t))||\nabla N_1(x,t)|\, dx \\
&- \frac{m_1}{4}\alpha^2 \int_{\Omega_2(t)\cup\Omega_3(t)} |\nabla N_1(x,t)|^2\, dx + \frac{m_1}{2} \int_{\Omega_2(t)\cup\Omega_3(t)} |\varphi^\perp(x,t)|^2 |\nabla N_1(x,t)|\, dx .
\end{aligned}
$$

Hölder's and Young's inequality with $\varepsilon = m_1(2L_f\|\overline{N}\|_{L^\infty(\Omega)})^{-1}\alpha^2$ and extension to Ω give

$$\frac{d}{dt}\|\nabla N_1(t)\|_{L^2(\Omega)}^2 \leq \frac{2L_f^2\|\overline{N}\|_{L^\infty(\Omega)}^2}{m_1\alpha^2}\|\nabla u(t)\|_{L^2(\Omega)}^2 + m_1\|\varphi^\perp(t)\|_{L^\infty(\Omega)}^2\|\nabla N_1(t)\|_{L^2(\Omega)}^2 .$$

For $n \leq 3$ there is the Sobolev space imbedding $H^2(\Omega) \hookrightarrow L^\infty(\Omega)$ with constant $C_{H^2} > 0$ and by use of Corollary 8 we can further estimate

$$\leq \underbrace{\frac{2L_f^2\|\overline{N}\|_{L^\infty(\Omega)}^2}{m_1\alpha^2}}_{=:C_{24}}\|\nabla\varphi^\perp(t)\|_{L^2(\Omega)}^2 + \underbrace{m_1 C_{H^2}^2(C_W^4 + C_W^2 + 1)}_{=:C_{25}}\|\Delta\varphi^\perp(t)\|_{L^2(\Omega)}^2\|\nabla N_1(t)\|_{L^2(\Omega)}^2.$$

Integrating over $\int_0^t ds$, we obtain

$$\|\nabla N_1(t)\|_{L^2(\Omega)}^2 \leq \underbrace{\|\nabla N_{1,0}\|_{L^2(\Omega)}^2 + C_{24}\int_0^\infty \|\nabla\varphi^\perp(t)\|_{L^2(\Omega)}^2\, dt}_{\leq C_{26} < \infty}$$
$$+ C_{25}\int_0^t \|\Delta\varphi^\perp(s)\|_{L^2(\Omega)}^2\|\nabla N_1(s)\|_{L^2(\Omega)}^2\, ds$$

and Gronwall's inequality together with (3.44) leads us to

$$\|\nabla N_1(t)\|_{L^2(\Omega)}^2 \leq C_{26}\, e^{C_{25}\int_0^\infty \|\Delta\varphi^\perp(t)\|_{L^2(\Omega)}^2\, dt} < \infty \quad \text{for all } t \geq T_\alpha,$$

i.e. it holds

$$\sup_{t \geq T_\alpha} \|\nabla N_1(t)\|_{L^2(\Omega)} < \infty.$$

In analogy to the calculations for $\nabla N_2(t)$ in $(0, t_0]$, by use of (3.58), Condition 1 (iii) and 3 we also obtain for the bounded intervall $(0, T_\alpha]$

$$\sup_{t \in (0,T_\alpha]} \|\nabla N_1(t)\|_{L^2(\Omega)} < \infty.$$

All together for case II) $u^\infty > C^-$, we obtain

$$\boxed{\sup_{t>0} \|\nabla N_1(t)\|_{L^2(\Omega)} < \infty.}$$

The boundedness of $\nabla N_2(t)$ in $L^2(\Omega)$ is shown in exactly the same way as for case I) $u^\infty \leq C^-$, since for the estimation of $\|\nabla N_2(t)\|_{L^2(\Omega)}$ we did not use the relation of u^∞ and C^-. This yields

$$\boxed{\sup_{t>0} \|\nabla N_2(t)\|_{L^2(\Omega)} < \infty}$$

and with that

$$\boxed{\|u(t) - u^\infty\|_{L^\infty(\Omega)} \longrightarrow 0 \quad \text{as } t \to \infty.}$$

In summary for both cases I) and II) we obtained uniform convergence of the solution $u(t)$ to $u^\infty \equiv a_1^\infty C_\varphi$

$\square$

Convergence rate

Theorem 14
Under the assumptions of Condition 3, the long-time behavior of the ODE solution (N_1, N_2, N_3) can be further characterized:

Partial swelling: $u^\infty < C^-$

$\exists\, T_p \geq \tilde{\delta} > 0$ *such that for all $x \in \Omega$ it holds*

$$N_1(x, t) \equiv N_1(x, T_p) \quad \text{for all } t \geq T_p$$

and we have the following exponential convergence rates for all $x \in \Omega$ and $t \geq T_p$:

$$N_2(x, t) \xrightarrow{t \to \infty} 0 \qquad\qquad\qquad in\ \mathcal{O}(e^{-g(\bar{\varrho})t})$$

$$N_3(x, t) \xrightarrow{t \to \infty} \overline{N}(x) - N_1(x, T_p) \quad in\ \mathcal{O}(e^{-g(\bar{\varrho})t})\,.$$

Complete swelling: $u^\infty > C^-$

$\exists\, T_c \geq \tilde{\delta} > 0$ *such that for all $x \in \Omega$ and all $t \geq T_c$ the following exponential convergence rates hold with some constants $\gamma > 0$, $\zeta > 0$, $\eta > 0$:*

$$N_1(x, t) \xrightarrow{t \to \infty} 0 \qquad\qquad\qquad in\ \mathcal{O}(e^{-f(C^- + \gamma)t})$$

$$N_2(x, t) \xrightarrow{t \to \infty} 0 \qquad\qquad\qquad in\ \mathcal{O}(e^{-g(\zeta)t})$$

$$N_3(x, t) \xrightarrow{t \to \infty} \overline{N}(x) \qquad\qquad\quad in\ \mathcal{O}(e^{-\eta t})\,.$$

Here exponential convergence of $v(t) \to v^\infty$ is given if there exist some constants $C > 0$ and $k > 0$ such that
$$|v(t) - v^\infty| \leq C e^{-kt}\,.$$

Proof

1.) Partial swelling
We start with the partial swelling case. By the uniform convergence of $u(x, t)$ to $u^\infty < C^-$ follows the existence of a time $T_p \geq \tilde{\delta} > 0$ such that

$$u(x, t) \leq C^- \qquad \forall x \in \Omega \quad \forall t \geq T_p$$

and consequently

$$f(u(x, t)) = 0 \qquad \forall x \in \Omega \quad \forall t \geq T_p\,. \tag{3.64}$$

Remark
For this relation it was crucial to have uniform convergence.

From the model equation (3.2) it follows immediately for all $x \in \Omega$

$$\partial_t N_1(x, t) = 0 \quad \forall t \geq T_p\,,$$

which implies

$$\boxed{N_1(x,t) \equiv N_1(x,T_p) \qquad \forall t \geq T_p\,.}$$

For equation (3.3), by (3.64) and the definition of $\overline{\varrho}$, it holds for all $t \geq T_p \geq \tilde{\delta}$

$$\partial_t N_2(x,t) = -g(u(x,t))N_2(x,t) \leq -g(\overline{\varrho})N_2(x,t)\,,$$

which yields with Gronwall's inequality

$$\boxed{N_2(x,t) \leq N_{2,0}(x)e^{-g(\overline{\varrho})t} \leq \|N_{2,0}\|_{L^\infty(\Omega)}e^{-g(\overline{\varrho})t} \quad \forall x \in \Omega \quad \forall t \geq T_p} \qquad (3.65)$$

i.e. we have exponential convergence of $N_2(x,t)$ to 0. From the conservation law (3.8) we know

$$N_3(x,t) = \overline{N}(x) - N_1(x,T_p) - N_2(x,t) \quad \forall t \geq T_p$$

and consequently

$$N_{3,p}^\infty(x) = \overline{N}(x) - N_1(x,T_p)\,.$$

This gives

$$|N_3(x,t) - N_{3,p}^\infty(x)| = N_2(x,t) \quad \text{for } t \geq T_p$$

and with the previous result (3.65) it follows

$$\boxed{|N_3(x,t) - N_{3,p}^\infty(x)| \leq \|N_{2,0}\|_{L^\infty(\Omega)}e^{-g(\overline{\varrho})t} \quad \forall x \in \Omega \quad \forall t \geq T_p\,,}$$

i.e. exponential convergence of $N_3(x,t)$ to $N_{3,p}^\infty(x)$.

2.) Complete swelling
In the complete swelling case where $u^\infty > C^-$, the uniform convergence of $u(x,t)$ to u^∞ yields the existence of a time $T_c \geq \tilde{\delta} > 0$ and a constant $\beta > 0$ such that

$$u(x,t) \geq C^- + \beta > C^- \quad \forall x \in \Omega \quad \forall t \geq T_c\,.$$

In order to show the positivity of $f(u(x,t))$, we have to distinguish between two cases in accordance with Condition 2:

- $u(x,t) \geq C^- + \delta$, where $\delta > 0$ denotes the constant from Condition 2, i.e. $\beta \geq \delta$. In that case, Condition 2 (iii) holds and it follows

$$f(u(x,t)) \geq f(C^- + \delta) > 0 \quad \forall x \in \Omega \quad \forall t \geq T_c\,.$$

- $u(x,t) \in (C^-, C^- + \delta)$, which means we are in the case of Condition 2 (ii), where we have the relation $f'(u(x,t)) \geq m_1\beta > 0$, i.e. the function is strictly increasing and with that

$$f(u(x,t)) \geq f(C^- + \beta) > 0 \quad \forall x \in \Omega \quad \forall t \geq T_c\,.$$

In summary we conclude for the situation of complete swelling

$$f(u(x,t)) \geq f(C^- + \gamma) > 0 \quad \forall x \in \Omega \quad \forall t \geq T_c \,, \text{ where } \gamma := \min(\beta, \delta) \qquad (3.66)$$

and in addition by Condition 2 (iii), (iv)

$$g(u(x,t)) \geq g(\zeta) > 0 \qquad \forall x \in \Omega \quad \forall t \geq T_c \,, \text{ where } \zeta := \min(\overline{\varrho}, C^- + \beta)\,. \qquad (3.67)$$

Substituting relation (3.66) into the model equation

$$\partial_t N_1(x,t) = -f(u(x,t))N_1(x,t) \,,$$

we obtain exponential convergence of $N_1(x,t)$ to 0:

$$\boxed{N_1(x,t) \leq N_{1,0}(x)e^{-f(C^-+\gamma)t} \leq \|N_{1,0}\|_{L^\infty(\Omega)}e^{-f(C^-+\gamma)t} \quad \forall x \in \Omega \quad \forall t \geq T_c \,.}$$

The second ODE

$$\partial_t N_2(x,t) = f(u(x,t))N_1(x,t) - g(u(x,t))N_2(x,t)$$

can be estimated by means of the previous result, Condition 1 (ii) and (3.67). This yields for $x \in \Omega$ and $t \geq T_c$

$$\partial_t N_2(x,t) \leq f^*\|N_{1,0}\|_{L^\infty(\Omega)}e^{-f(C^-+\gamma)t} - g(\zeta)N_2(x,t) \,.$$

Integration over $\int_0^t ds$ gives

$$N_2(x,t) \leq \underbrace{\|N_{2,0}\|_{L^\infty(\Omega)} + \frac{f^*}{f(C^- + \gamma)}\|N_{1,0}\|_{L^\infty(\Omega)}}_{=:\, C_{27} < \infty} - g(\zeta)\int_0^t N_2(x,s)\, ds \,,$$

whence follows with Gronwall's inequality the exponential convergence to 0:

$$\boxed{N_2(x,t) \leq C_{27}e^{-g(\zeta)t} \quad \forall x \in \Omega \quad \forall t \geq T_c \,.}$$

In analogy to the previous case, the conservation law (3.8) implies

$$N_{3,c}^\infty(x) = \overline{N}(x)$$

and it immediately follows with $\eta := \min\big(f(C^- + \gamma), g(\zeta)\big)$

$$\boxed{|N_3(x,t) - \overline{N}(x)| \leq \big(\|N_{1,0}\|_{L^\infty(\Omega)} + C_{27}\big)e^{-\eta t} \quad \forall x \in \Omega \quad \forall t \geq T_c \,.}$$

$$\square$$

Remark

For the third case $u^\infty = C^-$ no further details about the type of convergence can be made.

Proposition 15

Let the assumptions of Theorem 14 hold.

Then the solution $u(t)$ converges to u^∞ "exponentially fast", i.e. there exists $t_0 > 0$ and constants $k > 0$, $C > 0$ such that

$$\|u(t) - u^\infty\|_{L^2(\Omega)} \leq Ce^{-kt_0} \quad \text{for all } t \geq t_0,$$

which means we can obtain an arbitrary small norm by the choice of t_0 sufficiently large.

Proof

From Theorem 14 we know that $N_2(t)$ converges exponentially to 0 in $\mathcal{O}(e^{-kt})$, where $k := \min(g(\overline{\varrho}), g(\zeta))$. In addition, (3.33) states that the main part of the decomposition of $u(x,t)$ is non-decreasing, whence follows

$$\frac{d}{dt}a_1(t) \leq d_2 C_\varphi g^* \int_\Omega N_2(x,t)\, dx \leq d_2 C_\varphi g^* \lambda(\Omega) \|N_{2,0}\|_{L^\infty(\Omega)} e^{-kt}.$$

Integration over $\int_t^\infty ds$ yields

$$0 \leq a_1^\infty - a_1(t) \leq \underbrace{d_2 C_\varphi \frac{g^*}{k} \lambda(\Omega) \|N_{2,0}\|_{L^\infty(\Omega)}}_{=:C_{28} < \infty} e^{-kt},$$

i.e.

$$a_1^\infty - a_1(t) = |a_1^\infty - a_1(t)| \leq C_{28} e^{-kt} \quad \forall t > 0.$$

By the characterizaton of the first Fourier coefficient (3.32), the definition (3.30) of C_φ and the fact $u^\infty = a_1^\infty C_\varphi$, it follows for $t > 0$

$$a_1^\infty - a_1(t) = C_\varphi \int_\Omega u^\infty\, dx - C_\varphi \int_\Omega u(x,t)\, dx = C_\varphi \left(\|u^\infty\|_{L^1(\Omega)} - \|u(t)\|_{L^1(\Omega)} \right) \leq C_{28} e^{-kt}.$$

This relation induces that not $u(t)$ itself, but the mean value over Ω converges exponentially to the mean value of u^∞.

Remark

1.) Since we do not know the sign of $u^\infty - u(x,t)$ in Ω, we can not deduce exponential convergence of $u(t)$ to u^∞ in $L^1(\Omega)$.

2.) This kind of exponential mean value convergence is also known from the standard heat equation.

Now we take a look at second part of the decomposition. From (3.40) it follows with Condition 1 (ii)

$$\frac{d}{dt}\|\varphi^\perp(t)\|_{L^2(\Omega)}^2 + \gamma\|\varphi^\perp(t)\|_{L^2(\Omega)}^2 \leq C_{29}\|N_2(t)\|_{L^2(\Omega)}^2$$

and by Proposition 5 together with the exponential convergence of N_2, we have

$$\|\varphi^{\perp}(t)\|_{L^2(\Omega)}^2 \leq \|\varphi^{\perp}(t_0)\|_{L^2(\Omega)}^2 e^{-\gamma(t-t_0)} + C_{29} \int_{t_0}^{t} \|N_2(s)\|_{L^2(\Omega)}^2 \, ds$$

$$\leq \|\varphi^{\perp}(t_0)\|_{L^2(\Omega)}^2 e^{-\gamma(t-t_0)} + \frac{C_{29}}{k} \|N_{2,0}\|_{L^\infty(\Omega)}^2 \lambda(\Omega) \left(e^{-2kt_0} - e^{-2kt} \right)$$

for every $t \geq t_0$. Taking the limit, we obtain

$$\|\varphi^{\perp}(t)\|_{L^2(\Omega)}^2 \leq \underbrace{\frac{C_{29}}{k} \|N_{2,0}\|_{L^\infty(\Omega)}^2 \lambda(\Omega)}_{=: C_{30}} e^{-2kt_0} \quad \text{for every fixed } t_0 > 0 \text{ and } t \geq t_0.$$

In summary we obtain with the previous results for $t \geq t_0$

$$\|u(t) - u^\infty\|_{L^2(\Omega)}^2 = \int_\Omega |a_1(t) C_\varphi + \varphi^{\perp}(x,t) - a_1^\infty C_\varphi|^2 \, dx$$

$$\leq 2 C_\varphi^2 \lambda(\Omega) |a_1(t) - a_1^\infty|^2 + 2 \|\varphi^{\perp}(t)\|_{L^2(\Omega)}^2$$

$$\leq 2 C_\varphi^2 \lambda(\Omega) C_{28}^2 e^{-2kt} + 2 C_{30} e^{-2kt_0}$$

$$\leq (2 C_\varphi^2 \lambda(\Omega) C_{28}^2 + 2 C_{30}) e^{-2kt_0}$$

and the proof is complete.

□

3.2　Dirichlet boundary conditions

The mathematical analysis of the previous section is highly dependent on the chosen Neumann boundary conditions. We now want to study another *in vitro* model, where the test tube wall contains a substance that binds calcium ions. That means, more and more Ca^{2+} gets lost during the process and as we will see, we end up with $u = 0$.

For that we consider the same model with replaced boundary conditions:

$$\partial_t u = d_1 \Delta u + d_2 g(u) N_2 \tag{3.68}$$

$$\partial_t N_1 = -f(u) N_1 \tag{3.69}$$

$$\partial_t N_2 = f(u) N_1 - g(u) N_2 \tag{3.70}$$

$$\partial_t N_3 = g(u) N_2 \tag{3.71}$$

with boundary condition

$$u = 0 \text{ on } \partial\Omega. \tag{3.72}$$

Our aim now is to study the influence of this replacement.

In the following let $(u^D, N_1^D, N_2^D, N_3^D)$ denote the solution of (3.68) - (3.72). It turns out that the small change in the model description has a high impact on the mathematical results. There are three main differences occurring in the Dirichlet problem:

(i) Hopf's principle can not be applied any more.

(ii) The corresponding eigenvalue problem has different properties.

(iii) Wirtinger's inequality does not hold any more.

These will be explored in the sequel.

Hopf's principle

One main property that was used to study the asymptotic behavior of solutions was the boundedness of $u(x,t)$ by a positive constant $\varrho > 0$ for sufficiently large $t \geq t_0$ (c.f. Proposition 4). In order to obtain this lower bound, it was crucial to create a contradiction by use of Hopf's maximum principle, which states that the normal derivative at the boundary can not be zero. This fact was contrary to the assumption of homogenous Neumann boundary conditions, however it does not yield a contradiction in the Dirichlet case any more.

Hence with that we can not show that u^D stays away from zero and consequently the transition function $g(u^D)$ is not assured to be positive. In order to show the convergence result $N_2^{D,\infty}(x) \equiv 0$ in Theorem 6 we needed Proposition 4, which now does not hold any more. Due to $g(u^D)$ not necessarily being positive, we can not deduce that all mitochondria entering the state N_2^D will be transferred to N_3^D.

Corresponding eigenvalue problem

In Theorem 6 we also showed that the calcium concentration u strongly converges to a constant C. To prove this fact we essentially used the orthogonal decomposition

$$u(x,t) = a_1(t)\varphi_1(x) + \varphi^\perp(x,t)$$

with $\varphi_1(x)$ being the first eigenfunction of the corresponding eigenvalue problem

$$-\Delta\varphi_j(x) = \lambda_j\varphi_j(x), \quad x \in \Omega$$
$$\partial_\nu\varphi_j\big|_{\partial\Omega} = 0\,.$$

For this type of boundary condition it is known that $\varphi_1(x)$ is constant and with that we could show

$$u(x,t) \to u^\infty(x) = \lim_{t\to\infty} a_1(t)\,\varphi_1(x) \equiv C \quad \text{as } t \to \infty\,.$$

On the contrary for the corresponding Dirichlet eigenvalue problem

$$-\Delta\varphi_j^D(x) = \lambda_j^D\varphi_j^D(x), \quad x \in \Omega$$
$$\varphi_j^D\big|_{\partial\Omega} = 0$$

we can only deduce that the first eigenfunction is positive, but not constant. Even if we could show that the orthogonal complement $\varphi^{D,\perp}$ converges to 0 as in the Neumann case, like that we can not obtain information about the limit function $u^{D,\infty}(x)$. Thus the orthogonal decomposition is only helpful for the Neumann problem.

Wirtinger's inequality

In order to show some of the convergence results in Theorem 6 and Corollary 9, it was necessary to estimate $\|\varphi^\perp(t)\|_{L^2(\Omega)}$ by $\|\nabla\varphi^\perp(t)\|_{L^2(\Omega)}$. As a result of the orthogonality between $\varphi^\perp(t)$ and the constant eigenfunction $\varphi_1(x) \equiv C_\varphi$ in the Neumann case, we could apply Wirtinger's inequality (c.f. Lemma 7) to obtain this estimate.

However, for the Dirichlet problem this is not the case any more. But this problem can be easily solved, since due to the boundary condition we are now looking at functions from the Sobolev space $H_0^1(\Omega)$. In that space the well known Poincaré inequality is valid and we can work with the analogous estimate

$$\|v\|_{L^2(\Omega)} \le C_P \|\nabla v\|_{L^2(\Omega)} \quad \text{for } v \in H_0^1(\Omega)\,.$$

By use of this inequality we can show that in the Dirichlet case $\|u^D(t)\|_{L^2(\Omega)}$ stays bounded for all $t > 0$. Multiplying (3.68) by u^D and integrating over $\int_\Omega dx$, we get

$$\frac{1}{2}\frac{d}{dt}\|u^D(t)\|_{L^2(\Omega)}^2 + d_1\|\nabla u^D(t)\|_{L^2(\Omega)}^2 = d_2 \int_\Omega g(u^D(x,t))N_2^D(x,t)u^D(x,t)\,dx\,. \quad (3.73)$$

Remark
Integration by parts yields

$$\int_\Omega \Delta u\,u\,dx = \int_{\partial\Omega} \nabla u\,u\,\vec{n}\,dS - \int_\Omega \nabla u\,\nabla u\,dx = -\|\nabla u\|_{L^2(\Omega)}^2$$

regardless of which choice of homogenous boundary condition.

It turns out that (3.73) is exactly equation (3.39) from the Neumann case with $\varphi^\perp$ replaced by u^D. From here we can proceed in the same way by use of Poincaré's instead of Wirtinger's inequality and obtain

$$\frac{d}{dt}\|u^D(t)\|_{L^2(\Omega)}^2 + \underbrace{\frac{d_1}{C_P^2}}_{=:\,\gamma\,>\,0} \|u^D(t)\|_{L^2(\Omega)}^2 \le \frac{d_2^2 C_P^2}{d_1}\|g(u^D(t))N_2^D(t)\|_{L^2(\Omega)}^2 \quad (3.74)$$

$$\le \frac{d_2^2 C_P^2}{d_1}\lambda(\Omega)g^{*2}\|\overline{N}\|_{L^\infty(\Omega)}^2 =: C < \infty\,.$$

Now Proposition 5 can be applied with $y(t) := \|u^D(t)\|_{L^2(\Omega)}^2$ and yields

$$\|u^D(t)\|_{L^2(\Omega)}^2 \le \|u_0\|_{L^2(\Omega)}^2 + \frac{C}{\gamma} =: C_D < \infty \quad \text{for all } t > 0\,,$$

hence

$$\boxed{\sup_{t>0}\|u^D(t)\|_{L^2(\Omega)} \le C_D\,.} \quad (3.75)$$

By the continuous imbedding $L^2(\Omega) \hookrightarrow L^1(\Omega)$ it immediately follows

$$\boxed{\sup_{t>0}\|u^D(t)\|_{L^1(\Omega)} \le C_D\,.} \quad (3.76)$$

From (3.74) we can not directly deduce $u^D(x,t) \to 0$ in $L^2(\Omega)$ as we did in the analogous Neumann case for $\varphi^\perp$. For that we need $\|N_2^D\|_{L^1(0,\infty;L^1(\Omega))} < \infty$ in order to have $\int_0^\infty a(t)\,dt < \infty$ with $a(t) := \|g(u^D(t))N_2^D(t)\|_{L^2(\Omega)}^2$ to apply Proposition 5. This was shown in (3.36) and is, amongst others, based on Proposition 4, which is not valid any more.

However, we can derive the L^2-summability in a different way:

Since we will see that Theorem 2 also holds true in the Dirichlet case, it follows from (3.71) that $N_3^D(x,t)$ is non-decreasing in t for each $x \in \Omega$ and is bounded due to the conservation law: $N_3^D(x,t) \le \|\overline{N}\|_{L^\infty(\Omega)}$ (c.f. (3.24)). Thus the sequence converges and we have $N_3^D(x,t) \to N_3^{D,\infty}(x) \le \|\overline{N}\|_{L^\infty(\Omega)}$ as $t \to \infty$. Hence integrating (3.71) over $\int_0^t dt$ and passing to the limit, we obtain

$$\int_0^\infty g(u^D(x,t))N_2^D(x,t)\,dt = N_3^{D,\infty}(x) - N_{3,0}(x) < \infty \quad \forall x \in \Omega\,.$$

This yields $g(u^D)N_2^D \in L^1(0,\infty;L^1(\Omega))$, since we can estimate

$$\int_0^\infty \int_\Omega g(u^D(x,t))N_2^D(x,t)\,dx\,dt \le \lambda(\Omega)\int_0^\infty \sup_{x \in \Omega} g(u^D(x,t))N_2^D(x,t)\,dt < \infty\,.$$

Finally we arrive at the desired result

$$\int_0^\infty a(t)\,dt = \int_0^\infty \|g(u^D(t))N_2^D(t)\|_{L^2(\Omega)}^2\,dt \le g^*\|\overline{N}\|_{L^\infty(\Omega)}\|g(u^D)N_2^D\|_{L^1(0,\infty;L^1(\Omega))} < \infty\,,$$
(3.77)

which implies by use of Proposition 5

$$\boxed{u^D(x,t) \xrightarrow{t \to \infty} u^{D,\infty}(x) \equiv 0 \quad \text{strongly in } L^2(\Omega)\,.}$$
(3.78)

Remark
This convergence to zero makes clear that it is not possible to obtain a result like Proposition 4 in this case.

Summary

For the homogenous Dirichlet problem in comparison with the Neumann case major differences occur and hence we are not able to obtain all results from Section 3.1. Due to the facts noted above, we can not deduce uniform convergence of u^D and in particular we can not deduce a classification of partial and complete swelling. However as a result of $u^{D,\infty} \equiv 0 < C^-$, we assume that only partial swelling can occur. Nevertheless, many findings are in agreement with those from the Neumann problem as they are summarized in the next theorem.

Theorem 16
For the solution $(u^D, N_1^D, N_2^D, N_3^D)$ of the homogenous Dirichlet problem (3.68) - (3.72) the following assertions hold:

  (i) *Theorem 1 holds true.*

 (ii) *Theorem 2 holds true.*

(iii) *Under the assumptions of Theorem 2 we have the strong convergence results*

$$N_1^D(x,t) \xrightarrow{t \to \infty} N_1^{D,\infty}(x) \geq 0 \qquad in\ L^p(\Omega), \quad 1 \leq p < \infty$$

$$N_2^D(x,t) \xrightarrow{t \to \infty} N_2^{D,\infty}(x) \geq 0 \qquad in\ L^p(\Omega), \quad 1 \leq p < \infty$$

$$N_3^D(x,t) \xrightarrow{t \to \infty} N_3^{D,\infty}(x) \leq \|\overline{N}\|_{L^\infty(\Omega)} \quad in\ L^p(\Omega), \quad 1 \leq p < \infty$$

$$u^D(x,t) \xrightarrow{t \to \infty} u^{D,\infty}(x) \equiv 0 \qquad in\ L^2(\Omega)$$

and the solution u^D is bounded in the following sense:

$$\sup_{t>0} \|u^D(t)\|_{L^1(\Omega)} < \infty$$

$$\sup_{t>0} \|u^D(t)\|_{L^2(\Omega)} < \infty\,.$$

Proof

  (i) In the proof of existence and uniqueness of a global solution, the Dirichlet boundary
       condition comes only into play in the pure PDE (c.f. (3.16))

$$\partial_t \hat{u} = d_1 \Delta \hat{u} + d_2 g(\hat{u}) N_2^u$$
$$\hat{u}(x,0) = u_0(x)$$
$$\hat{u}\big|_{\partial\Omega} = 0\,.$$

       In analogy to the Neumann case, equations of such kind are treated in [2] or [13] and
       can also be embedded into the abstract framework of [40], which yield the desired
       results.

 (ii) The proof of solutions preserving non-negativity proceeds with exactly the same
       arguments as in the Neumann boundary case. Equation (3.22) also holds for ho-
       mogenous Dirichlet boundary conditions since $u\big|_{\partial\Omega} = 0$ implies $u^-\big|_{\partial\Omega} = 0$.

(iii) The convergence results of N_1^D, N_2^D, N_3^D follow without any influence of the modified
       boundary condition. However, as noted before we can not conclude $N_2^\infty(x) \equiv 0$ any
       more. The main effect of the Dirichlet boundary conditions becomes noticeable at the
       analysis of u^D. Here most of the results get lost due to the three reasons introduced
       earlier. The only information we can obtain with this method are the upper bounds
       (3.75) and (3.76) and the convergence (3.78).

$$\square$$

Remark
For the proof of Theorem 16 we do not require Conditions 2 and 3. The assumptions of
Condition 1 together with non-negative initial conditions are sufficient.

3.3 Robin boundary conditions

Now we want to proceed to the biologically more interesting case and study the behavior in the whole cell. Here the cell membrane is permeable and it is of major importance that the calcium concentration between the cell and the extracellular regime is maintained. In Section 2.3 we introduced the arguments leading to the following *in vivo* model:

$$
\begin{align}
\partial_t u &= d_1 \Delta(u) + d_2 g(u) N_2 & (3.79) \\
\partial_t N_1 &= -f(u) N_1 & (3.80) \\
\partial_t N_2 &= f(u) N_1 - g(u) N_2 & (3.81) \\
\partial_t N_3 &= g(u) N_2 & (3.82)
\end{align}
$$

with non-homogeneous Robin boundary conditions

$$
-\partial_\nu u = a(x)(u - \alpha) \text{ on } \partial\Omega , \qquad (3.83)
$$

where the constant $\alpha \geq 0$ represents the balance of concentration that is to be maintained. The boundary function $a(x)$ may be used to distinguish between different parts of the cell membrane.

Remark
Here we note again that the different initial conditions described in Section 2.3 are covered by the general case and hence we do not need to study them seperatly.

For the mathematical analysis we need to impose a condition on the function $a(x)$, i.e. a has to be bounded below by a positive constant:

$$
a \in L^\infty(\partial\Omega), \quad 0 < a_0 \leq a(x) \quad \text{for a.e. } x \in \partial\Omega . \qquad (\text{Cond.}a)
$$

In the following we denote by $(u^R, N_1^R, N_2^R, N_3^R)$ the corresponding solution of the Robin problem (3.79) - (3.83). In analogy to the previous section, here many mathematical tools do not apply anymore.

- First of all we do not have the the relation $(-\Delta u, u)_{L^2(\Omega)} = \|\nabla u\|_{L^2(\Omega)}^2 \geq 0$ as we had for the Neumann and Dirichlet case, since it now holds

$$
\int_\Omega -\Delta u^R u^R \, dx = \int_{\partial\Omega} a(x)(u^R - \alpha) \, u^R \, dS + \|\nabla u^R\|_{L^2(\Omega)}^2 .
$$

- By the same arguments as for the Dirichlet problem, we can not obtain a lower positive bound for $u^R(x,t)$ due to Hopf's principle not inducing a contradiction. Furthermore, we do not have an orthogonal decomposition with the first component being constant and neither Wirtinger's nor Poincaré's inequality are valid.

These facts pose many problems in applying the previous techniques to analyze the model. In particular for the existence of a unique solution of the pure PDE we need to introduce a new mathematical concept, which will also be of great importance for the degenerate diffusion model examined in Chapter 4.

Homogeneous case

At first we take a look at the homogeneous case $\alpha = 0$, i.e. (3.83) now reads

$$- \partial_\nu u = a(x)u \quad \text{on } \partial\Omega. \tag{3.84}$$

Then we obtain the following result similar to Theorem 16 of the previous section:

Theorem 17
For the solution $(u^R, N_1^R, N_2^R, N_3^R)$ of the homogeneous Robin problem (3.79) - (3.82) with boundary condition (3.84), the following assertions hold under the additional assumption of (Cond.a)*:*

  (i) Theorem 1 holds true.

  (ii) Theorem 2 holds true.

  (iii) Under the assumptions of Theorem 2 we have the strong convergence results

$$
\begin{aligned}
N_1^R(x,t) &\xrightarrow{t\to\infty} N_1^{R,\infty}(x) \geq 0 && in\ L^p(\Omega), \quad 1 \leq p < \infty \\
N_2^R(x,t) &\xrightarrow{t\to\infty} N_2^{R,\infty}(x) \geq 0 && in\ L^p(\Omega), \quad 1 \leq p < \infty \\
N_3^R(x,t) &\xrightarrow{t\to\infty} N_3^{R,\infty}(x) \leq \|\overline{N}\|_{L^\infty(\Omega)} && in\ L^p(\Omega), \quad 1 \leq p < \infty \\
u^R(x,t) &\xrightarrow{t\to\infty} u^{R,\infty}(x) \equiv \alpha = 0 && in\ L^2(\Omega).
\end{aligned}
$$

Proof

  (i) Again, the modified boundary condition comes only into play in the analysis of the pure PDE (c.f. (3.16))

$$
\begin{aligned}
\partial_t \hat{u} &= d_1 \Delta \hat{u} + d_2 g(\hat{u}) N_2^u \\
\hat{u}(x,0) &= u_0(x) \\
-\partial_\nu \hat{u} &= a(x)\hat{u} \qquad \text{for } x \in \partial\Omega.
\end{aligned} \tag{3.85}
$$

The existence and uniqueness of a global solution of such a problem can be obtained by applying the theory of maximal monotone operators, which is described in [9]. In Chapter 4 we will intensely use this mathematical concept, for which reason we introduce it in detail in Section 4.2. It states that we can rewrite (3.85) in the form

$$\partial_t \hat{u} = -d_1 M(\hat{u}) - B(\hat{u}) \tag{3.86}$$
$$\hat{u}(x,0) = u_0(x), \tag{3.87}$$

where M is a maximal monotone operator (c.f. Definition 22) in the phase space $L^2(\Omega)$ and $\hat{u} \mapsto B(\hat{u}) = -d_2 g(\hat{u}) N_2^u$ is Lipschitz continuous on $L^2(\Omega)$. Here the boundary condition is contained in the domain $D(M)$. Problems of this type are treated in [9], which yields the desired result and gives the properties of $\hat{u}$ stated in Theorem 1.

Hence it remains to choose an appropriate maximal monotone operator M. For that we need the notion of the subdifferential ∂ (c.f. Definition 20) and by Theorem 24 it follows $M = \partial\varphi$, where φ is a lower semi-continuous convex functional. In the sequel will we see that the function $\varphi : L^2(\Omega) \to [0, \infty]$ defined by

$$\varphi(u) := \begin{cases} \dfrac{1}{2} \displaystyle\int_\Omega |\nabla u|^2 \, dx + \dfrac{1}{2} \displaystyle\int_{\partial\Omega} a|u|^2 \, dS & \text{if } u \in H^1(\Omega) \\ \infty & \text{if } u \in L^2(\Omega) \setminus H^1(\Omega) \end{cases}$$

satisfies these properties.

In analogy to the proof of Proposition 25 we can show that φ is convex, lower semicontinuous and Gâteaux differentiable, which implies $\partial\varphi(u) = \{u^*\}$, where u^* is to be determined. Thus it remains to prove $u^* = -\Delta u$. By definition, a subgradient $u^* \in \partial\varphi(u)$ fulfills

$$\langle u^*, v - u \rangle = (u^*, v - u)_{L^2(\Omega)} \overset{!}{\leq} \varphi(v) - \varphi(u)$$

and for functions $u \in L^2(\Omega)$ satisfying the boundary condition (3.84) it holds

$$\int_\Omega -\Delta u \, (v - u) \, dx = \int_{\partial\Omega} au \, (v - u) \, dx + \int_\Omega \nabla u \, \nabla (v - u) \, dx \, .$$

This can be further estimated by use of Hölder's and Young's inequality

$$\begin{aligned} \leq \ & \frac{1}{2} \int_{\partial\Omega} a|u^2| \, dS + \frac{1}{2} \int_{\partial\Omega} a|v^2| \, dS - \int_{\partial\Omega} a|u^2| \, dS \\ & + \frac{1}{2} \int_\Omega |\nabla u|^2 \, dx + \frac{1}{2} \int_\Omega |\nabla v|^2 \, dx - \int_\Omega |\nabla u|^2 \, dx \\ = \ & \varphi(v) - \varphi(u) \end{aligned}$$

and thus $u^* = -\Delta u$. Since we know that $\partial\varphi$ is single-valued, $\partial\varphi : u \mapsto -\Delta u$ is a mapping from $L^2(\Omega)$ into $L^2(\Omega)$ defined for u satisfying (3.84). That implies

$$D(\partial\varphi) = \{u \in H^2(\Omega) : -\partial_\nu u = a(x)u \text{ on } \partial\Omega\} \, ,$$

i.e. the domain $D(\partial\varphi)$ includes the boundary condition and we found an appropriate function φ to obtain (3.86), (3.87). This yields the existence of a unique global solution of the pure PDE (3.85).

In order to assure the local and global existence of $(u^R, N_1^R, N_2^R, N_3^R)$ to the original system, we can repeat the same arguments as for the Neumann boundary case. This is possible since for $\alpha = 0$ we have by (Cond.a)

$$\int_\Omega -\Delta u^R u^R \, dx = \int_{\partial\Omega} a(x)|u^R|^2 \, dS + \|\nabla u^R\|_{L^2(\Omega)}^2 \geq 0 \, .$$

(ii) We assume non-negative initial data $u_0(x) \geq 0$ and $N_{i,0}(x) \geq 0$ for $i = 1, 2, 3$. Then the non-negativity of $N_i^R(x, t)$ for $t > 0$ is shown by exactly the same arguments as in the proof of Theorem 2. Multiplying (3.79) by the negative part u^{R-} and integrating $\int_\Omega dx$, we obtain

$$-\frac{1}{2}\frac{d}{dt}\|u^{R-}\|_{L^2(\Omega)}^2 = d_1 \int_{\partial\Omega} a|u^{R-}|^2\, dS + \|\nabla u^{R-}\|_{L^2(\Omega)}^2 + d_2 \int_\Omega g(u^R)N_2^R u^{R-} \geq 0$$

and hence

$$\frac{d}{dt}\|u^{R-}\|_{L^2(\Omega)}^2 \leq 0\,,$$

which implies the property of preserving non-negativity.

(iii) The convergence of $N_i^R(x, t) \to N_i^{R,\infty}(x)$ in $L^p(\Omega)$, $1 \leq p < \infty$ can be proved with the same arguments as in Neumann boundary case. However, as we already noted in Section 3.2, we can not verify $N_2^{R,\infty} \equiv 0$, since we can not obtain the strict positivity of u as in Proposition 4.

In the following we show that for the Robin boundary problem the solution u^R converges to zero in $L^2(\Omega)$. Here we can neither apply Wirtinger's nor Poincaré's inequality, but the following lemma finds a remedy:

Lemma 18 (Friedrich's inequality)
Let $v \in H^1(\Omega)$. Then there exists a positive constant C_F such that

$$\|v\|_{L^2(\Omega)}^2 \leq C_F \left(\|\nabla v\|_{L^2(\Omega)}^2 + \int_{\partial\Omega} |v|^2\, dS \right).$$

A proof of this inequality can be found in [52].

Remark
Friedrich's inequality is a generalization of Poincaré's inequality for functions satifsying arbitrary boundary conditions.

In order to derive the convergence of $\|u^R\|_{L^2(\Omega)}$, we multiply (3.79) by u^R and integrate over $\int_\Omega dx$. This yields with (Cond.a)

$$\frac{1}{2}\frac{d}{dt}\|u^R\|_{L^2(\Omega)}^2 + \int_\Omega |\nabla u^R|^2\, dx + a_0 \int_{\partial\Omega} |u^R|^2\, dS \leq d_2\|g(u^R)N_2^R\|_{L^2(\Omega)}\|u^R\|_{L^2(\Omega)}\,.$$

By Friedrich's inequality there exists a positive constant $C > 0$ such that

$$\|u^R\|_{L^2(\Omega)}^2 \leq C_F C \left(\|\nabla u^R\|_{L^2(\Omega)}^2 + a_0 \int_{\partial\Omega} |u^R|^2\, dS \right).$$

Inserting this estimate we obtain

$$\frac{1}{2}\frac{d}{dt}\|u^R\|_{L^2(\Omega)}^2 + \frac{1}{C_F C}\|u^R\|_{L^2(\Omega)}^2 \leq d_2\|g(u^R)N_2^R\|_{L^2(\Omega)}\|u^R\|_{L^2(\Omega)}$$

and Young's inequality yields

$$\frac{1}{2}\frac{d}{dt}\|u^R\|_{L^2(\Omega)}^2 + \frac{1}{2C_FC}\|u^R\|_{L^2(\Omega)}^2 \le \frac{d_2^2 C_F C}{2}\|g(u^R)N_2^R\|_{L^2(\Omega)}^2.$$

From Proposition 5 it follows with the same arguments as in the previous cases by use of (3.77)

$$\boxed{u^R(x,t) \xrightarrow{t\to\infty} u^{R,\infty}(x) \equiv 0 \quad \text{strongly in } L^2(\Omega)\,.}$$

This finishes the proof of Theorem 17.

$\square$

Inhomogeneous case

Based on these findings we now consider the model (3.79) - (3.82) with inhomogeneous Robin boundary conditions (3.83) for the general case $\alpha \ge 0$. Here we obtain a similar result

Theorem 19

For the general Robin problem (3.79) - (3.83) *all assertion of Theorem 17 hold true with*

$$u^{R,\infty} \equiv \alpha \ge 0\,.$$

Proof

In order to study this type of boundary condition, we define

$$\boxed{v(x,t) := u(x,t) - \alpha\,.}$$

Then v satisfies

$$\partial_t v = d_1 \Delta v + d_2 g(v+\alpha)N_2$$

with homogeneous Robin boundary condition

$$-\partial_\nu v = a(x)v \text{ on } \partial\Omega\,.$$

By the properties of f and g, shifting $v \curvearrowright v + \alpha$ does not change the mathematical analysis and hence applying the previous arguments we can prove Theorem 17 with u replaced by v. Consequently it also follows $\|v\|_{L^2(\Omega)} \to 0$, i.e.

$$\boxed{u^R(x,t) \xrightarrow{t\to\infty} u^{R,\infty}(x) \equiv \alpha \quad \text{strongly in } L^2(\Omega)\,.}$$

It only remains to show the non-negativity of u^R for general $\alpha \ge 0$. We proceed in analogy to (*ii*) of the proof of Theorem 17. Here it holds

$$\int_\Omega \Delta u^R u^{R-}\,dx = \int_\Omega |\nabla u^{R-}|^2\,dx - \int_{\partial\Omega} a((u^{R+} - u^{R-}) - \alpha)u^{R-}\,dS$$

$$= \int_\Omega |\nabla u^{R-}|^2\,dx + \int_{\partial\Omega} a(|u^{R-}|^2 + \alpha u^{R-})\,dS \ge 0$$

and hence by the same arguments the property of preserving non-negativity follows.

$\square$

Biological interpretation

Biologically the convergence of $u(x,t)$ to α is exactly the result we expected. Additional Ca^{2+} is removed from the cell and the calcium gradient is again stabilized. Here it is interesting to take a look at the relation of α and the swelling threshold C^-. Based on the classification of partial and complete swelling we obtained for the *in vitro* model, one could conjecture that we have an analogous classification here, i.e. $\alpha > C^-$ leading to complete swelling and $\alpha < C^-$ inducing partial swelling.

However, $u(x,t) \equiv \alpha$ is also the situation when the whole system is in rest, that means when we do not have any induction of mitochondrial swelling. α being greater than C^- would hence imply that without any outer influence the cell dies immediately by apoptosis due to all mitochondria getting swollen. This allows only for the conclusion $\alpha < C^-$.

Now the distinction between partial and complete swelling is only dependent on the parameter values:

- A low diffusion rate d_1 together with a high feedback rate d_2 can lead to **complete swelling**, when the initially high calcium peak is not dissolved too fast and the resulting calcium wave reaches every mitochondrion with a sufficiently high amplitude bigger than C^-.

- On the other hand, the opposite direction of high diffusion and small feedback brings forward the fast diffusion of calcium, which then leads to **partial swelling**.

- As we will see in the numerical simulations, this distinction is also highly dependent on the boundary parameter a, which determines the speed of the calcium efflux.

3.4 Numerical simulation

Now we want to verify the obtained mathematical results numerically. The varying settings for the *in vitro* and the *in vivo* model are elaborated in Section 2.3.

As described earlier, the model functions f and g have a sigmoidal shape determined in the following way:

$f(u)$: Transition rate from unswollen to swelling mitochondria dependent on the local Ca^{2+} concentration

$$
f(s) = \begin{cases}
0 & \text{for } s < C^- \\
f^* & \text{for } s > C^+ \\
-\frac{f^*}{2} \cos\left(\frac{s - C^-}{C^+ - C^-}\pi\right) + \frac{f^*}{2} & \text{else}
\end{cases}
$$
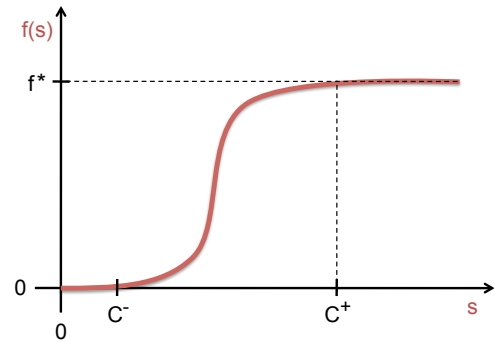
Figure 3.1 – Transition rate f

$g(u)$: "Dying" term describing the transition of mitochondria in the swelling process to completely swollen ones where the membrane is ruptured and stored Ca^{2+} is released

$$
g(s) = \begin{cases}
g^* & \text{for } s > C^+ \\
-\frac{g^*}{2} \cos\left(\frac{s}{C^+}\pi\right) + \frac{g^*}{2} & \text{else}
\end{cases}
$$
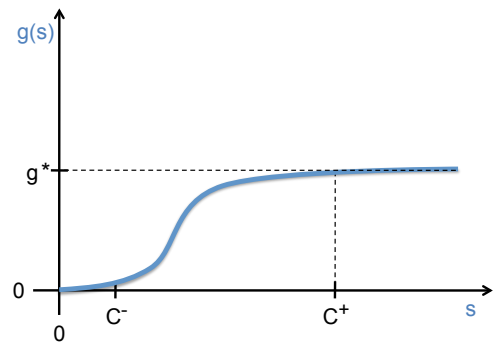
Figure 3.2 – Transition rate g

3.4.1 The *in vitro* model

Model parameters

The model parameters we used for the *in vitro* simulations are noted in Table 3.1.

Name	Description	Value
d_1	diffusion parameter	0.2
d_2	feedback parameter	30
f^*	maximal transition rate $N_1 \curvearrowright N_2$	1
g^*	maximal transition rate $N_2 \curvearrowright N_3$	0.1
C^-	threshold of initiating $N_1 \curvearrowright N_2$	20
C^+	saturation threshold	200
$h_x = \frac{1}{N}$	step size of space discretization	$\frac{1}{40}$
h_t	step size of time discretization	1

Table 3.1 – *In vitro* simulation: Model parameters I

Discretization

The domain Ω is discretized with step size $h_x = \frac{1}{N}$ leading to the discrete domain

$$\Omega_h = \{(x_i, x_j)\}_{i,j=0,\dots,N} = \{(ih_x, jh_x) : i = 0, \dots, N, \ j = 0, \dots, N\}$$

of size $(N + 1) \times (N + 1)$.

The time interval will be discretized with time steps of length h_t which results in the discrete time interval

$$T_h = \{t_k\}_{k \in \mathbb{N}_0} = \{kh_t : k \in \mathbb{N}_0\}\,.$$

On that domain $\Omega_h \times T_h$ we define the grid solution $(u_h, N_{1h}, N_{2h}, N_{3h})$.

Numerical approximation

The PDE describing the calcium diffusion process is discretized with respect to space by means of the standard finite difference approach. Here the Laplacian is approximated by use of the five point star. Doing so, the PDE is transferred into an ODE and we end up with an ODE system on the discrete domain Ω_h, that shall be solved for the discrete time steps $t_k \in T_h$. Due to the low numerical complexity of the model, this can be easily achieved by using the explicit Euler method. The homogeneous Neumann boundary condition is realized by introducing phantom points in order to calculate the normal derivative at the boundary.

Initial values

As we pointed out earlier, in the beginning all mitochondria are intact and with that neither in the swelling process nor completely swollen, i.e.

$$N_{1,0}(x) \equiv 1, \quad N_{2,0}(x) \equiv 0, \quad N_{3,0}(x) \equiv 0\,.$$

For the calcium concentration it is not so clear how to determine the initial state. The initial value $u_0(x)$ defines the distribution of the added Ca^{2+} amount. At this the rate of diffusion progression as well as the dosage location is of great importance. Therefore one can imagine different possible initial states. Here we take a look at the grid solution u_h and determine initial values u_{0h}. In all cases we assume that the total amount of added Ca^{2+} is the same, i.e.

$$\sum_{x_i,x_j \in \Omega_h} u_{0h}(x_i, x_j) \equiv C_{tot} \,.$$

1) Highly localized: The total calcium amount C_{tot} is located at one single point (x_k, x_l) in Ω_h:

$$u_{0h}(x_k, x_l) = C_{tot}$$
$$u_{0h}(x_i, x_j) = 0 \qquad \text{for } i \neq k, j \neq l, \quad x_i, x_j \in \Omega_h \,.$$

Figure 3.3 shows two possible distributions.

(a) Center: $(x_k, x_l) = (0.5, 0.5)$ (b) Close to boundary: $(x_k, x_l) = (0.5, 0.95)$
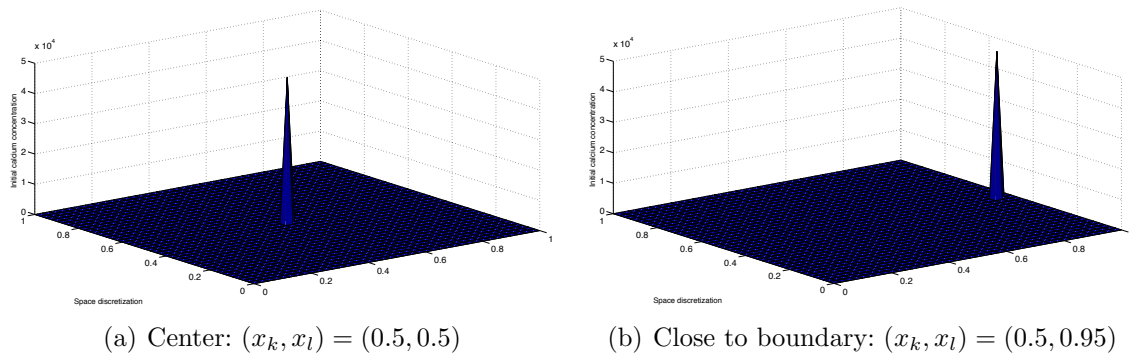
Figure 3.3 – Localized initial calcium distribution

2) Normally distributed: The initial calcium concentration is determined by a sector of the standard normal distribution. Figure 3.4 depicts the meaning of a sector of the normal distribution for the 1D case .
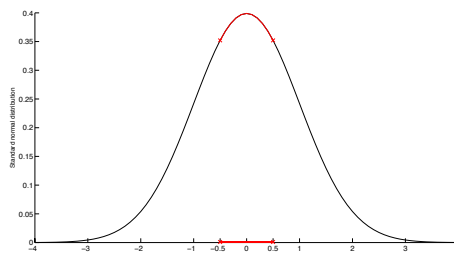
Figure 3.4 – Sector of the 1D standard normal distribution

In 2D the density function is given by

$$N(y_1, y_2) = \frac{1}{2\pi} \exp\left(-\frac{1}{2}(y_1^2 + y_2^2) \right)$$

and the sector for the interval $[y_l, y_r]$ is obtained by the translation

$$y \curvearrowright \tilde{y} := (y_r - y_l) \cdot y + y_l \,.$$

Thus the initial Ca^{2+} concentration adapted to the total calcium amount is given by

$$u_{0h}(x_i, x_j) = C_{tot} \cdot \frac{N(\tilde{x}_i, \tilde{x}_j)}{\sum_{x_i, x_j \in \Omega_h} N(\tilde{x}_i, \tilde{x}_j)} \,, \quad x_i, x_j \in \Omega_h \,.$$

The next Figure 3.5 shows the resulting initial calcium distributions for different sector intervals $[y_l, y_r]$.

(a) $y_l = -0.5$, $y_r = 0.5$

(b) $y_l = -1$, $y_r = 1$

(c) $y_l = -2$, $y_r = 2$

(d) $y_l = -3$, $y_r = 3$

(e) $y_l = -0.8$, $y_r = 0.2$

(f) $y_l = -1$, $y_r = 3$
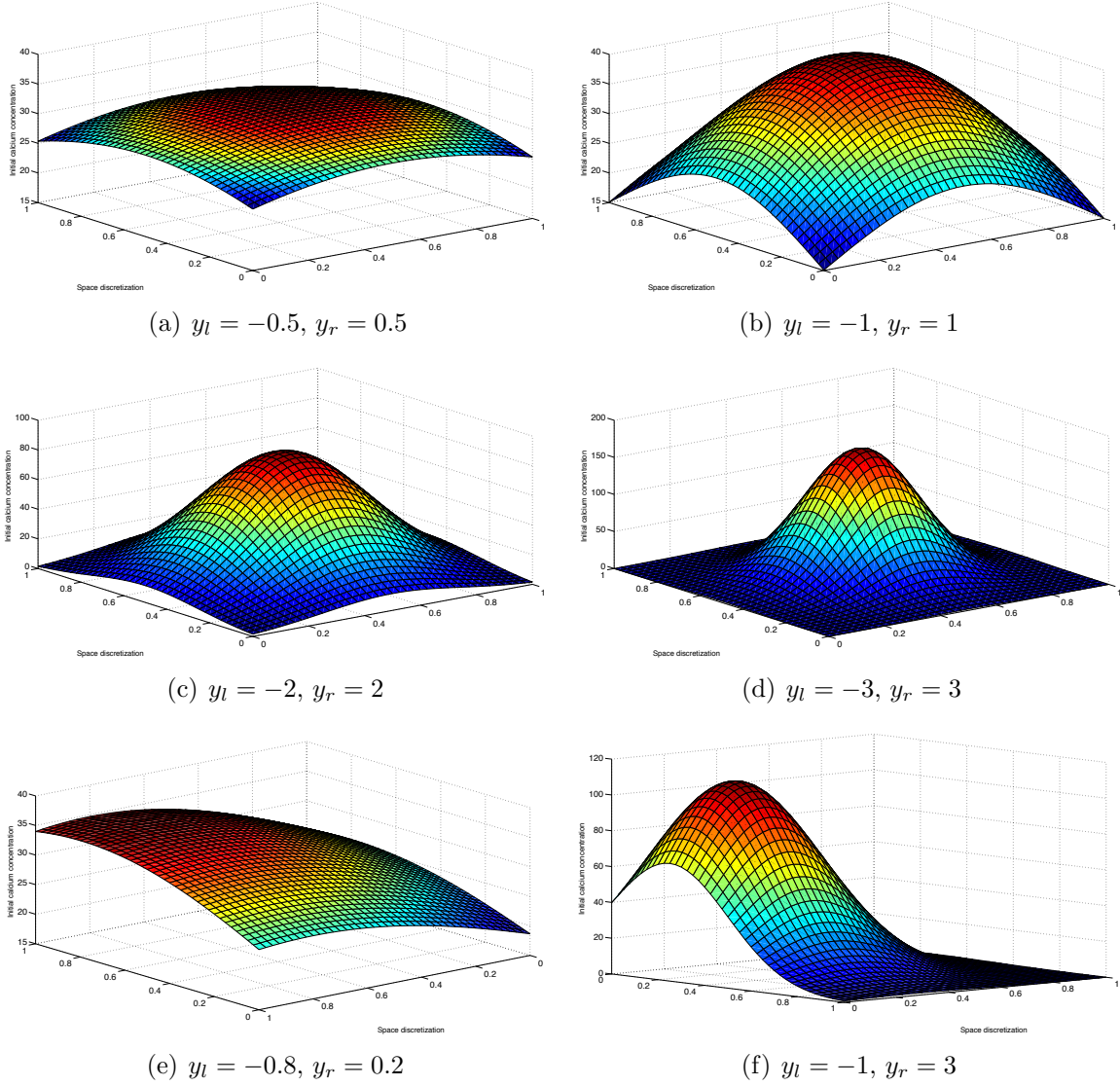
Figure 3.5 – Normally distributed initial calcium distribution

3) Constant: As a consequence of complete diffusion the initial calcium distribution is constant, i.e.

$$u_{0h}(x_i, x_j) = \frac{C_{tot}}{(N+1)^2} \,, \quad x_i, x_j \in \Omega_h \,.$$

Simulation

Now everything is prepared for the numerical simulations, which were done using the commercial software MATLAB.

The following pages show the time evolution of the numerical solutions for five different initial calcium concentrations displayed column by column:

Column $\boxed{1}$	Column $\boxed{2}$	Column $\boxed{3}$	Column $\boxed{4}$	Column $\boxed{5}$
Localized at point $x = (0.5, 0.5)$	Localized at point $x = (0.5, 0.95)$	Normally distributed on sector $[-1, 3]$	Normally distributed on sector $[-2, 2]$	Normally distributed on sector $[-0.5, 0.5]$
$\boxed{t = t_1}$	$\boxed{t = t_1}$	$\boxed{t = t_1}$	$\boxed{t = t_1}$	$\boxed{t = t_1}$
$\vdots$	$\vdots$	$\vdots$	$\vdots$	$\vdots$
$\boxed{t = t_{10}}$	$\boxed{t = t_{10}}$	$\boxed{t = t_{10}}$	$\boxed{t = t_{10}}$	$\boxed{t = t_{10}}$

For every data collection we used the same total amount of initial Ca^{2+}

$$C_{tot} = 30 \cdot (N + 1)^2 \,,$$

i.e. the difference between each column only lies in the localization and the degree of calcium diffusion. The simulations show that for every constellation this calcium amount is high enough to induce *complete swelling*.

Figures 3.6 - 3.9 show the evolution of the model variables u_h, N_{1h}, N_{2h} and N_{3h} column-wise for the five different initial conditions mentioned above. Each row displays the different states at one time step. From the simulations it becomes clear that the choice of the initial calcium distribution is of great importance for the duration as well as the dynamics of the whole process.

One remarkable result is the clearly visible spreading calcium wave. If we compare the dynamics with those of simple diffusion without any feedback, the resulting calcium evolution induced by mitochondrial swelling is indeed completely different.

The numerical simulations also show that at much lower initial calcium concentrations, the model outcome depends on the location and type of the initial calcium distribution. As we can see there, a small change in the initial distribution of Ca^{2+} is enough to shift the behavior from partial to complete swelling.
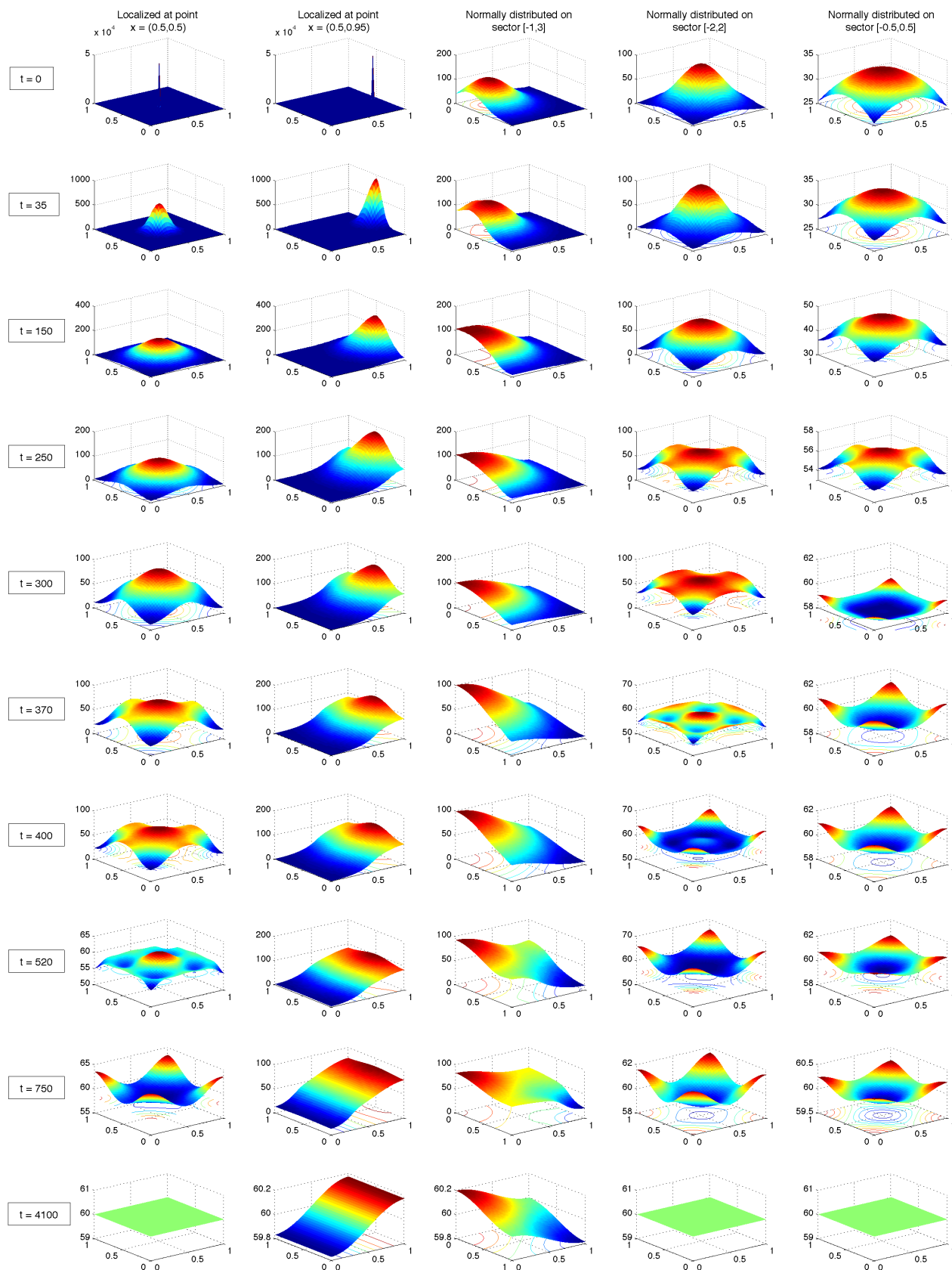
Figure 3.6 – Time development of the **calcium concentration u_h** for different initial calcium concentrations
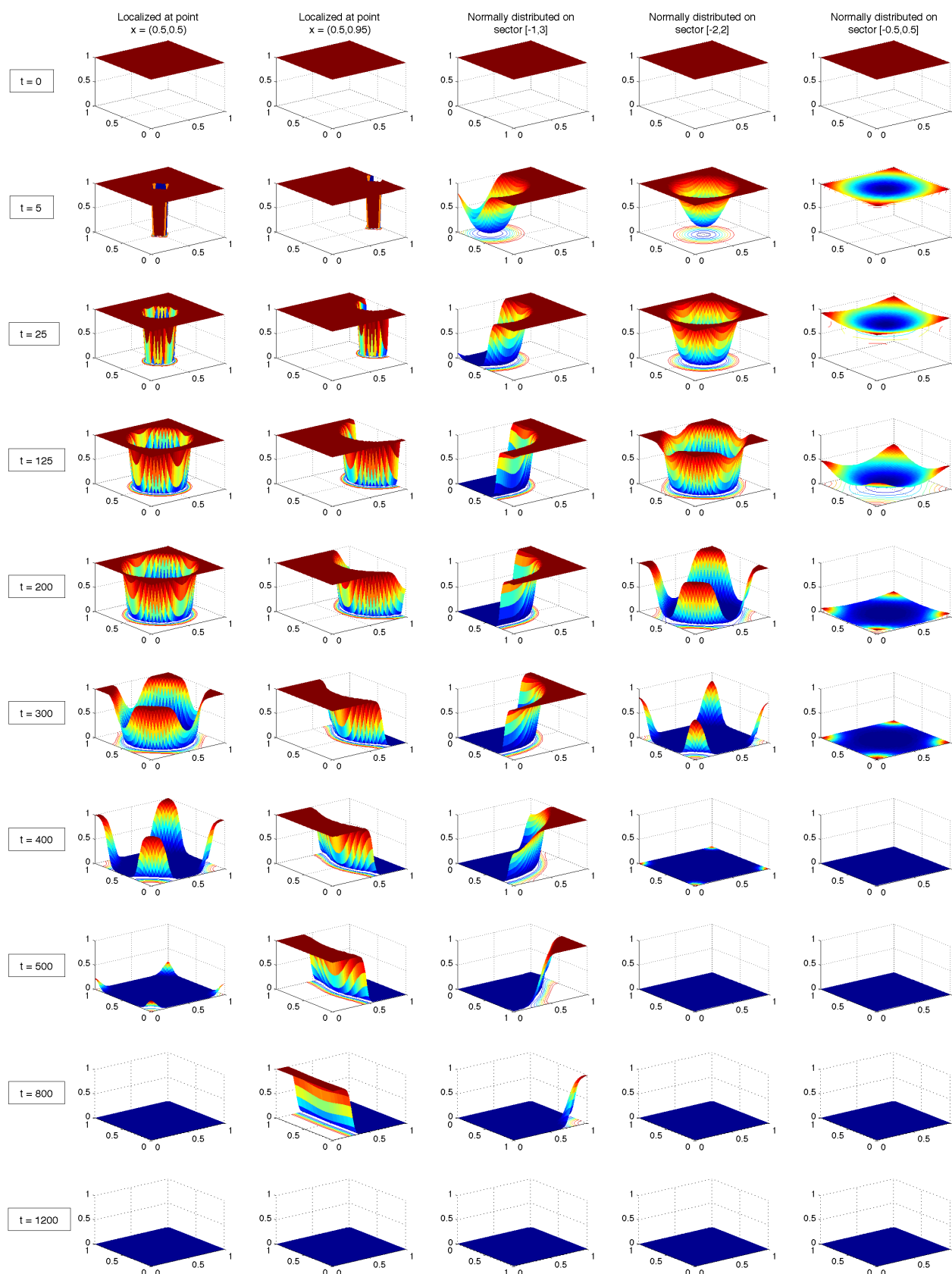
Figure 3.7 – Time development of the **unswollen mitochondrial subpopulation N_{1h}** for different initial calcium concentrations
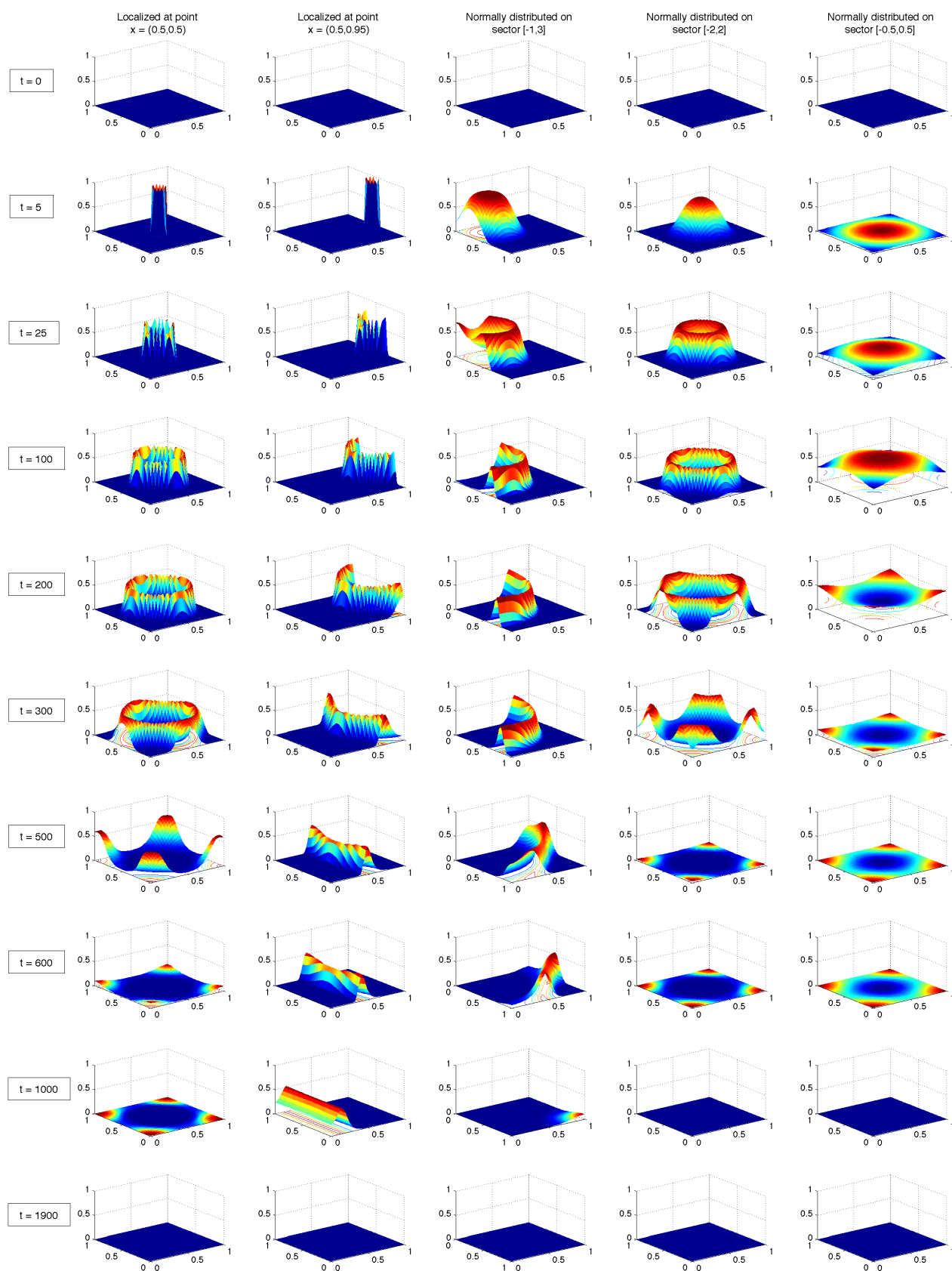
Figure 3.8 – Time development of the **intermediate mitochondrial subpopulation N_{2h}** for different initial calcium concentrations
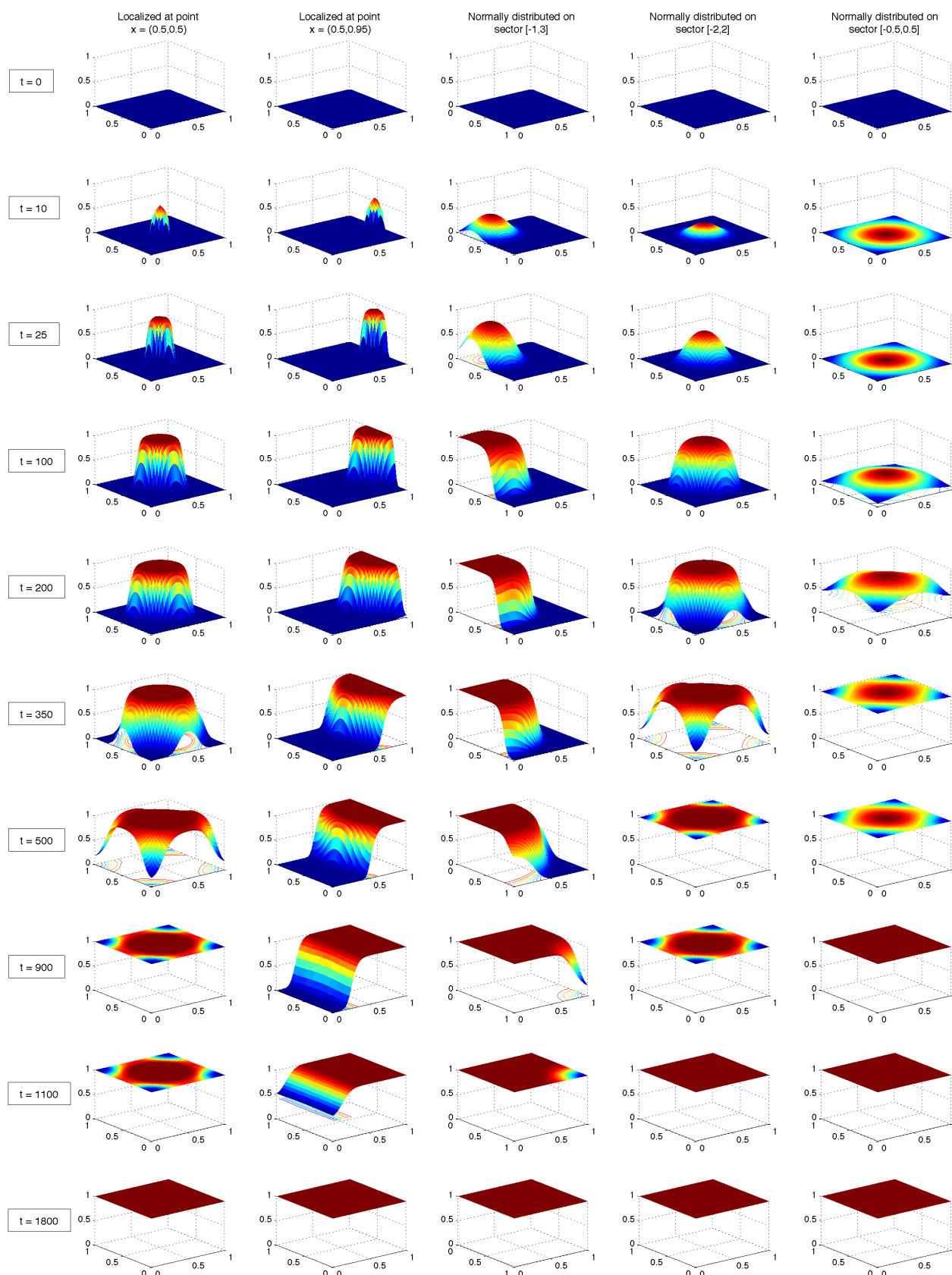
Figure 3.9 – Time development of the **swollen mitochondrial subpopulation N_{3h}** for different initial calcium concentrations
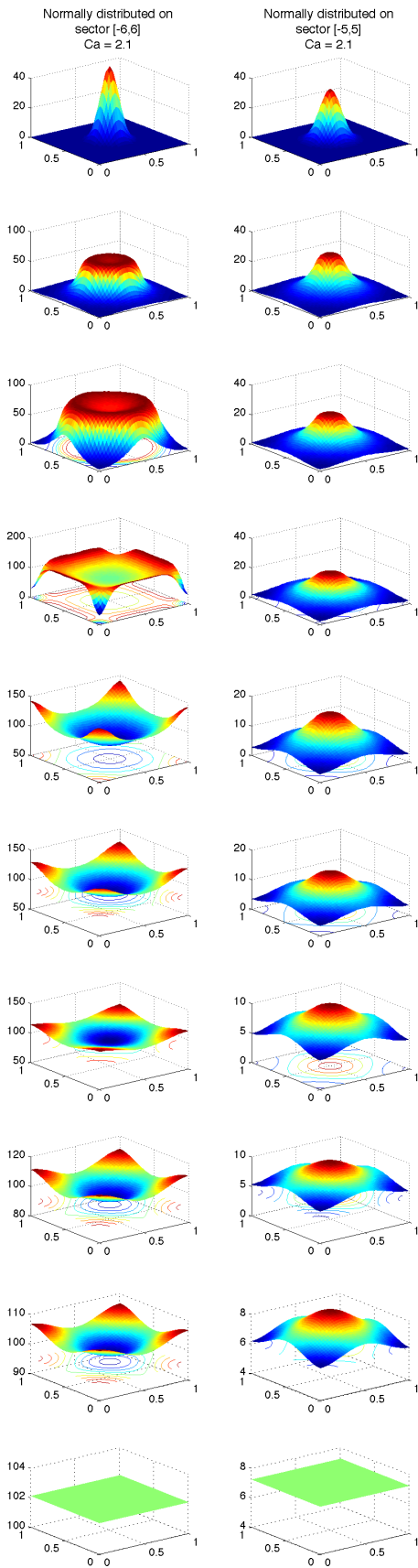
Here we consider a much lower total amount of calcium, $C_{tot} = 2.1 \cdot (N + 1)^2$ added in two varying initial distributions. The simulations show that this small change in the degree of localization decides between partial and complete swelling. Here we only show the evolution of u_h and N_{1h} in order to get a qualitative description of the difference between partial and complete swelling. The remaining variable N_{3h} behaves in a similar manner, whereas N_{2h} converges to zero regardless of the situation. We know that $N_{1h}^\infty + N_{3h}^\infty = 1$, hence N_{3h}^∞ represents the complement of N_{1h}^∞.
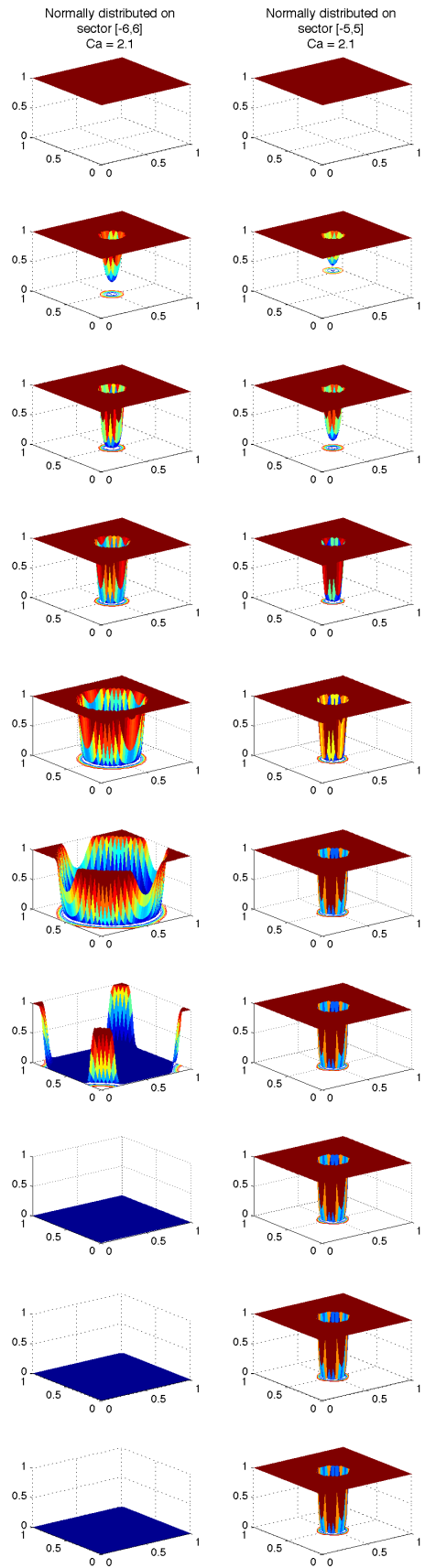
Comparison with experimental data

Up to now, we do not have any experimental data including the spatial development. As we already explained, the existing data measure mitochondrial swelling in terms of light scattering at different calcium concentrations as can again be seen in Figure 3.10:
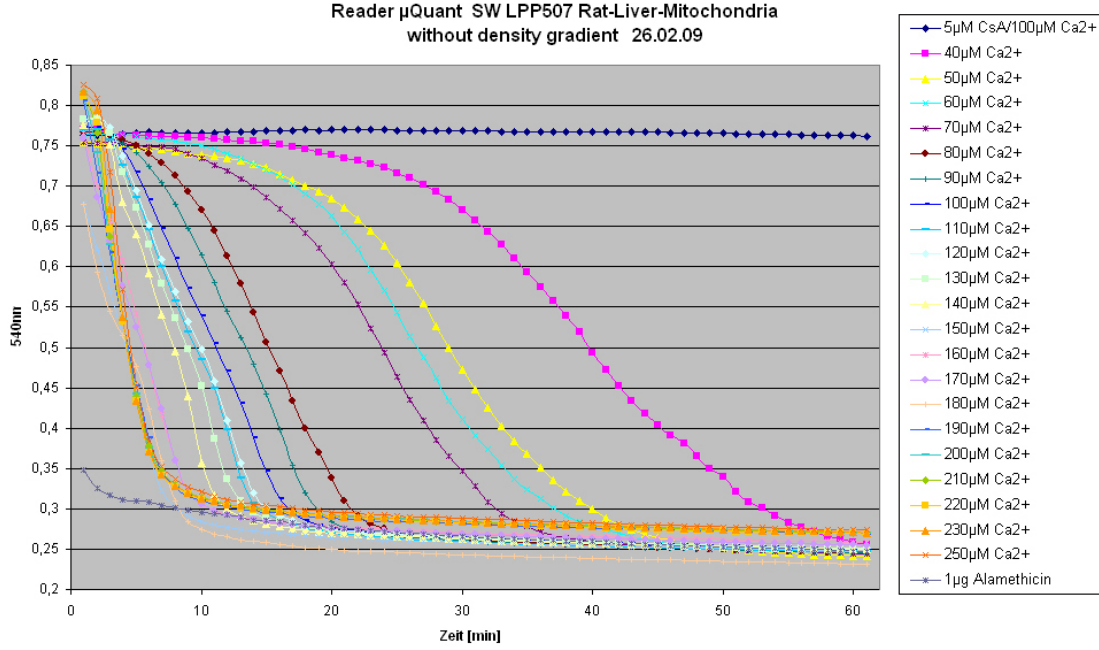
Figure 3.10 – Experimental data of mitochondrial swelling at different Ca^{2+} concentrations

In order to compare the obtained solutions with the experimental data, we now have to take a look at the combined volume of all three subpopulations. As described in Section 2.2.1, this is obtained by summing the weighted mean values over the whole domain Ω_h. These averages are given by

$$I_{1h}(t_k) = \frac{1}{(N+1)^2} \sum_{x_i, x_j \in \Omega_h} N_{1h}(x_i, x_j, t_k)$$

$$I_{2h}(t_k) = \frac{1}{(N+1)^2} \sum_{x_i, x_j \in \Omega_h} N_{2h}(x_i, x_j, t_k)$$

$$I_{3h}(t_k) = \frac{1}{(N+1)^2} \sum_{x_i, x_j \in \Omega_h} N_{3h}(x_i, x_j, t_k)$$

and with that in accordance with the previously introduced volume equation (2.4), the volume is set up as

$$V(t_k) = V_0 \cdot I_{1h}(t_k) + kV_p \cdot I_{2h}(t_k) + V_p \cdot I_{3h}(t_k), \quad t_k \in T_h. \tag{3.88}$$

Here we choose the initial mitochondrial volume V_0 and the volume of completely swollen mitochondria V_p in accordance with [43]. The parameter $0 < k < 1$ determines the volume

of mitochondria in the swelling process as a fixed percentage of the final volume V_p. For the simulations we used the values from Table 3.2.

Name	Description	Value
V_0	initial volume	1.2
V_p	final volume	1.7
k	intermediate volume parameter	0.68

Table 3.2 – *In vitro* simulation: Model parameters II

As we showed in [22], there is a linear dependence between the total mitochondrial volume and the measured light scattering change. Thus for the simulation, the optical density values are given by $0.95 - V(t_k)$, $t_k \in T_h$ resulting in the biologically reasonable range between 0.25 and 0.75.

In the experiment the added Ca^{2+} concentrations are high enough to induce complete swelling. Thus we apply volume formula (3.88) to the solution $(u_h, N_{1h}, N_{2h}, N_{3h})$ of the complete swelling case as depicted in Figures 3.6 - 3.9.

Figure 3.11 shows the evolution of each subpopulation in total and displays the resulting optical density values. Here it becomes clear that different initial calcium conditions indeed result in completely different curve shapes. In the following we want to explain the varying curve progressions biologically.
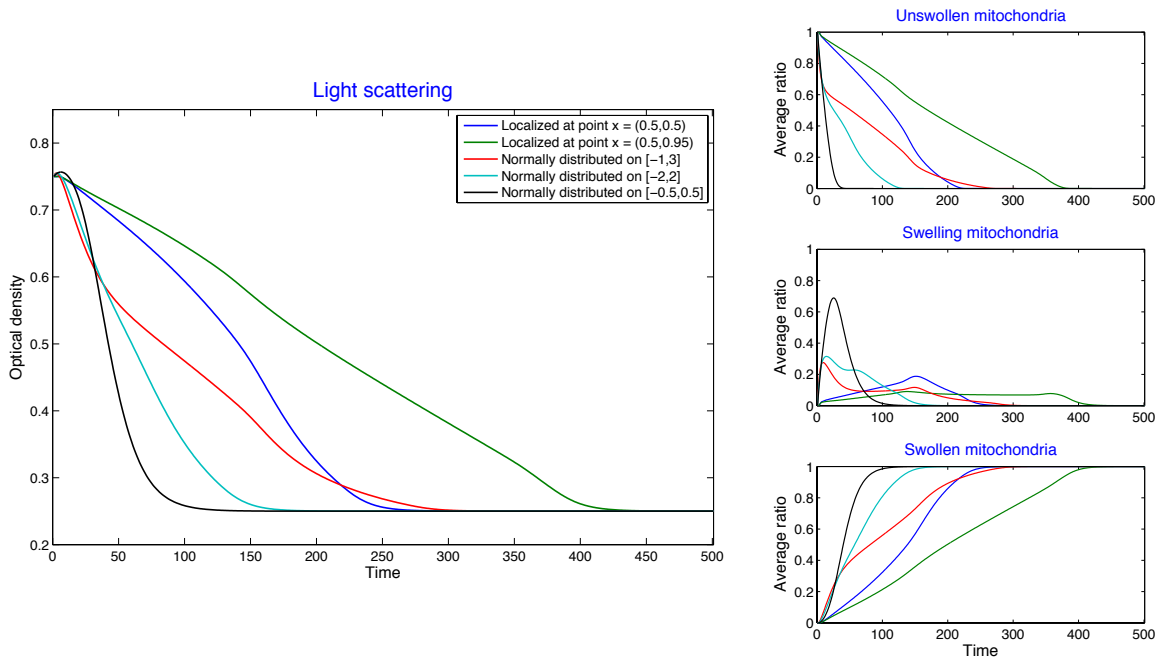
Figure 3.11 – Time development of the average mitochondrial subpopulations and the resulting light scattering values for different initial calcium concentrations

1) *Swelling time*

As one can expect from the 2D simulations, the green line (column $\boxed{2}$) is the slowest one. Due to the most "unfavorable" initial calcium distribution it takes the longest time until all mitochondria are swollen and the lowest optical density value is reached. The shape of the swelling curve displays the linear style of wave propagation.

On the other hand the black line (column $\boxed{5}$) presents the most "favorable" initial condition and the equilibrium is reached soon. The initial calcium concentration at every point in Ω_h lies above the initiation threshold C^- and thus all mitochondria start swelling immediately. Since there is only little variation over the domain, the whole process is running in a very uniform way. If we take a look at the corresponding 'Swelling mitochondria' curve, it is clearly to be seen how the black line increases and decreases very steep within a short period of time. This shows the simultaneity of the incidents because first all mitochondria enter the swelling process at the same time and subsequently complete the swelling process nearly simultaneously. However the transition $N_2 \curvearrowright N_3$ is dependent on the local calcium concentration, which is locally not so high compared to the other situations due to the high rate of dispersion. This fact explains why the black swelling curve is the slowest one in the very beginning.

The remaining curves (columns $\boxed{1}$, $\boxed{3}$ and $\boxed{4}$) lie in between and we see that the centered normally distributed initial conditions produce the fastest swelling times.

2) *Number of phases*

Another thing that immediately attracts attention are the different types of curve progression. In particular for the red line (column $\boxed{3}$) the two-phase shape becomes very obvious. This special appearance can be explained by the different dynamics of calcium diffusion. Figure 3.12 studies the two dimensional diffusion process on the quadratic domain Ω. It depicts the dependence of the spreading dynamics on the source location under the assumption of zero flux conditions on the boundary.

| (a) Center | (b) Close to egde | (c) Close to corner |
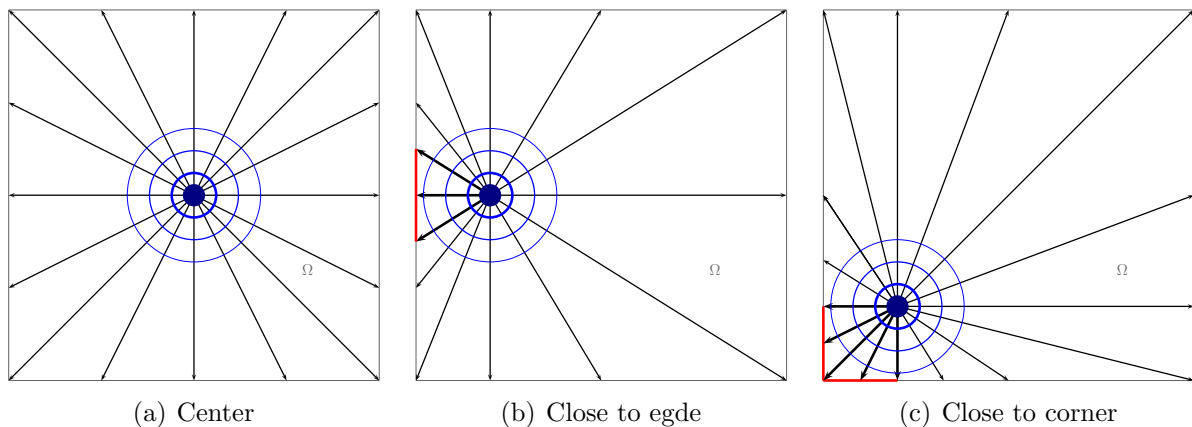
Figure 3.12 – Effects of the source location to the diffusion process in 2D

In the first image 3.12(a) the source location is the center of Ω. Since calcium diffusion on a homogenous domain is symmetric, the whole process is radially symmetric and leads

to uniform expansion.

The second image 3.12(b) considers the situation of the source located close to an edge of the boundary. Here radial symmetry is lost and due to the zero Neumann condition calcium reaching this edge (marked in red) is reflected. Meanwhile calcium is diffusing without interruption in the three remaining directions. The reflection at the boundary has two consequences: 1) Around the reflection area the calcium diffusion is constricted and thus the local concentration here is higher. 2) This blocked amount of calcium is missing on the other side of the calcium wave and it takes a longer time until all mitochondria are reached. Furthermore this blocked calcium reaches the mitochondria at a later time where they have already been confronted with the freely diffusing calcium. Thus the influence of the "delayed" calcium is diminished.

In the last image 3.12(c) the situation is tightened and now the source is located close to a corner, i.e. close to two edges at once. Here the diffusing calcium is reflected and blocked in two directions and can only spread freely in the two remaining directions. Now all the consequences from before apply and are even self-enhanced due to interactions.

Remark
Of course the same effects occur in the weakened case where the domain is not quadratic but round.

Conclusion

The influence of different initial calcium distributions was experimentally studied in the previously described Figure 2.4, which is again depicted here.
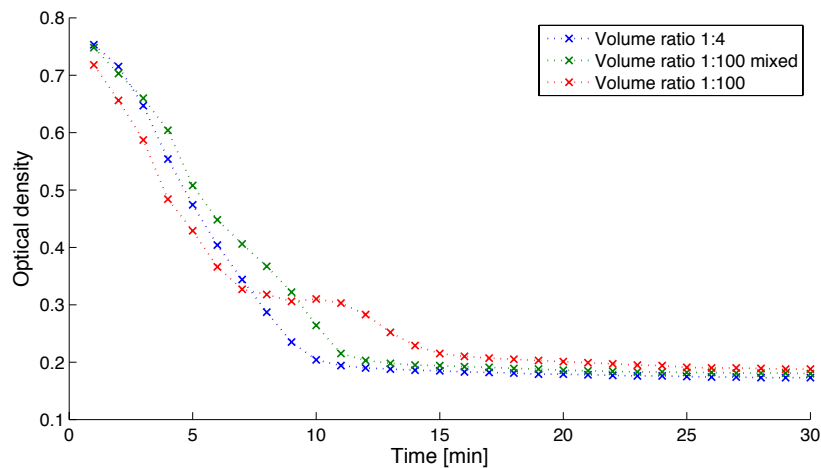
If we compare these data with the simulated swelling curves from Figure 3.11, we see that we indeed obtain similar curve progressions.

The first case Volume ratio 1:4 corresponds to the most distributed case of column $\boxed{5}$, whereas the highly localized case Volume ratio 1:100 shows the same two-phase behavior as the red line (column $\boxed{3}$).

As we saw in the previous simulations, the experimental setting is displayed in the most appropriate way when assuming an initial calcium concentration which is normally distributed on the interval $[-0.5, 0.5]$. Adding different total amounts of calcium in this distribution, we can obtain a qualitative description of the experimental data as it is shown in Figure 3.13.
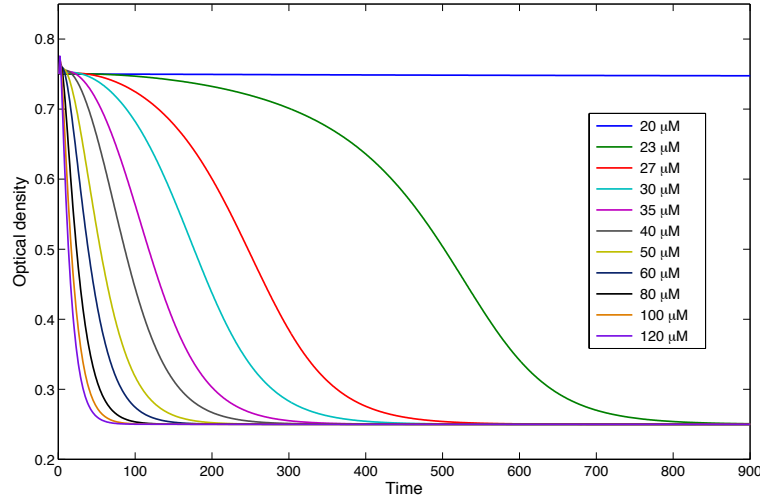
Figure 3.13 – Comparison: Different calcium concentrations

In summary, the derived mathematical model gives a realistic description of the mitochondrial swelling taking place *in vitro*. All experimental data could be verified and furthermore it also yields spatial data. By use of this new model we are now able to study the local processes, which is of major importance in order to understand the underlying biological mechanism in more detail.

3.4.2   The *in vivo* model

As a next step we now want to simulate the processes taking place *in vivo* as described in Section 2.3. Here we have to choose a different discrete domain Ω_h, which now represents the whole cell. In order to do this in an appropriate way, we utilize another method of space discretization, the finite element method.

For that we use the MATLAB Partial Differential Equation Toolbox, which provides a graphical user interface to draw arbitrary domains. Using this interface, we can also describe the mitochondrial regions, i.e. $N_{1h}(0)$, define the Robin boundary conditions and initialize the finite element mesh. The resulting domain description is shown in Figure 3.14. Here the green regions depict two mitochondrial groups and the purple circle represents the nucleus, which is excluded from the domain.

The numerical simulation of the *in vivo* model is then obtained in the following way:

- Calculate the calcium evolution by the MATLAB routine `parabolic.m`. Due to the dependence on N_{2h}, in every time step the present distribution of N_{2h} is calculated on the run by means of one Euler iteration.

- Interpolate the obtained solution u_h in order to evaluate it on predefined time steps $t_k \in T_h$ and then use this values to calculate N_{1h}, N_{2h} and N_{3h} by use of the explicit Euler method.
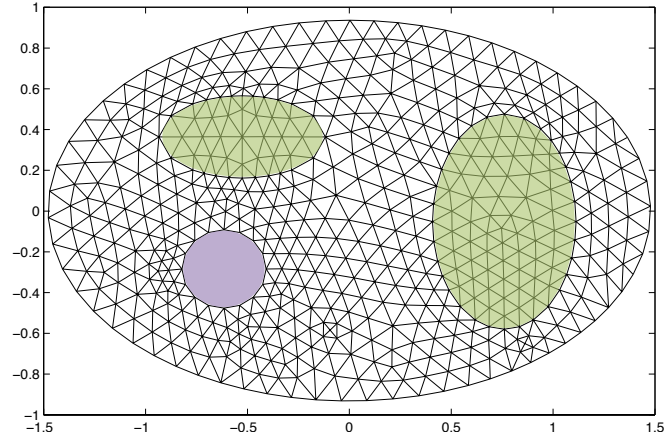
Figure 3.14 – Finite element mesh initialization of the cell including the nucleus and two regions of mitochondria

At this we use the parameter values noted in Table 3.3.

Name	Description	Value
d_1	diffusion parameter	0.01
d_2	feedback parameter	100
f^*	maximal transition rate $N_1 \curvearrowright N_2$	1
g^*	maximal transition rate $N_2 \curvearrowright N_3$	0.1
C^-	threshold of initiating $N_1 \curvearrowright N_2$	20
C^+	saturation threshold	200
h_t	step size of time discretization	0.1
α	intracellular Ca^{2+} concentration at rest	1

Table 3.3 – *In vivo* simulation: Model parameters

The initial calcium distribution is highly localized representing either calcium influx from the extracellular regime through a channel in the cell membrane or the release of calcium from the endoplasmic reticulum.

The total amount is given by

$$C_{tot} = 18 \, \# \, \text{points in } \Omega_h \, .$$

The *in vivo* model with the domain described in Figure 3.14 is now simulated. Here we analyze the influence of two different parameter values a in the description of the boundary condition. All other parameter values remain identical.

For the simulations we assume a to be constant and study the cases

$$a = 1 \cdot 10^{-4} \quad \text{and} \quad a = 3 \cdot 10^{-4} \, ,$$

i.e. in the second case the flux over the boundary is three times higher. Like that more calcium vanishes per time step and as we will see in the following Figures 3.15 - 3.18, this small difference decides between partial and complete swelling.

The simulations on the left represent the complete swelling case, i.e. here both mitochondrial regions are affected, whereas on the right only one region gets swollen and the other one remains intact.

Special model function g

The following figures are obtained by setting $C^+ = 0$ in the description of the model function g, i.e. here g is a constant function $g \equiv g^*$. Like that the transition of mitochondria from N_2 to N_3 proceeds independent of calcium, representing the osmotically driven influx of water once the membrane got permeable.

We chose the function to be constant, since for the *in vivo* case in contrast to the *in vitro* case, calcium vanishes over the cell membrane and hence $g(u)$ gets smaller and smaller. But it stays positive due to the assumed intracellular calcium concentration $u = \alpha$ of the system in rest. However, this would lead to very slow dynamics. Also the effect of the positive feedback gets more visible by taking a constant g.

Remark
For the *in vitro* case it is not necessary to change the description of g, since there the local calcium concentration remains higher compared to the *in vivo* case. This happens because added calcium does not leave the test tube.

Conclusion

The presented simulations show the wide capability of the derived mathematical model. The *in vitro* as well as the *in vivo* swelling mechanism is modeled in perfect accordance with the biological description and we are now able to study the local processes taking place in whole cells.

Using the MATLAB Partial Differential Toolbox we can also simulate the degenerate diffusion case and take into account space dependencies of the model functions f, g and the boundary function a. This offers a wide applicability of the developed model, which may lead to important new biological findings about the underlying mechanism.

Figure 3.15 shows the time development of the calcium concentration for two values of a. As we pointed out in the model description, for the *in vivo* model the calcium source is always very localized. This leads to a high difference $u - \alpha$ and hence the calcium efflux is very high near to the calcium pulse. On the left the value of a is lower and hence this efflux proceeds slower. Like that more calcium is available to induce mitochondrial swelling, which leads to complete swelling on the left and partial swelling on the right. In the beginning calcium diffuses in a similar manner, however the right concentration is not sufficient to induce swelling in both mitochondria regions. In contrast on the left side the positive feedback coming from the second mitochondria group can be immediately identified by the additional calcium bump appearing at $t = 900$. This leads to a different calcium evolution, however they both converge to the constant function $u \equiv \alpha$. This convergence appears to be very slow due to the low values of a.
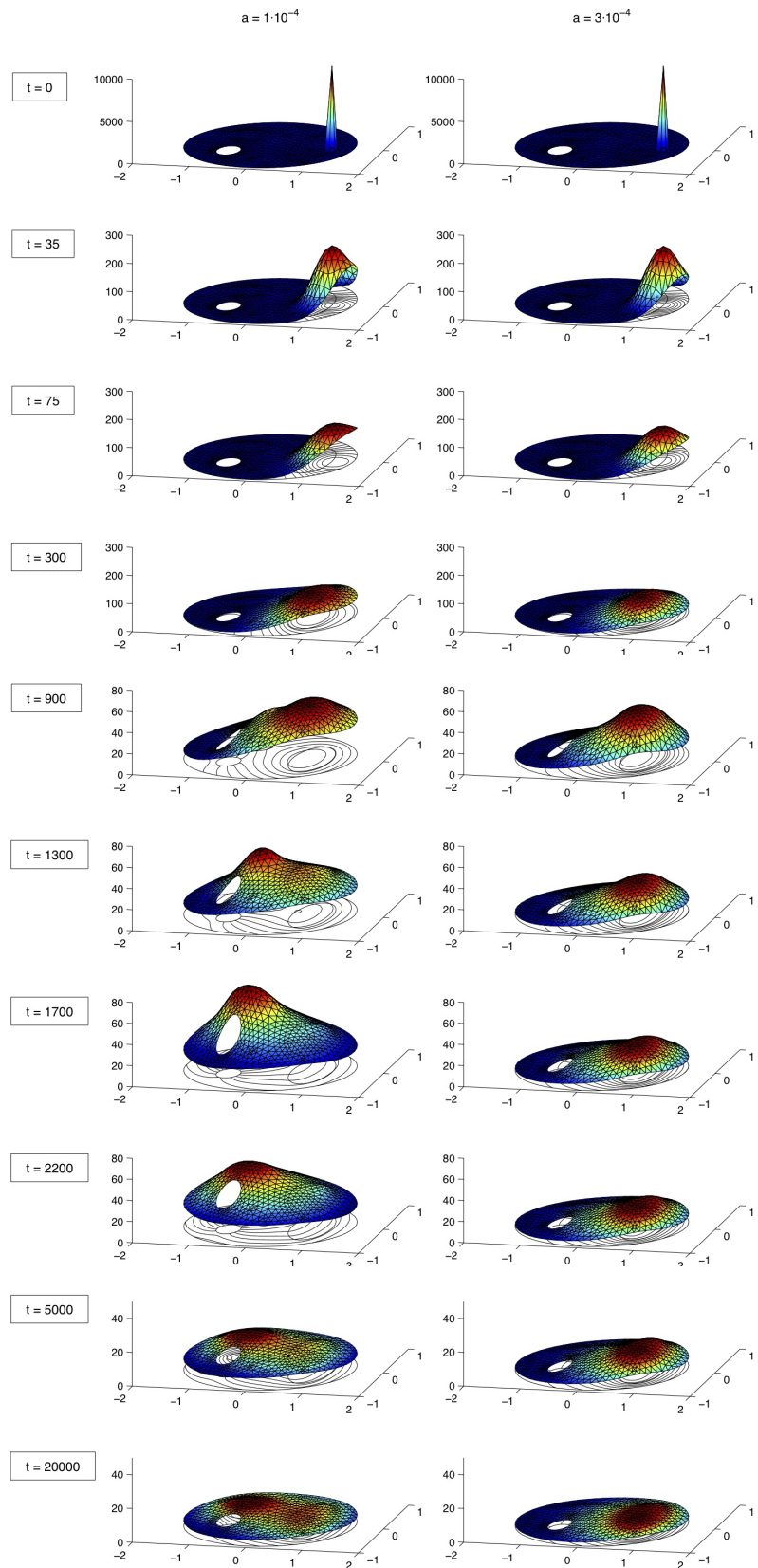
Figure 3.15 – Calcium evolution at *in vivo* swelling
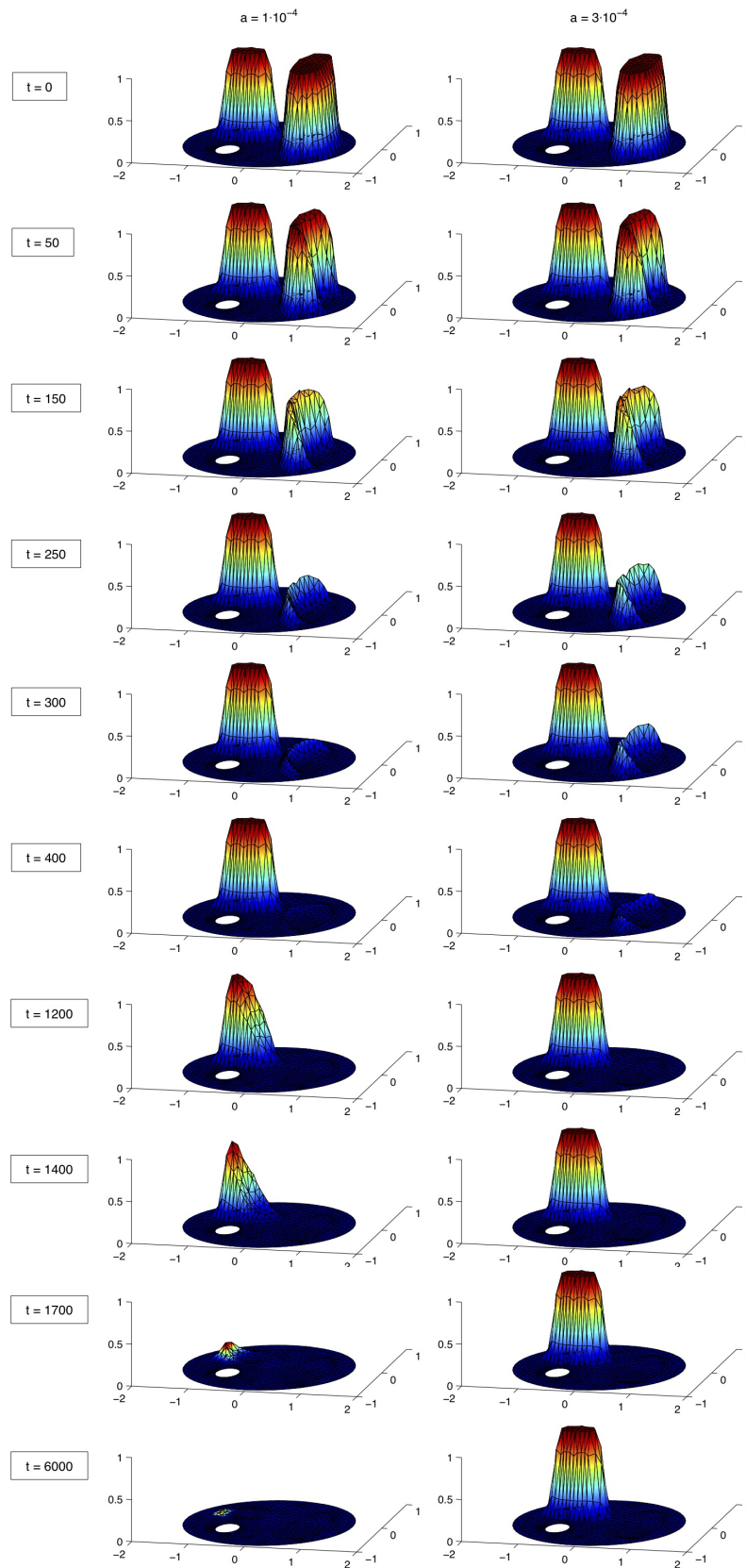
Figure 3.16 – Unswollen mitochondria at *in vivo* swelling

The next Figure 3.16 shows the corresponding behavior of the unswollen mitochondrial population. Starting from initially distributed mitochondria residing in the two regions introduced in Figure 3.14, we either end up with no intact mitochondria on the left or only one intact population on the right. Due to the location of the calcium source, at the beginning only one group is affected. In the partial swelling case the remaining calcium concentration is not high enough to trigger also swelling in the second group. However, this effect is dependent on the distance between both groups. We also saw in other simulations that if these groups are more contiguous and hence calcium does not diffuse to the same degree on the way from one region to the other, then under the same conditions swelling is induced in both groups. As one can imagine, here also the diffusion rate plays an important role with higher diffusion leading to a higher probability of partial swelling and vice versa.

Taking a look at the population of mitochondria that are in the swelling process but not completely swollen presented in Figure 3.17, the direction of the calcium wave gets clearly visible. Starting from the source near to the cell membrane, calcium spreads to the left where it hits the first group of mitochondria. When it made its way through the whole region, it hits the second group. Since the calcium concentration is positive by definition of the cell milieu, we can deduce the convergence of N_2 to zero. However, this convergence appears to be very slow.

In the mathematical description of the cell we excluded the nucleus from the domain, because calcium can not diffuse through it. At this inner boundary we assume to have homogeneous Neumann boundary conditions.

Using the graphical user interface provided by the MATLAB Partial Differential Equation Toolbox, it is also possible to build a more realistic model of the cell taking into account more biological details.
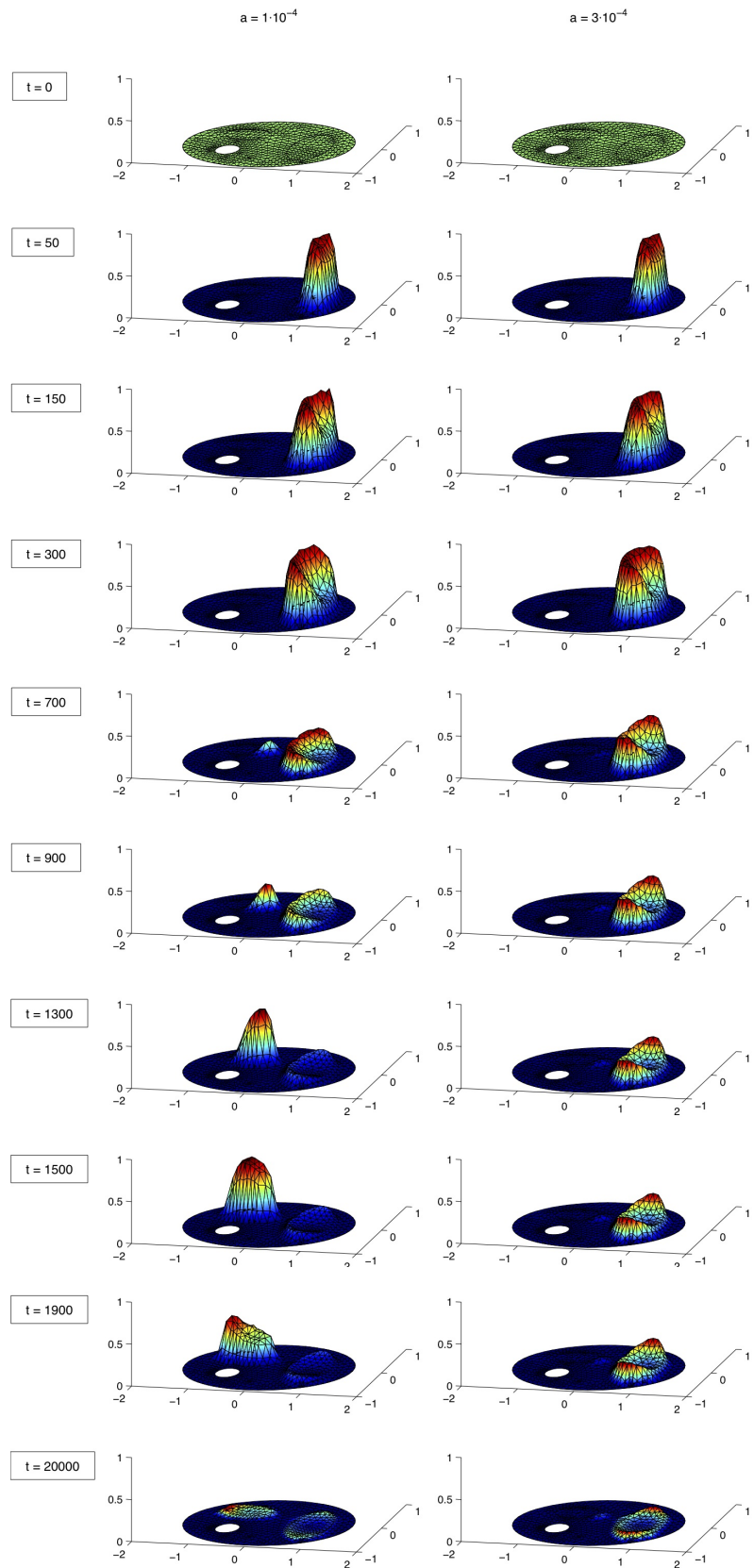
Figure 3.17 – Swelling mitochondria at *in vivo* swelling
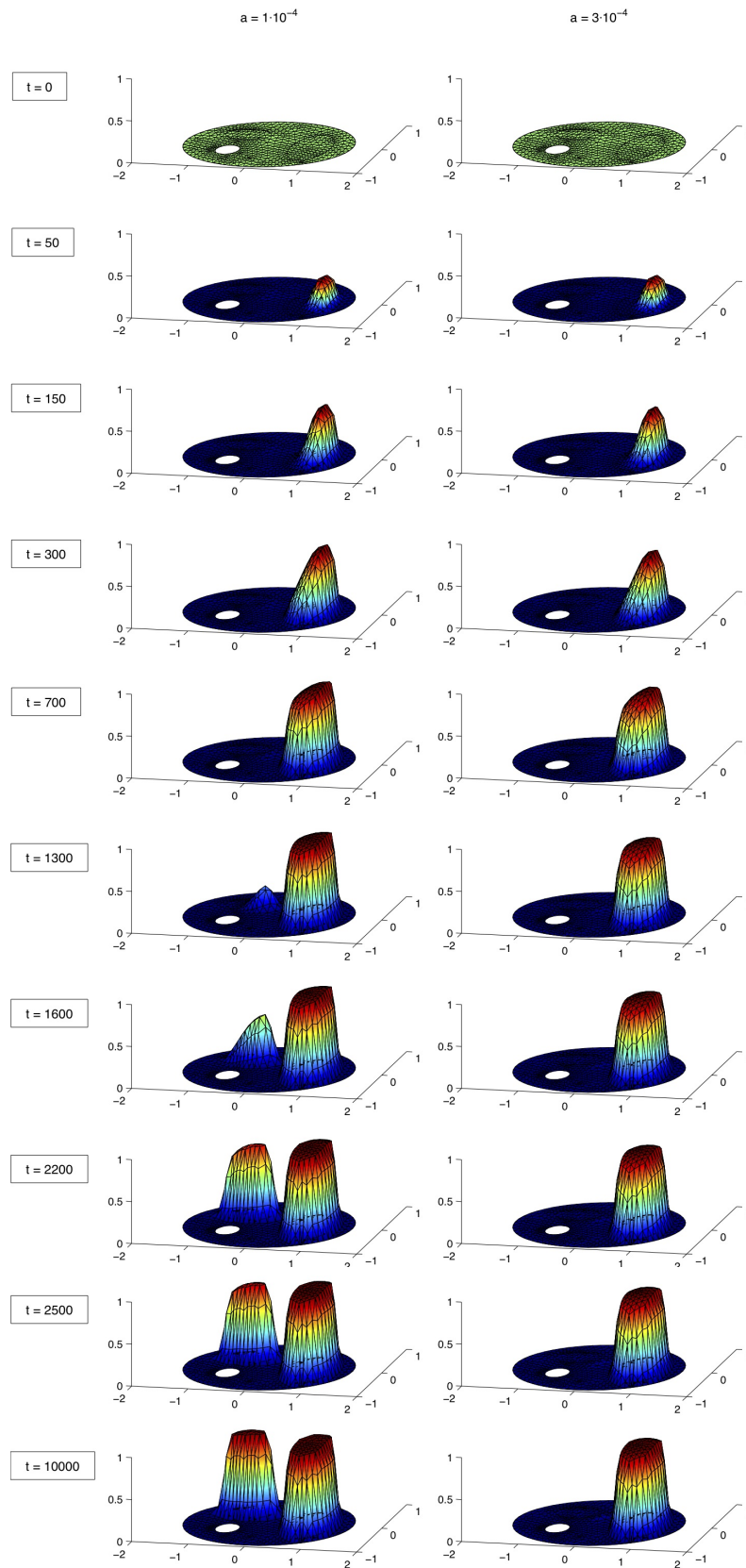
Figure 3.18 – Swollen mitochondria at *in vivo* swelling

The last Figure 3.18 displays the behavior of the remaining mitochondrial population, the completely swollen ones. In the case of complete swelling, the final distribution is the same as the initial distribution of intact mitochondria. This is an immediate consequence of the conservation law, which states that the total population of mitochondria does not change with time. In the partial swelling case hence mitochondria from the first region are all completely swollen, whereas those from the second group are still intact. If we take a look at the dynamics and focus on the beginning of the whole process, we see that the increase of N_3 in the first region proceeds nearly identical for both cases. This is justified by an almost identical high calcium source at the very beginning. The more diffusion comes into play, the more the process dynamic changes. However, at this also the extent of the positive feedback plays an important role. The higher the additionally released calcium, the higher the probability of complete swelling.

CHAPTER 4

Degenerate mitochondria model

The previous models were governed by the concept of standard diffusion. A classical property of the heat equation is its *infinite speed of propagation*, i.e. for every $t > 0$ the solution $u(t)$ starting from non-negative initial values u_0 gets automatically positive on the whole domain. We saw this fact in Proposition 4 and the reason becomes reliable by the divergence form representation

$$\Delta u = \operatorname{div}(1 \cdot \nabla u)$$

with the constant diffusion coefficient $D \equiv 1$ determining the speed of diffusion.

Remark
This classical property can also be shown for the Dirichlet problem (3.68) - (3.72).

However, from the application point of view this property is not realistic, since there are no substances that can diffuse infinitely fast. Imagine a huge domain Ω and the calcium source u_0 being a delta distribution. Then biologically it is not possible that after an arbitrary small time the calcium reaches any point of the domain.

Remark
Besides knowing this disadvantage, the use of the standard Laplacian to describe diffusion processes is a generally accepted mathematical idealization. Furthermore, this effect does not appear in the numerical simulations. Here the domain is discretized and the diffusion at one point is only dependent on its neighboring points, which may all be zero for compactly supported initial conditions.

4.1 Degenerate diffusion

In order to obtain a more realistic setting, in the following the standard Laplacian is not the method of choice anymore. It is replaced by the porous medium operator

$$\Delta u^{m-1} = \operatorname{div}\left((m-1)u^{m-2} \cdot \nabla u\right) \quad \text{with } m > 2 \,, \tag{4.1}$$

which is a nonlinear generalization of Δu representing the case $m = 2$. For more general information the reader is referred to [54], where the mathematical theory of the porous

medium equation

$$\partial_t u = \Delta u^{m-1}$$

and its applications are studied.

The nonlinear expression (4.1) is only defined for non-negative functions, since m does not have to be an integer. In our application u represents the calcium concentration, which is biologically restricted to be non-negative. However, from the beginning we can not mathematically assure that the solution u is non-negative, this is why in the following we work with the signed operator

$$\Delta(|u|^{m-2}u) = \mathrm{div}\Big(\underbrace{(m-1)|u|^{m-2}}_{=:\,D(u)}\cdot\nabla u\Big)\,,\quad m > 2\,. \tag{4.2}$$

The absolute value assures that the definition is valid regardless of the sign of u and the function $|s|^{m-2}s$ is monotone.

This leads to the new model equation

$$\boxed{\partial_t u = d_1\Delta(|u|^{m-2}u) + d_2 g(u)N_2\,,} \tag{4.3}$$

which will be studied in the sequel.

Finite propagation speed

In contrast to the standard Laplace operator, now the diffusion coefficient

$$D(u) = (m-1)|u|^{m-2}$$

is dependent on u and not constant anymore. This has a huge influence on the speed of propagation. Now starting from a compactly supported initial condition, diffusion only appears dependent on u. That means $D(u)$ is only positive for locations where calcium is already present, which leads to a consecutive spreading.

As it can e.g. be read in [54], starting from a compactly supported initial value u_0, the solution $u(t)$ has compact support for every $t > 0$, which signifies *finite speed of propagation*. Furthermore the sets

$$B(t) := \{x \in \Omega : u(x,t) > 0\} \subset \Omega$$

satisfy

$$\bigcup_{t>0} B(t) = \Omega \quad \text{and} \quad B(t_2) \subset B(t_1) \quad \text{for } t_2 > t_1\,.$$

The diffusion coefficient vanishes outside the set $B(t)$ if $m > 2$ and therefore the rate of diffusion is extremely small near the boundary of $B(t)$, hence the set expands slowly. On the other hand, if $m = 2$ representing the Laplacian, the diffusion coefficient remains identically constant in Ω, therefore in this case supp $u(\cdot,t)$ spreads all over $\overline{\Omega}$ instantly.

Figure 4.1 depicts the differences between infinite and finite propagation speed and makes clear why the degenerate diffusion (4.2) is more suitable to represent the process in reality compared to the standard Laplacian with infinite speed.

(a) infinite speed

(b) finite speed
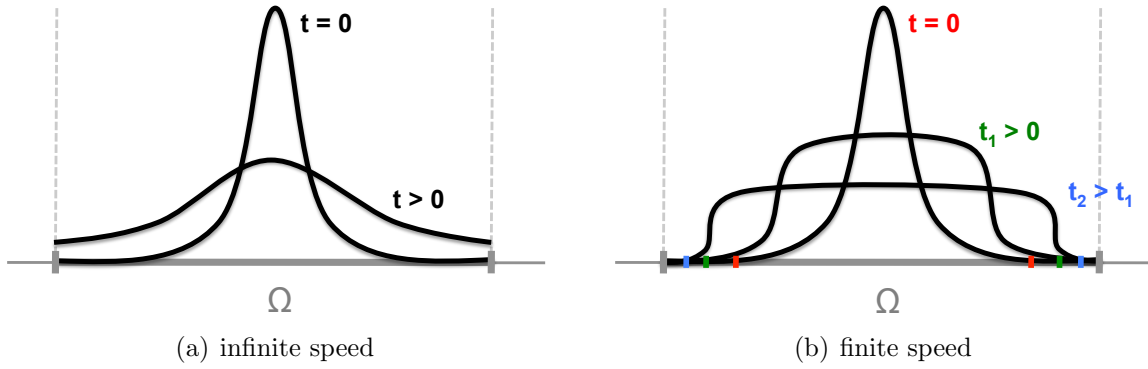
Figure 4.1 – Propagation of compactly supported initial data

Degeneracy

The most important property of this new type of equation is its degeneracy, i.e. the diffusion coefficient depends on u in a sense that it vanishes for $u = 0$. In that case the PDE (4.3) is not parabolic anymore and we name it a *degenerate parabolic equation*.

Example

For the case $u \geq 0$ and $m = 3$ we obtain

$$\partial_t u = 2d_1(u\Delta u + |\nabla u|^2) + d_2 g(u)N_2 \,.$$

That means for $u \to 0$ the equation becomes

$$\partial_t u = 2d_1|\nabla u|^2 + d_2 g(u)N_2 \,,$$

where the diffusion term is completely lost and we have to deal with another class of equation.

Understandably the degeneracy is challenging for the mathematical analysis and in the following we will see that we need additional theoretical concepts to treat this type of equation.

4.2 Preliminaries

At first we want to introduce some mathematical tools to handle degenerate parabolic equations. Our aim is to embed the nonlinear diffusion operator into a wider class of equations, namely maximal monotone operators. At this we restrict ourselves to Hilbert spaces, however there are analogous concepts for Banach spaces. The following facts can be found in the standard literature [9], [54] and [57].

Subdifferential

The notion of the derivate can be generalized in order to be also applied for functions that are not differentiable in the classical sense, i.e. Gâteaux differentiable in the case of infinite dimensional spaces.

Definition 20
Let X be a real Banach space with dual X^* and $\varphi : X \to [-\infty, \infty]$ a functional. An element $u^* \in X^*$ is called $\underline{subgradient}$ of φ at $u \in X$ if and only if $\varphi(u) \neq \infty$ and

$$\varphi(v) \geq \varphi(u) + \langle u^*, v - u \rangle \quad \forall v \in X , \tag{4.4}$$

where $\langle \cdot, \cdot \rangle$ denotes the pairing between X and X^*. The set

$$\partial\varphi(u) := \{u^* : u^* \in X^*, u^* \text{ subgradient of } \varphi \text{ in } u\}$$

is called $\underline{subdifferential}$ of φ in u.

Remark
Here we list some important properties of the subdifferential:

(i) In contrast to the Gâteaux differential $D\varphi$, the subdifferential can be multivalued, i.e. $\partial\varphi$ is a mapping from the space X into the set of subsets of the dual space X^*:

$$\partial\varphi : X \to 2^{X^*} .$$

(ii) If the function φ is convex, then

$$\partial\varphi(u) \neq \emptyset \qquad \forall u \in X .$$

(iii) If the function φ is convex and Gâteaux differentiable at u, then $\partial\varphi(u)$ is singlevalued:

$$\partial\varphi(u) = \{D\varphi(u)\} .$$

(iv) Let $\varphi : \mathbb{R} \to \mathbb{R}$. Then the subdifferential $\partial\varphi(x)$ can be geometrically described as the set containing all slopes of straight lines through the point $(x, \varphi(x))$, that lie underneath the graph of φ.

(v) The subdifferential is dependent on the choice of the pairing $\langle \cdot, \cdot \rangle$ between X and X^*.

The following example explains the subdifferential of a function $\varphi : \mathbb{R} \to \mathbb{R}$, which is not differentiable at $x = 0$.

Example
Let $\varphi : \mathbb{R} \to \mathbb{R}$ and $a, b \in \mathbb{R}^+$. We define

$$\varphi(x) := \begin{cases} -bx & \text{if } x < 0 \\ ax & \text{if } x \geq 0 . \end{cases}$$

Then $\varphi(x)$ is differentiable for $x \in \mathbb{R} \setminus 0$ and thus in that case we have $\partial\varphi(x) = \{\varphi'(x)\}$. It remains to determine $\partial\varphi(0)$. For $x = 0$ condition (4.4) reads

$$\varphi(y) \geq x^*y \quad \Leftrightarrow \quad \begin{cases} x^* \geq -b & \text{if } y < 0 \\ x^* \leq a & \text{if } y \geq 0 \end{cases} \quad \Leftrightarrow \quad x^* \in [-b, a] \qquad \forall y \in \mathbb{R}$$

and it follows $\partial\varphi(0) = [-b, a]$.

Figure 4.2 (a) shows all solid lines through the point $(0,0)$ and marks the feasible (green) and not feasible (red) slopes to stay underneath the graph. Figure 4.2 (b) then displays the subdifferential $\partial\varphi$ as it was obtained by calculation as well as geometrical observation.

(a) Admissibility of the solid lines   (b) Corresponding subdifferential
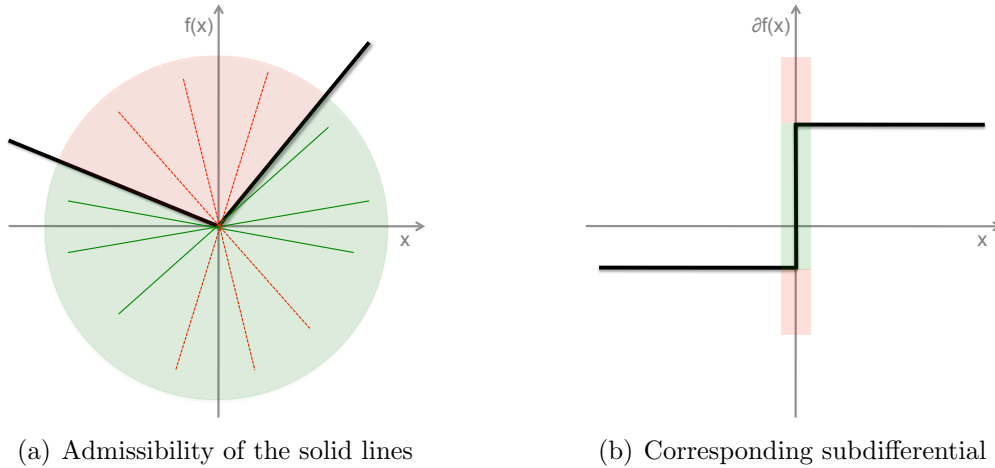
Figure 4.2 – Geometrical explanation of the subdifferential

Multivalued operators

The theory of nonlinear operators often includes multivalued operators as for instance the subdifferential of a convex function.

Definition 21
Let X, Y be real Banach spaces and $A : X \to 2^Y$ a multivalued operator that maps $u \in X$ to $A(u) \subseteq Y$.

Then the <u>effective domain</u> $D(A)$, the <u>range</u> $R(A)$ and its <u>graph</u> $G(A)$ are defined as follows:

$$D(A) := \{u \in X : A(u) \neq \emptyset\}$$
$$R(A) := \bigcup_{u \in D(A)} A(u)$$
$$G(A) := \{(u,v) \in X \times Y : u \in D(A), v \in A(u)\}.$$

One remarkable property of multivalued operators is that the inverse operator

$$A^{-1} : Y \to 2^X \quad \text{defined by} \quad A^{-1}(v) = \{u \in X : v \in A(u)\} \subseteq X$$

always exists. Here we have

$$D(A^{-1}) = R(A), \quad R(A^{-1}) = D(A), \quad (u,v) \in G(A) \Leftrightarrow (v,u) \in G(A^{-1}).$$

Remark
For single-valued maps it holds $A(u) = \{v\}$.
However, every single-valued map $A : D(A) \subseteq X \to Y$ can be identified with a multivalued map $\overline{A} : X \to 2^Y$ by setting

$$\overline{A}(u) = \begin{cases} \{A(u)\} & \text{if } u \in D(A) \\ \emptyset & \text{else} . \end{cases}$$

Maximal monotone operators

Another important feature of operators is maximal monotonicity, which is generally defined in the following way:

Definition 22
Let H be a Hilbert space and $A : D(A) \subset H \to H$ a (possibly nonlinear and multivalued) operator.

A is called <u>monotone</u>, if for every $u_1, u_2 \in D(A)$ and every $v_1 \in A(u_1)$, $v_2 \in A(u_2)$ it holds

$$(A(u_1) - A(u_2), u_1 - u_2)_H \geq 0 .$$

A is called <u>maximal monotone</u>, if it is monotone and satisfies the range condition

$$R(I + A) = H .$$

Maximal monotonicity can be geometrically characterized in the following way:

Proposition 23
Let $A : D(A) \subset H \to H$ be a monotone operator.

Then A is maximal monotone if and only if its graph $G(A)$ is maximal.

Example
The following examples show the application to functions $f : \mathbb{R} \to \mathbb{R}$.

  1) Let f be non-decreasing. Then f is montone.

  2) Let f be non-increasing. Then f is not monotone, but $-f$ is.

  3) Let f be non-decreasing and continuous. Then f is maximal monotone.

  4) Let f be non-decreasing and discontinuous. Then f can be extended to a maximal monotone function, which is multivalued.
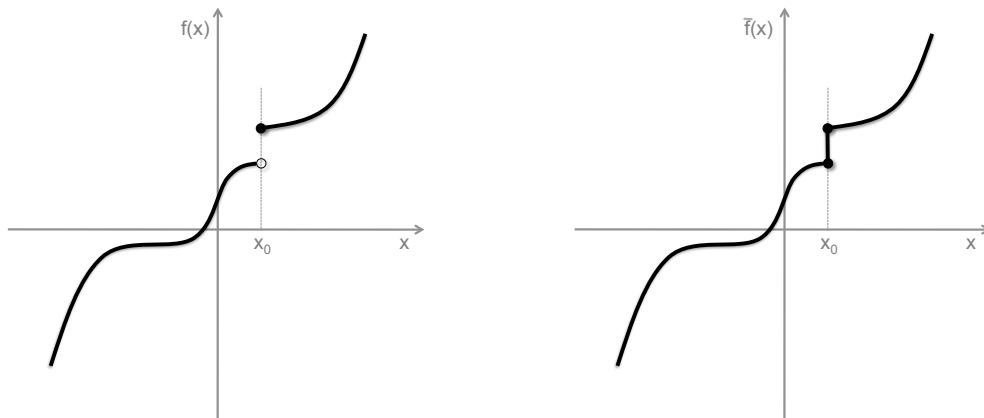
Figure 4.3 – Obtaining a maximal montone function by extension

This situation is shown in Figure 4.3, where the function f on the left has a discontinuity at x_0 and due to the resulting "hole", the graph is not maximal. Extending this function by filling up the hole, we obtain the maximal monotone function $\overline{f}$ depicted on the right hand side, which is multivalued at point x_0.

Remark

The theory of maximal monotone operators also applies to the standard Laplacian, since we can show that the non-negative linear operator $-\Delta : D(A) \subset H \rightarrow H$ with $H = L^2(\Omega)$ fulfills the required properties

(i) monotone:

$$(A(u_1) - A(u_2), u_1 - u_2)_H = \|\nabla(u_1 - u_2)\|^2_{L^2(\Omega)} \geq 0$$

(ii) maximal: The range condition $R(I + A) = H$ reads in this case

$$\forall f \in H \text{ there exists } u \in D(A) \text{ such that } u - \Delta u = f.$$

In other words we are looking for the solution of this elliptic PDE, whose existence is e.g. reported in [24].

The most important result for the analysis of the porous medium model is the fact that under some conditions the subdifferential is a maximal monotone operator [47].

Theorem 24

Let H be a Hilbert space and $\varphi : H \rightarrow (-\infty, \infty]$ be a proper function, i.e. $\varphi \not\equiv \infty$.

If φ is convex and lower semicontinuous, then its subdifferential $\partial\varphi : H \rightarrow 2^{H^*}$ is a maximal monotone operator.

4.3 Model analysis

In the following we want to apply the theory of [40] to prove existence and uniqueness for the **porous medium type model**

$$
\begin{align}
\partial_t u &= d_1 \Delta(|u|^{m-2} u) + d_2 g(u) N_2 \tag{4.5}\\
\partial_t N_1 &= -f(u) N_1 \tag{4.6}\\
\partial_t N_2 &= f(u) N_1 - g(u) N_2 \tag{4.7}\\
\partial_t N_3 &= g(u) N_2 \tag{4.8}
\end{align}
$$

with homogeneous Dirichlet boundary condition

$$u = 0 \text{ on } \partial\Omega. \tag{4.9}$$

At this the PDE has to be rewritten in the form

$$\boxed{\partial_t u(t) = -d_1 \partial\varphi(u(t)) - B(u(t)),} \tag{4.10}$$

where the subdifferential $\partial\varphi$ is maximal monotone and B is a possibly nonmonotone multivalued nonlinear operator.

Phase space

In contrast to the non-degenerate cases, now the phase space is changed to

$$H := H^{-1}(\Omega) = H_0^1(\Omega)^* \,,$$

for which on bounded domains we have the well-known continuous and dense embeddings

$$H_0^1(\Omega) \hookrightarrow L^2(\Omega) \subset\subset H^{-1}(\Omega) \,. \tag{4.11}$$

Remark
The theory of [40] deals with abstract Cauchy problems, where the boundary condition is contained in the phase space definition. In our case, the homogeneous Dirichlet boundary condition (4.9) is reflected by the choice of $H_0^1(\Omega)$.

The subdifferential shall be applied to a function $\varphi : H \to [0, \infty]$. By definition of the subdifferential, it obviously follows

$$D(\partial\varphi) \subseteq D(\varphi) \subseteq H$$

and for the operator $B : D(B) \subset H \to H$ determined by $B(u) = d_2 g(u) N_2$ we also require

$$D(\partial\varphi) \subseteq D(B) \,.$$

The subdifferential

In terms of Theorem 24, at first we have to find a suitable proper, convex, lower semicontinuous function φ. Here we denote by $\|\cdot\|_p$ the L^p-norm $\|\cdot\|_{L^p(\Omega)}$.

Proposition 25
Let $m > 2$. The function $\varphi : H \to [0, \infty]$ defined by

$$\varphi(u) := \begin{cases} \frac{1}{m}\|u\|_m^m & \text{if } u \in L^m(\Omega) \\ \infty & \text{otherwise} \end{cases} \tag{4.12}$$

possesses in H the maximal monotone subdifferential

$$\partial\varphi(u) = -\Delta(|u|^{m-2}u) \,. \tag{4.13}$$

Proof

1) *φ is proper*
We have $\varphi \not\equiv \infty$ due to the embedding

$$L^m(\Omega) \hookrightarrow L^2(\Omega) \subset\subset H^{-1}(\Omega) = H \,.$$

2) *φ is convex*
In order to show the convexity, we define $\tilde{\varphi} := g \circ f$

$$\tilde{\varphi} : L^m(\Omega) \to [0, \infty)$$

with $f : L^m(\Omega) \to [0, \infty)$ and $g : [0, \infty) \to [0, \infty)$ given by

$$f(u) := \|u\|_m \quad \text{and} \quad g(s) := \frac{1}{m} s^m .$$

Then f is convex by the triangle inequality valid of every norm and g is convex since $g''(s) \geq 0$ for every $s \in [0, \infty)$. Furthermore g is non-decreasing and it follows for every $\lambda \in (0, 1)$

$$g\big(f(\lambda u + (1 - \lambda)v)\big) \leq g\big(\lambda f(u) + (1 - \lambda)f(v)\big) \leq \lambda g\big(f(u)\big) + (1 - \lambda)g\big(f(v)\big),$$

thus $\tilde{\varphi}$ is convex. Knowing that, it immediately follows that

$$\varphi(u) := \begin{cases} \tilde{\varphi}(u) & \text{if } u \in L^m(\Omega) \\ \infty & \text{otherwise} \end{cases} \tag{4.14}$$

is also convex.

3) φ is lower semicontinuous

Here we again use the composition $\tilde{\varphi} = g \circ f$ as described above. It is basic knowledge that every norm is lower semicontinuous with respect to weak convergence and so we have lower semicontinuity of f. Furthermore g as a polynomial is continuous and increasing on its domain $[0, \infty)$. This implies that $\tilde{\varphi}$ is lower semicontinuous as it is e.g. proved in [14]. Again, this is also satisfied by the extension (4.14).

By Theorem 24 it follows that the subdifferential $\partial\varphi$ is maximal monotone, but it remains to show that it is given by (4.13). For that we will show that φ is Gâteaux differentiable and consequently $\partial\varphi(u) = \{u^*\}$. Then will prove that $u^* = -\Delta|u|^{m-2}u$ in $H^{-1}(\Omega)$.

4) φ is Gâteaux differentiable

For $h > 0$ we have to show

$$\lim_{h \to 0} \frac{\varphi(u + hv) - \varphi(u)}{h} = D\varphi(u)(v)$$

where the derivative $D\varphi(u)(v)$ of φ at u in direction v is linear and bounded in v.

In accordance with Definition 20, the subdifferential of φ is only defined for $u \in L^m(\Omega)$, hence we only need Gâteaux differentiability in $L^m(\Omega)$. Here we have $\varphi(u) = \frac{1}{m}\|u\|_m^m$ and it is e.g. proven in [55], that this functional is Gâteaux (and also Fréchet) differentiable for $1 < m < \infty$. The proof is done using the auxiliary function $\psi(h) := \varphi(u + hv)$, which is differentiable in h. Then by the standard differentiability it holds

$$\psi'(0) = \lim_{h \to 0} \frac{\psi(h) - \psi(0)}{h} = \lim_{h \to 0} \frac{\varphi(u + hv) - \varphi(u)}{h} .$$

Hence it follows that $\partial\varphi(u)$ consists of only one element for every $u \in L^m(\Omega)$. According to this, if we can find $u^* \in \partial\varphi(u)$, then this element defines the subdifferential.

5) $u^* = |u|^{m-2}u \in \partial\varphi(u)$

We want to determine $u^* \in \varphi(u)$ for the phase space $H = H^{-1}(\Omega)$, i.e. by Definition 20 we have to find $u^* \in H_0^1(\Omega)$ such that

$$\langle u^*, v - u \rangle \leq \varphi(v) - \varphi(u) \qquad \forall v \in H^{-1}(\Omega). \tag{4.15}$$

Again we only need to study $u \in L^m(\Omega)$, and since (4.15) with $v \in H^{-1}(\Omega) \setminus L^m(\Omega)$ holds for every $u^* \in H_0^1(\Omega)$, it is also sufficient to take $v \in L^m(\Omega)$. Hence in fact we treat (4.15) in $L^m(\Omega)$, where we want to find $u^* \in L^{\frac{m}{m-1}}(\Omega) = L^m(\Omega)^*$ with

$$\int_\Omega u^*(v - u)\,dx \leq \frac{1}{m}\left(\|v\|_m^m - \|u\|_m^m\right) \qquad \forall v \in L^m(\Omega). \tag{4.16}$$

In the following we will show that $u^* = |u|^{m-2}u \in L^{\frac{m}{m-1}}(\Omega)$ for $u \in L^m(\Omega)$ satisfies the desired property in $L^m(\Omega)$.

It holds

$$\int_\Omega |u|^{m-2}u(v - u)\,dx = \int_\Omega |u|^{m-2}uv\,dx - \int_\Omega |u|^m\,dx\,,$$

which can be estimated by applying Hölder's and Young's inequality both with $p = m$ and its conjugate $q = \frac{m}{m-1}$

$$\leq \||u|^{m-2}u\|_{\frac{m}{m-1}}\|v\|_m - \|u\|_m^m \leq \frac{m-1}{m}\|u^{m-1}\|_{\frac{m}{m-1}}^{\frac{m}{m-1}} + \frac{1}{m}\|v\|_m^m - \|u\|_m^m$$

$$= \frac{m-1}{m}\|u\|_m^m + \frac{1}{m}\|v\|_m^m - \|u\|_m^m = \frac{1}{m}\left(\|v\|_m^m - \|u\|_m^m\right).$$

Hence (4.16) is fulfilled and we have $|u|^{m-2}u \in \partial\varphi(u)$ in $L^m(\Omega)$.

In summary, for the subdifferential $\partial\varphi$ in $L^m(\Omega) \subset H^{-1}(\Omega)$ we were able to show

$$\partial\varphi(u) = |u|^{m-2}u \qquad \forall u \in L^m(\Omega). \tag{4.17}$$

6) *Identifying $\tilde{u} = -\Delta(|u|^{m-2}u) \in \partial\varphi(u)$ for the phase space $H^{-1}(\Omega)$*

However, the PDE (4.5) is defined on the phase space $H^{-1}(\Omega)$ and thus our aim now is to determine the corresponding subdifferential in $H^{-1}(\Omega)$. For that we need to choose an appropriate scalar product on $H = H^{-1}(\Omega)$. This can be done by defining

$$(u, v)_H := \langle(-\Delta)^{-1}u, v\rangle \qquad \forall u, v \in H, \tag{4.18}$$

where $\langle\cdot,\cdot\rangle$ denotes the duality pairing $_{H_0^1(\Omega)}\langle\cdot,\cdot\rangle_{H^{-1}(\Omega)}$. This definition is justified by the isomorphism $-\Delta : H_0^1(\Omega) \to H^{-1}(\Omega)$ provided by the famous Lax-Milgram Theorem. In accordance the inverse operator $(-\Delta)^{-1} : H^{-1}(\Omega) \to H_0^1(\Omega)$ exists and inherits the property of being self-adjoint.

Our purpose now is to find the identification $\tilde{u} \in H^{-1}(\Omega)$ of $u^* = |u|^{m-2}u$. For every element $\tilde{u}$ of $H^{-1}(\Omega)$ we have in accordance with the subdifferential definition

$$(\tilde{u}, v)_H = \langle(-\Delta)^{-1}\tilde{u}, v\rangle \stackrel{!}{=} \langle u^*, v\rangle \quad \forall v \in H \quad \Leftrightarrow \quad \tilde{u} = -\Delta u^* \in H^{-1}(\Omega).$$

$\square$

Existence of a unique global solution

In analogy to Theorem 1, we obtain a similar existence result for the degenerate model by using the theory of maximal monotone operators.

Theorem 26

Let $\Omega \subset \mathbb{R}^n$ be bounded. Under the assumptions of Condition 1 it holds:

For all initial data $u_0 \in L^m(\Omega)$, $N_{1,0} \in L^\infty(\Omega)$, $N_{2,0} \in L^\infty(\Omega)$ and $N_{3,0} \in L^\infty(\Omega)$ the system (4.5) - (4.9) with $m > 2$ and

$$\|N_{1,0}\|_{L^\infty(\Omega)} + \|N_{2,0}\|_{L^\infty(\Omega)} \neq 0$$

possesses a unique global solution (u, N_1, N_2, N_3) satisfying

$$u \in C([0,T]; H^{-1}(\Omega))$$
$$\partial_t u \in L^2(0,T; H^{-1}(\Omega))$$
$$|u|^{m-2}\nabla u \in L^2(0,T; L^2(\Omega))$$
$$N_i \in L^\infty(0,T; L^\infty(\Omega)), \quad i = 1, 2, 3,$$

for all $T > 0$.

Proof

The approach to prove existence of a solution proceeds in the same way as for the non-degenerate diffusion case stated in the proof of Theorem 1. The system is splitted up into a pure ODE system and a pure PDE for which we separately show the existence of solutions. Then both are reunited and we have the existence of a unique solution of the whole system if we can show that the corresponding map

$$\mathcal{B} : u \in X \mapsto N^u := \begin{pmatrix} N_1^u \\ N_2^u \end{pmatrix} \mapsto \hat{u} = \mathcal{B}(u)$$

is a contraction.

1.) Existence for the pure ODE system

Since the modifications only apply to the PDE part, the pure ODE system is again given by (3.9), (3.10) dependent on a fixed parameter u. It turns out that for this case it is more suitable to take u from the space $X := C([0,T]; L^1(\Omega))$ and search for the global solution of the ODE in the space $Y := L^\infty(\Omega) \times L^\infty(\Omega)$ with the corresponding norm $\|(A_1, A_2)\|_Y = \|A_1\|_{L^\infty(\Omega)} + \|A_2\|_{L^\infty(\Omega)}$ for $A = (A_1, A_2) \in Y$.

It is easy to see that F is also Lipschitz continuous in the space Y, which yields the existence of a unique global solution $N^u = (N_1^u, N_2^u) \in C([0,\infty]; Y)$.

$$\square \text{ 1.})$$

Remark

Since we deal with functions from $L^m(\Omega)$ with $m > 2$, one can also choose Y to be the space $L^\infty(\Omega) \times L^\infty(\Omega)$ instead of $L^2(\Omega) \times L^2(\Omega)$ as we did in Section 3.1.1.

2.) Existence for the pure PDE

The main difference here consists in showing the existence of a solution $\hat{u}$ to the degenerate pure PDE problem dependent on N_2^u

$$\partial_t \hat{u} = d_1 \Delta(|\hat{u}|^{m-2}\hat{u}) + d_2 g(\hat{u}) N_2^u \tag{4.19}$$
$$\hat{u}(x,0) = u_0(x) \tag{4.20}$$
$$\hat{u}\big|_{\partial\Omega} = 0\,. \tag{4.21}$$

As stated before, this PDE can be reformulated and embedded in a more abstract context by searching for the solution $\hat{u}(t)$ of

$$\partial_t \hat{u}(t) + d_1 \partial\varphi(\hat{u}(t)) + B(\hat{u}(t)) = 0 \tag{4.22}$$
$$\hat{u}(0) = u_0 \tag{4.23}$$

in the phase space $H = H^{-1}(\Omega)$. Here the subdifferential is applied to the function φ defined in Proposition 25 and we set

$$B(\hat{u}) := -d_2 g(\hat{u}) N_2^u\,.$$

Remark
By the subdifferential definition, $\partial\varphi(u)$ is only defined for $u \in L^m(\Omega)$ since $\varphi(u) = \infty$ for $u \in H \setminus L^m(\Omega)$.

Our aim now is to apply Theorem IV of [40], which then assures the existence of a global solution $\hat{u}$. In order to do that, several conditions have to be satisfied. The theory developed in [40] is capable for a much larger class of equations and deals with multivalued operators. In our case we only have single-valued operators and so it is sufficient to show that the following three conditions hold:

(B.1) *The level set* $\mathcal{K}_L := \{v \in H : \|v\|_H + \varphi(v) \leq L\}$ *is compact in* H *for every* $L > 0$

(B.2) *The function B is φ-demiclosed:*

$$
\left.
\begin{array}{rrcll}
i) & v_n & \rightarrow & v & \text{in} \quad C([0,T];H) \\
ii) & \partial\varphi(v_n) & \rightharpoonup & \partial\varphi(v) & \text{in} \quad L^2(0,T;H) \\
iii) & B(v_n) & \rightharpoonup & \chi & \text{in} \quad L^2(0,T;H)
\end{array}
\right\}
\implies \quad \chi = B(v)
$$

(B.3) *The function B is bounded in H:*

$$\|B(v)\|_H \leq C \text{ and consequently } (B(v),v)_H \leq C\|v\|_H \quad \forall v \in H$$

Lemma 27
For the given problem (4.22), (4.23) *conditions* **(B.1)**, **(B.2)** *and* **(B.3)** *imply all necessary assumptions of Theorem IV in [40].*

Proof

In the following we will check the validity of the necessary assumptions $(\mathbf{A}.\varphi^t)$, $(\mathbf{A.1})$, $(\mathbf{A.2})$, $(\mathbf{A.6})$ and $(\mathbf{A.4})$ with $(\mathbf{3.7})$ from [40] replaced by $(\mathbf{3.7})'$.

$(\mathbf{A}.\varphi^t)$ Since φ is not dependent on the time t, this assumption is automatically satisfied.

$(\mathbf{A.1}) = (\mathbf{B.1})$.

$(\mathbf{A.2})$ The perturbation term $B(u)$ does not depend on t and is single-valued, hence $(\mathbf{i})$ and $(\mathbf{ii})$ are always satisfied, $(\mathbf{iii})$ follows from $(\mathbf{B.2})$.

$(\mathbf{A.4})$ Follows from $(\mathbf{B.3})$.

$(\mathbf{A.6})$ It holds

$$(\partial\varphi(v), v)_H = (-\Delta(|v|^{m-2}v), v)_H \overset{(4.18)}{=} \langle |v|^{m-2}v, v \rangle = \int_\Omega |v|^m \, dx = m\varphi(v) \quad (4.24)$$

and thus from $(\mathbf{B.3})$ it follows

$$(-\partial\varphi(v) - B(v), v)_H + m\varphi(v) = (-B(v), v)_H \leq C\|v\|_H \leq 2C(\|v\|_H^2 + 1)$$

which implies $(\mathbf{A.6})$.

$\square$

Now we want to prove that these three necessary assumptions are satisfied.

Property $(\mathbf{B.1})$ can be justified by the definition of φ according to (4.12). From the non-negativity of $\|v\|_H$ it immediately follows

$$\mathcal{K}_L \subseteq L^m(\Omega) \subset L^2(\Omega) \subset\subset H$$

since $m > 2$ and thus $\mathcal{K}_L$ is a compact subset of H.

For the demonstration of $(\mathbf{B.2})$ we define the cylinder $Q_T := \Omega \times (0, T)$ with elements $\tilde{x} := (x, t)$. Then on Q_T it holds

$$\|v\|_{L^2(0,T;L^2(\Omega))}^2 = \int_0^T \|v(t)\|_{L^2(\Omega)}^2 \, dt = \int_0^T \int_\Omega |v(x,t)|^2 \, dx \, dt = \int_{Q_T} |v(\tilde{x})|^2 \, d\tilde{x} = \|v\|_{L^2(Q_T)}^2.$$

At first we recall the meaning of weak convergence in Bochner spaces. For bounded domains we have the Gelfand triple (4.11) and consequently there is an analogous embedding

$$L^2(0, T; H_0^1(\Omega)) \hookrightarrow L^2(0, T; L^2(\Omega)) \hookrightarrow L^2(0, T; H^{-1}(\Omega)). \quad (4.25)$$

Remark

The compact embedding $V \subset\subset W$ does not imply $L^2(0, T; V) \subset\subset L^2(0, T; W)$ and vice versa. However, under additional assumptions such an implication can be shown see e.g. [51].

By definition, for a weakly convergent sequence $\{w_n\}_{n\in\mathbb{N}}$ in $L^2(0,T;H^{-1}(\Omega))$ it holds for every $\psi \in L^2(0,T;H^{-1}(\Omega))^* = L^2(0,T;H_0^1(\Omega))$ due to the embedding (4.25)

$$
\begin{aligned}
&\langle \psi, w_n \rangle \to \langle \psi, w \rangle \\
\Leftrightarrow \quad &(\psi, w_n)_{L^2(0,T;L^2(\Omega))} \to (\psi, w)_{L^2(0,T;L^2(\Omega))} \\
\Leftrightarrow \quad &\int_0^T (\psi(t), w_n(t))_{L^2(\Omega)}\, dt \to \int_0^T (\psi(t), w(t))_{L^2(\Omega)}\, dt \\
\Leftrightarrow \quad &\int_{Q_T} \psi(\tilde{x}) w_n(\tilde{x})\, d\tilde{x} \to \int_{Q_T} \psi(\tilde{x}) w(\tilde{x})\, d\tilde{x} \\
&\Leftrightarrow \quad w_n \rightharpoonup w \quad \text{in } L^2(Q_T) \quad \Rightarrow \quad w_n \to w \quad \text{in } \mathcal{D}'(Q_T).
\end{aligned}
$$

Based on this consideration we now want to show **(B.2)**, the φ-demiclosedness of B.

As we just demonstrated, the third convergence assumption $B(v_n) \rightharpoonup \chi$ in $L^2(0,T;H^{-1}(\Omega))$ implies the weakest type of convergence, i.e. convergence of $B(v_n)$ to χ in distributional sense on Q_T. The aim now is to identify $\chi = B(v)$. If we can show almost everywhere convergence

$$v_n \to v \quad \text{a.e. in } Q_T, \tag{4.26}$$

then by the continuity of g given by Condition 1 it follows

$$B(v_n) = -d_2 g(v_n) N_2^u \to -d_2 g(v) N_2^u = B(v) \quad \text{a.e. in } Q_T.$$

Since almost everywhere convergence implies convergence in distributional sense and the $\mathcal{D}'$-limit is unique, under this assumption it follows $\chi = B(v)$.

Thus it remains to deduce (4.26) from the supposed convergences *i)* and *ii)*. First of all they imply that $\partial\varphi(v_n)$ and v_n are bounded in $L^2(0,T;H) \supset C([0,T];H)$, from which we can deduce by (4.24)

$$\infty > (\partial\varphi(v_n), v_n)_{L^2(0,T;H)} = \int_0^T (\partial\varphi(v_n), v_n)_H\, dt = \int_0^T \int_\Omega |v_n|^m\, dx\, dt = \|v_n\|_{L^m(Q_T)}^m.$$

Hence v_n is also bounded in the reflexive Banach space $L^m(Q_T)$, which yields the existence of a weakly convergent subsequence

$$v_{n_k} \rightharpoonup v \quad \text{in } L^m(Q_T). \tag{4.27}$$

Furthermore it holds

$$\|v_{n_k}\|_{L^m(\Omega)}^m = (\partial\varphi(v_{n_k}), v_{n_k})_H \overset{ii)}{\to} (\partial\varphi(v), v_{n_k})_H \overset{i)}{\to} (\partial\varphi(v), v)_H = \|v\|_{L^m(\Omega)}^m$$

and consequently

$$\|v_{n_k}\|_{L^m(Q_T)} \to \|v\|_{L^m(Q_T)}. \tag{4.28}$$

Since $L^m(Q_T)$ is reflexive and with that uniformly convex due to the Milman-Pettis Theorem, the weak convergence (4.27) together with the norm convergence (4.28) implies

$$v_{n_k} \rightharpoonup v \quad \text{in } L^m(Q_T), \tag{4.29}$$

which in turn gives the desired result (4.26) for a subsequence

$$v_{n_{k_l}} \to v \quad \text{a.e. in } Q_T.$$

and **(B.2)** is shown.

The implication (4.29) can e.g. be found in [10] and is a generalization of the basic result for Hilbert spaces.

Remark
For a Hilbert space H the strong convergence follows immediately:

$$\|v_{n_k} - v\|_H^2 = (v_{n_k} - v, v_{n_k} - v)_H = \|v_{n_k}\|_H^2 - 2(v_{n_k}, v)_H + \|v\|_H^2 \to 0,$$

since by assumption we have $\|v_{n_k}\|_H \to \|v\|_H$ and $(v_{n_k}, w)_H \to (v, w)_H$ for all $w \in H$ and in particular $w = v$.

The third condition **(B.3)** is assured by the continuous embedding $L^\infty(\Omega) \hookrightarrow L^2(\Omega) \hookrightarrow H$. Here we have

$$\|B(v)\|_H \leq C_{L^2}\|B(v)\|_{L^2(\Omega)} \leq C_{L^2}C_{L^\infty}\|B(v)\|_{L^\infty(\Omega)} = C_{L^2}C_{L^\infty}\| - d_2 g(v) N_2^u\|_{L^\infty(\Omega)}$$
$$\leq C_{L^2}C_{L^\infty}d_2 g^*\|\overline{N}\|_{L^\infty(\Omega)} =: C < \infty$$

and consequently

$$(B(v), v)_H \leq \|B(v)\|_H\|v\|_H \leq C\|v\|_H.$$

Hence all conditions of Theorem IV in [40] are satisfied. It yields the existence of a global solution $\hat{u}$ to the degenerate pure PDE (4.22), (4.23) and thus also to the original problem (4.19) - (4.21).

$$\square \text{ 2.)}$$

3.) Uniqueness of $\hat{u}$

The uniqueness of the solution is shown by use of Kato's inequality, which is introduced in [31].

Theorem 28 (Kato's inequality)
Let $v \in H^2(\Omega)$ satisfy homogeneous Dirichlet boundary conditions. Then it holds

$$(\Delta v, sgn(v))_{L^2(\Omega)} \leq 0.$$

Let $\hat{u}_1, \hat{u}_2$ be two solutions of (4.19) - (4.21) and define $\hat{w} := \hat{u}_1 - \hat{u}_2$. We multiply (4.19) by $\text{sgn}(\hat{u}_1 - \hat{u}_2)$ and obtain due to the Lipschitz continuity of g (c.f. Condition 1 (iii))

$$\frac{d}{dt}\|\hat{w}\|_{L^1(\Omega)} \leq \int_\Omega \Delta(|\hat{u}_1|^{m-2}\hat{u}_1 - |\hat{u}_2|^{m-2}\hat{u}_2)\,\text{sgn}(\hat{u}_1 - \hat{u}_2)\,dx + d_2 L_g\|\overline{N}\|_{L^\infty(\Omega)}\|\hat{w}\|_{L^1(\Omega)}.$$

The function $h(s) := |s|^{m-2}s$ is non-decreasing since $h'(s) = (m-1)|s|^{m-2} \geq 0$ and thus it holds

$$\text{sgn}(\hat{u}_1 - \hat{u}_2) = \text{sgn}(|\hat{u}_1|^{m-2}\hat{u}_1 - |\hat{u}_2|^{m-2}\hat{u}_2)$$

and we can apply Kato's inequality, which yields

$$\frac{d}{dt}\|\hat{w}\|_{L^1(\Omega)} \leq d_2 L_g \|\overline{N}\|_{L^\infty(\Omega)}\|\hat{w}\|_{L^1(\Omega)}.$$

By Gronwall's inequality it follows

$$\|\hat{w}(t)\|_{L^1(\Omega)} \leq \|\hat{w}(0)\|_{L^1(\Omega)}e^{d_2 L_g \|\overline{N}\|_{L^\infty(\Omega)}T} = 0$$

and consequently

$$\hat{u}_1 \equiv \hat{u}_2.$$

$$\square\ \textbf{3.)}$$

4.) Properties of the $\hat{u}$

Our aim now is to show that this solution satisfies the following properties:

$$\hat{u} \in C([0,T];H^{-1}(\Omega)) \tag{4.30}$$
$$\partial_t\hat{u} \in L^2(0,T;H^{-1}(\Omega)) \tag{4.31}$$
$$\partial\varphi(\hat{u}) \in L^2(0,T;H^{-1}(\Omega)) \tag{4.32}$$

Proof of (4.30):   The continuity of the solution with respect to $t \in [0,T]$ will be shown by use of the following Theorem:

Theorem 29
Let H be a Hilbert space, E a Banach space with embedding structure

$$E \subset H \cong H^* \subset E^*.$$

If a function u satisfies $u \in L^p(0,T;E)$ and $\partial_t u \in L^q(0,T;E^*)$ with $\frac{1}{p} + \frac{1}{q} = 1$, then it holds

$$u \in C([0,T];H)$$

for every $T > 0$.

This basic fact in the theory of evolution equations can e.g. be found in [13].

For our purpose we choose $E := L^m(\Omega)$ and $H = H^{-1}(\Omega)$ as before. Then again we have the compact embedding $E \subset\subset H$. Furthermore H can be identified with its dual $H_0^1(\Omega)$, which is continuously embedded into $L^{\frac{m}{m-1}}(\Omega) = L^m(\Omega)^*$. This follows from the Sobolev embedding theorem in dimensions $n = 2,3$ due to $m > 2$.

Hence in accordance with Theorem 29, we have to show

$$\hat{u} \in L^m(0,T;L^m(\Omega)) \text{ and } \partial_t\hat{u} \in L^{\frac{m}{m-1}}(0,T;L^{\frac{m}{m-1}}(\Omega)).$$

For that we multiply (4.19) by $\hat{u}$. At this the following term occurs:

$$\int_\Omega \Delta(|\hat{u}|^{m-2}\hat{u})\hat{u}\,dx = -(-\Delta(|\hat{u}|^{m-2}\hat{u}),\hat{u})_H \overset{(4.18)}{=} -\langle|\hat{u}|^{m-2}\hat{u},\hat{u}\rangle = -(|\hat{u}|^{m-2}\hat{u},\hat{u})_{L^2(\Omega)}$$
$$= -\|\hat{u}\|^m_{L^m(\Omega)}\,,$$

which yields due to $m > 2$

$$\frac{1}{2}\frac{d}{dt}\|\hat{u}(t)\|^2_{L^2(\Omega)} + d_1\|\hat{u}(t)\|^m_{L^m(\Omega)} \leq d_2\lambda(\Omega)^{\frac{1}{2}-\frac{1}{m}}\|g(\hat{u}(t)N_2^u(t)\|_{L^2(\Omega)}\|\hat{u}(t)\|_{L^m(\Omega)}$$

and by Young's inequality

$$\frac{d}{dt}\|\hat{u}(t)\|^2_{L^2(\Omega)} + d_1\|\hat{u}(t)\|^m_{L^m(\Omega)} \leq \frac{d_2^2}{d_1}\lambda(\Omega)^{2-\frac{2}{m}}g^{*2}\|\overline{N}\|^2_{L^\infty(\Omega)}\,.$$

Integration over $\int_0^T dt$ then gives

$$\int_0^T \|\hat{u}(t)\|^m_{L^m(\Omega)}\,dt \leq \frac{1}{d_1}\|u_0\|^2_{L^2(\Omega)} + T\frac{d_2^2}{d_1^2}\lambda(\Omega)^{2-\frac{2}{m}}g^{*2}\|\overline{N}\|^2_{L^\infty(\Omega)} < \infty\,,$$

i.e.

$$\boxed{\hat{u} \in L^m(0,T;L^m(\Omega))\,.} \tag{4.33}$$

For $\hat{u}(t) \in L^m(\Omega)$ we have by (4.17) $\partial\varphi(\hat{u}(t)) = |\hat{u}(t)|^{m-2}\hat{u}(t)$ and consequently

$$\int_0^T \|\partial\varphi(\hat{u}(t)\|^{\frac{m}{m-1}}_{L^{\frac{m}{m-1}}(\Omega)} = \int_0^T \int_\Omega \left||\hat{u}(x,t)|^{m-2}\hat{u}(x,t)\right|^{\frac{m}{m-1}}dx\,dt = \int_0^T \int_\Omega |\|\hat{u}(t)\|^m_{L^m(\Omega)}\,dt\,,$$

hence

$$\boxed{\partial\varphi(\hat{u}) \in L^{\frac{m}{m-1}}(0,T;L^{\frac{m}{m-1}}(\Omega))\,.}$$

The remaining term $g(\hat{u})N_2^u$ can be easily estimated:

$$\int_0^T \|g(\hat{u}(t))N_2^u(t)\|^{\frac{m}{m-1}}_{L^{\frac{m}{m-1}}}\,dt \leq Tg^{*\frac{m}{m-1}}\|\overline{N}\|^{\frac{m}{m-1}}_{L^\infty(\Omega)}\lambda(\Omega) < \infty$$

an with that it immediately follows

$$\boxed{\partial_t\hat{u} \in L^{\frac{m}{m-1}}(0,T;L^{\frac{m}{m-1}}(\Omega))\,.}$$

Thus Theorem 29 yields

$$\boxed{\hat{u} \in C([0,T];H^{-1}(\Omega))\,.}$$

Proof of (4.31):   Our next aim is to analyze

$$\|\partial_t \hat{u}\|_H^2 = (\partial_t \hat{u}, \partial_t \hat{u})_H \stackrel{(4.18)}{=} \langle (-\Delta)^{-1}(\partial_t \hat{u}), \partial_t \hat{u} \rangle = \int_\Omega (-\Delta)^{-1}(\partial_t \hat{u}) \, \partial_t \hat{u} \, dx \, ,$$

i.e. we multiply (4.19) by $(-\Delta)^{-1}(\partial_t \hat{u})$ and integrate over Ω. At this we have with integration by parts

$$\int_\Omega \Delta(|\hat{u}|^{m-2}\hat{u}) \, (-\Delta)^{-1}(\partial_t \hat{u}) \, dx = -\int_\Omega |\hat{u}|^{m-2}\hat{u} \, \partial_t \hat{u} \, dx = -\frac{1}{m}\frac{d}{dt}\int_\Omega |\hat{u}|^m \, dx \, .$$

The last term can be estimated by

$$d_2 \int_\Omega g(\hat{u}) N_2^u (-\Delta)^{-1}(\partial_t \hat{u}) \, dx = (g(\hat{u}) N_2^u, \partial_t \hat{u})_H \leq \|g(\hat{u}) N_2^u\|_H \|\partial_t \hat{u}\|_H \, .$$

Then Young's inequality together with the continuous embedding $L^2(\Omega) \hookrightarrow H$ yields

$$\|\partial_t \hat{u}(t)\|_H^2 + 2d_1 \frac{1}{m}\frac{d}{dt}\|\hat{u}(t)\|_{L^m(\Omega)}^m \leq d_2^2 C_{L^2} g^{*2} \|\overline{N}\|_{L^\infty(\Omega)}^2 \lambda(\Omega) =: C < \infty \, .$$

Integration $\int_0^T dt$ then finally gives

$$\int_0^T \|\partial_t \hat{u}(t)\|_H^2 \, dt \leq 2d_1 \frac{1}{m}\|u_0\|_{L^m(\Omega)}^m + CT < \infty$$

and hence

$$\boxed{\partial_t \hat{u} \in L^2(0,T;H^{-1}(\Omega)) \, .}$$

Proof of (4.32):   In analogy to the previous case we multiply (4.19) by $|\hat{u}|^{m-2}\hat{u}$ and obtain

$$\frac{1}{m}\frac{d}{dt}\|\hat{u}(t)\|_{L^m(\Omega)}^m + d_1 \|\partial\varphi(\hat{u}(t))\|_H^2 \leq d_2 g^* \|\overline{N}\|_{L^\infty(\Omega)} \|\hat{u}\|_{L^{m-1}(\Omega)}^{m-1} \, .$$

Integration with respect to t then yields

$$\int_0^T \|\partial\varphi(\hat{u}(t))\|_H^2 \, dt \leq \frac{1}{d_1 m}\|u_0\|_{L^m(\Omega)}^m + \frac{d_2}{d_1}g^* \|\overline{N}\|_{L^\infty(\Omega)} \underbrace{(\lambda(\Omega) \, T)}_{=\lambda(Q_T)}^{\frac{1}{m-1}-\frac{1}{m}} \|\hat{u}\|_{L^m(Q_T)} < \infty$$

due to (4.33) and hence

$$\boxed{\partial\varphi(\hat{u}) \in L^2(0,T;H^{-1}(\Omega)) \, .} \tag{4.34}$$

It remains to show (4.34) $\Leftrightarrow |\hat{u}|^{m-2}\nabla\hat{u} \in L^2(0,T;L^2(\Omega))$.

This equivalence is justified by the fact that for $\psi \in L^2(0,T;H_0^1(\Omega))$ and consequently $\nabla\psi \in L^2(0,T;L^2(\Omega))$ it holds

$$\infty > \int_0^T \langle -\Delta(|\hat{u}(t)|^{m-2}\hat{u}(t)), \psi(t) \rangle \, dt = \int_0^T (-\mathrm{div}((m-1)|\hat{u}(t)|^{m-2}\nabla\hat{u}(t)), \psi(t))_{L^2(\Omega)} \, dt$$

$$= (m-1)\int_0^T \int_\Omega |\hat{u}(x,t)|^{m-2}\nabla\hat{u}(x,t)\nabla\psi(x,t) \, dx \, dt = (m-1)(|\hat{u}|^{m-2}\nabla\hat{u}, \nabla\psi)_{L^2(Q_T)}.$$

$$\square \ 4.)$$

5.) The map $\mathcal{B} : u \mapsto \hat{u}$ is a contraction

Here we calculate the difference of two solutions $\hat{u}_1 = \mathcal{B}(u_1), \hat{u}_2 = \mathcal{B}(u_2)$ of the pure PDE dependent on different parameters u_1, u_2:

$$\partial_t \hat{u}_1 = d_1 \Delta(|\hat{u}_1|^{m-2}\hat{u}_1) + d_2 g(\hat{u}_1)N_2^{u_1} \qquad \hat{u}_1(x,0) = u_0(x) \qquad \hat{u}_1\big|_{\partial\Omega} = 0$$
$$\partial_t \hat{u}_2 = d_1 \Delta(|\hat{u}_2|^{m-2}\hat{u}_2) + d_2 g(\hat{u}_2)N_2^{u_2} \qquad \hat{u}_2(x,0) = u_0(x) \qquad \hat{u}_2\big|_{\partial\Omega} = 0\,.$$

Our aim is to show for $\delta\hat{u} := \hat{u}_1 - \hat{u}_2$ and $\delta u := u_1 - u_2$

$$\max_{0 \leq t \leq T_0} \|\delta\hat{u}(t)\|_{L^1(\Omega)} \leq \alpha \max_{0 \leq t \leq T_0} \|\delta u(t)\|_{L^1(\Omega)}$$

for $0 < \alpha < 1$ and T_0 sufficiently chosen.

In the proof of Theorem 1 we consider the space $C([0,T];L^2(\Omega))$, but for the degenerate case we have to use functions from $X = C([0,T];L^1(\Omega))$. This is due to the fact that we have to get rid of the diffusion operator term. For the non-degenerate case this is possible by multiplying with $\delta\hat{u}$, where we obtain

$$\int_\Omega \Delta\delta\hat{u}\,\hat{u}\,dx = -\|\nabla\hat{u}\|_{L^2(\Omega)}^2 \leq 0\,.$$

However, for the degenerate case the diffusion operator is nonlinear and we need to apply Kato's inequality as we did for the proof of uniqueness:

$$\int_\Omega \Delta(|\hat{u}_1|^{m-2}\hat{u}_1 - |\hat{u}_2|^{m-2}\hat{u}_2)\,\mathrm{sgn}(\hat{u}_1 - \hat{u}_2)\,dx \leq 0\,.$$

Thus in that case we multiply by the sign-function which in turn leads to the L^1-norm. In order to estimate $\delta\hat{u}$ we proceed in exactly the same way as we did in Section 3.1.1, with the only difference of multiplying by $\mathrm{sgn}(\delta\cdot)$. This yields with the same constants

① $\delta N_1 := N_1^{u_1} - N_1^{u_2}$

$$\|\delta N_1(t)\|_{L^1(\Omega)} \leq L_f C_1 \int_0^t \|\delta u(s)\|_{L^1(\Omega)}\,ds \quad \forall t \in [0,T]\,.$$

② $\delta N_2 := N_2^{u_1} - N_2^{u_2}$

$$\|\delta N_2(t)\|_{L^1(\Omega)} \leq C_3 \int_0^t \|\delta u(s)\|_{L^1(\Omega)}\,ds \quad \forall t \in [0,T] \text{ with } T \leq 1\,.$$

③ $\delta \hat{u} := \hat{u}_1 - \hat{u}_2$

$$\|\delta \hat{u}\|_X \leq \underbrace{d_2 g^* C_3 \, T e^{d_2 L_g C_2 T}}_{= C_4(T) > 0} \|\delta u\|_X \ \text{ with } T \leq 1 \, .$$

Now we are in exactly the same situation as in the proof of Theorem 1, where we show the existence of a time $T_0 \leq 1$ such that $C_4(T_0) < 1$.

This assures the existence of a unique local solution of the original problem (4.5) - (4.9) on the time interval $[0, T_0]$. Furthermore with the same arguments as before, the existence interval can be extended to any bounded interval $[0, T]$, which means the unique local solution can be continued globally. At this we also obtain $N_i \in L^\infty(0, T; L^\infty(\Omega))$.

$\square$ **5.)**

This finishes the proof of Theorem 26.

Further properties of the unique global solution are summarized in the next theorem.

Theorem 30

For the solution (u, N_1, N_2, N_3) of the degenerate problem (4.5) - (4.9) the following assertions hold:

(i) *Theorem 2 holds true.*

(ii) *Under the assumptions of Theorem 2 we have the strong convergence results*

$$
\begin{aligned}
N_1(x, t) & \xrightarrow{t \to \infty} N_1^\infty(x) \geq 0 && \text{in } L^p(\Omega), && 1 \leq p < \infty \\
N_2(x, t) & \xrightarrow{t \to \infty} N_2^\infty(x) \geq 0 && \text{in } L^p(\Omega), && 1 \leq p < \infty \\
N_3(x, t) & \xrightarrow{t \to \infty} N_3^\infty(x) \leq \|\overline{N}\|_{L^\infty(\Omega)} && \text{in } L^p(\Omega), && 1 \leq p < \infty \\
u(x, t) & \xrightarrow{t \to \infty} u^\infty(x) \equiv 0 && \text{in } L^m(\Omega) \, .
\end{aligned}
$$

Proof

(i) The proof of non-negativity and uniform boundedness of N_i, $i = 1, 2, 3$ is provided by exactly the same arguments as for the non-degenerate case.

It remains to show the non-negativity of $u(x, t)$ starting from non-negative initial data $u_0 \geq 0$.

Proceeding as in the proof of Theorem 2, we multiply (4.5) by the negative part u^- and integrate over $\int_\Omega dx$. Here we use the representation $u = u^+ - u^-$ and $|u| = u^+ + u^-$. This yields

$$-\frac{1}{2}\frac{d}{dt}\|u^-(t)\|_{L^2(\Omega)}^2 = d_1 \int_\Omega \Delta\big((u^+ + u^-)^{m-2}(u^+ - u^-)\big) \, u^- \, dx + d_2 \int_\Omega g(u) \, N_2 \, u^- \, dx \, .$$

Since we know $\int_\Omega u^+ u^- \, dx = 0$, the power function $(u^+ + u^-)^{m-2}$ can be resolved to $(u^+)^{m-2} + (u^-)^{m-2}$ and hence $(u^+ + u^-)^{m-2}(u^+ - u^-) = (u^+)^{m-1} - (u^-)^{m-1}$. With that we obtain

$$-\frac{1}{2}\frac{d}{dt}\|u^-(t)\|^2_{L^2(\Omega)} = -d_1 \int_\Omega \Delta((u^-)^{m-1}) \, u^- \, dx + d_2 \int_\Omega g(u) \, N_2 \, u^- \, dx$$

$$= d_1 \int_\Omega \nabla((u^-)^{m-1}) \, \nabla u^- \, dx + d_2 \int_\Omega g(u) \, N_2 \, u^- \, dx$$

$$= \underbrace{d_1 \int_\Omega (m-1)(u^-)^{m-2}|\nabla u^-|^2 \, dx + d_2 \int_\Omega g(u) \, N_2 \, u^- \, dx}_{\geq 0},$$

which implies $\|u^-(t)\|^2_{L^2(\Omega)} \leq \|u^-_0\|^2_{L^2(\Omega)} = 0$. This yields the desired result

$$u(x,t) \geq 0 \qquad \forall t \geq 0 \quad \forall x \in \Omega.$$

(ii) The convergence results of N_1, N_2 and N_3 are the same as for the non-degenerate case, since the ODEs of the model description are not changed. However, we can not deduce $N_2^\infty \equiv 0$. This is due to the fact that we can not obtain the strict positivity of u as we had in Proposition 4.

Remark
This phenomenon was already mentioned before. Whereas for the standard diffusion case it is possible to deduce the infinite speed of propagation, i.e. $u(t) > 0$ for $t > 0$, for the degenerate case it can be proven that we only have finite speed of propagation and the solution has compact support. Hence Proposition 4 can not hold in this case.

In order to obtain the convergence of $u(t)$ to 0 in $L^m(\Omega)$, we multiply (4.5) by $\partial\varphi(u) = -\Delta(|u|^{m-2}u)$ and take the inner product in H. Since we assume non-negative initial data, we know $u(x,t) \geq 0$ and thus $|u|^{m-2}u = u^{m-1}$. Then by the identification (4.18) we have

$$\langle \partial_t u, u^{m-1} \rangle = d_1 \langle \Delta(u^{m-1}), u^{m-1} \rangle + d_2 \langle g(u)N_2, u^{m-1} \rangle, \text{ i.e.}$$

$$\int_\Omega \partial_t u \, u^{m-1} \, dx = d_1 \int_\Omega \Delta(u^{m-1}) \, u^{m-1} \, dx + d_2 (g(u)N_2, u^{m-1})_{L^2(\Omega)}$$

and we further obtain

$$\frac{1}{m}\frac{d}{dt}\|u\|^m_{L^m(\Omega)} \leq -d_1\|\nabla u^{m-1}\|^2_{L^2(\Omega)} + d_2\|g(u)N_2\|_{L^2(\Omega)}\|u^{m-1}\|_{L^2(\Omega)}.$$

Applying Poincaré's inequality to $v = u^{m-1}$ we get $\|v\|_{L^2(\Omega)} \leq C_P\|\nabla v\|_{L^2(\Omega)}$. Inserting this estimate twice and using Young's inequality, we come up to

$$\frac{1}{m}\frac{d}{dt}\|u\|^m_{L^m(\Omega)} + \frac{d_1}{2C_P^2}\|u^{m-1}\|^2_{L^2(\Omega)} \leq \frac{d_2^2 C_P^2}{2d_1}\|g(u)N_2\|^2_{L^2(\Omega)}.$$

At this we have $\|u^{m-1}\|^2_{L^2(\Omega)} = \|u\|^{2(m-1)}_{L^{2(m-1)}(\Omega)}$ and due to $2(m-1) > m$ we can estimate $\|u\|_{L^m(\Omega)} \leq \lambda(\Omega)^{\frac{1}{m}-\frac{1}{2(m-1)}} \|u\|_{L^{2(m-1)}} =: C_\lambda \|u\|_{L^{2(m-1)}(\Omega)}$. This yields

$$\frac{d}{dt}\|u\|^m_{L^m(\Omega)} + C_\lambda^{-2(m-1)} \frac{md_1}{2C_P^2} \|u\|^{2(m-1)}_{L^m(\Omega)} \leq \frac{md_2^2 C_P^2}{2d_1} \|g(u)N_2\|^2_{L^2(\Omega)},$$

which is of the form

$$\frac{d}{dt}y(t) + \gamma y(t)^{p-1} \leq a(t)$$

with $y(t) := \|u(t)\|^m_{L^m(\Omega)}$, $\gamma > 0$ and $p = 1 + \frac{2(m-1)}{m} > 2$. The statements leading to (3.77) also apply to this case and so we have $\int_0^\infty a(t)\,dt < \infty$.

This differential inequality is different compared to the previous ones, since we now have the exponent $(p-1)$. Lemma 4.3 of [40] deals with this kind of inequalities and by using the argument in the proof of this lemma we arrive at

$$y(t) \leq \big(\gamma(p-2)(t-t_0)\big)^{-\frac{1}{p-2}} + \int_{t_0}^t a(s)\,ds \qquad (4.35)$$

for all $t_0 \in [0, T]$ and $t \in [t_0, T]$.

By the convergence of $\int_0^\infty a(t)\,dt$ we know that for any $\varepsilon > 0$ there exists $t_0 > 0$ such that $\int_{t_0}^\infty a(s)\,ds < \varepsilon$. Taking the limit $t \to \infty$ in (4.35), we get $\limsup_{t\to\infty} y(t) \leq \varepsilon$, whence follows $\lim_{t\to\infty} \|u\|^m_{L^m(\Omega)} = 0$, which implies

$$\boxed{u(x,t) \xrightarrow{t\to\infty} u^\infty(x) \equiv 0 \quad \text{strongly in } L^m(\Omega)\,.}$$

$\square$

Outlook

The derived mathematical model of mitochondrial swelling can be further extended. This will lead to interesting mathematical questions, that are also very important for the biological application.

- Take into account other boundary conditions for the degenerate model, in particular homogeneous Neumann and inhomogeneous Robin boundary conditions in order to account for the *in vitro* and *in vivo* processes as we did for the non-degenerate model.

- Try to get rid of the additional condition (Cond.*a*) in the Robin boundary case

$$-\partial_\nu u = a(x)(u - \alpha) \text{ on } \partial\Omega \, ,$$

  which states that the boundary function a has to be bounded below by a positive constant. If we could also allow $a(x)$ to be zero for special regions on the boundary, we could obtain a more detailed mathematical description of the cell membrane.

- Even if mitochondria do not diffuse within the cell, there are indications that mitochondria do move under special circumstances, e.g. dependent on the cell cycle phase [37]. This spatial evolution could be included in the mathematical model, which then leads to a coupled PDE-system.

Bibliography

[1] B. Alberts, A. Johnson, J. Lewis, M. Raff, K. Roberts, and P. Walter, *Molecular biology of the cell*, 5th ed., Garland Science, 2007.

[2] A.V. Babin and M.I. Vishik, *Attractors of evolution equations*, North Holland, 1992.

[3] S.V. Baranov, I.G. Stavrovskaya, A.M. Brown, A.M. Tyryshkin, and B.S. Kristal, *Kinetic model for Ca^{2+}-induced permeability transition in energized liver mitochondria discriminates between inhibitor mechanisms*, Journal of Biological Chemistry **283** (2008), no. 2, 665–676.

[4] S.B. Berman, S.C. Watkins, and T.G. Hastings, *Quantitative biochemical and ultrastructural comparison of mitochondrial permeability transition in isolated brain and liver mitochondria: Evidence for reduced sensitivity of brain mitochondria*, Experimental Neurology **164** (2000), no. 2, 415–425.

[5] P. Bernardi, A. Krauskopf, E. Basso, V. Petronilli, E. Blalchy-Dyson, F. Di Lisa, and M.A. Forte, *The mitochondrial permeability transition from in vitro artifact to disease target*, FEBS Journal **273** (2006), no. 10, 2077–2099.

[6] R. Bertram, J.L. Greenstein, R. Hinch, E. Pate, J. Reisert, M.J. Sanderson, T.R. Shannon, J. Sneyd (Ed.), and R.L. Winslow, *Tutorials in mathematical biosciences II: Mathematical modeling of calcium dynamics and signal transduction*, vol. 2, Springer, 2005.

[7] G.A. Blondin and D.E. Green, *The mechanism of mitochondrial swelling*, Proceedings of the National Academy of Sciences **58** (1967), no. 2, 612–619.

[8] C.D. Bortner and J.A. Cidlowski, *Apoptotic volume decrease and the incredible shrinking cell*, Cell Death and Differentiation **9** (2002), no. 12, 1307–1310.

[9] H. Brézis, *Opérateurs maximaux monotones et semi-groupes de contractions dans les espaces de Hilbert*, vol. 5, North Holland, 1973.

[10] H. Brezis, *Functional analysis, Sobolev spaces and partial differential equations*, Springer, 2010.

[11] N. Brustovetsky, T. Brustovetsky, K.J. Purl, M. Capano, M. Crompton, and J.M. Dubinsky, *Increased susceptibility of striatal mitochondria to calcium-induced permeability transition*, Journal of Neuroscience **23** (2003), no. 12, 4858–4867.

133

[12] G. Calamita, D. Ferri, P. Gena, G.E. Liquori, A. Cavalier, D. Thomas, and M. Svelto, *The inner mitochondrial membrane has aquaporin-8 water channels and is highly permeable to water*, Journal of Biological Chemistry **280** (2005), no. 17, 17149–17153.

[13] V.V. Chepyzhov and M.I. Vishik, *Attractors for equations of mathematical physics*, American Mathematical Society, 2002.

[14] G. Choquet, *Topology*, Elsevier Science & Technology, 1966.

[15] A. Deniaud, O. Sharaf el dein, E. Maillier, D. Poncet, G. Kroemer, C. Lemaire, and C. Brenner, *Endoplasmic reticulum stress induces calcium-dependent permeability transition, mitochondrial outer membrane permeabilization and apoptosis*, Oncogene **27** (2008), no. 3, 285–299.

[16] M.R. Duchen, *Mitochondria and calcium: From cell signalling to cell death*, The Journal of Physiology **529** (2000), no. 1, 57–68.

[17] M.A. Efendiev, *Evolution equations arising in the modelling of life sciences*, Birkhäuser, 2013.

[18] M.A. Efendiev, *Attractors of degenerate parabolic type equations*, in print.

[19] S. Eisenhofer, M.A. Efendiev, and M. Ôtani, *A mitochondria model with degenerate diffusion*, in preparation.

[20] S. Eisenhofer, M.A. Efendiev, M. Ôtani, S. Schulz, and H. Zischka, *On a ODE–PDE coupling model of the mitochondrial swelling process*, submitted to Discrete and Continuous Dynamical Systems (Series B).

[21] S. Eisenhofer, B.A. Hense, F. Toókos, and H. Zischka, *Modeling the volume change in mitochondria*, International Journal of Biomathematics and Biostatistics **1** (2010), 53–62.

[22] S. Eisenhofer, F. Toókos, B. A. Hense, S. Schulz, F. Filbir, and H. Zischka, *A mathematical model of mitochondrial swelling*, BMC Research Notes **3** (2010), no. 1, 67.

[23] S. Elmore, *Apoptosis: A review of programmed cell death*, Toxicologic Pathology **35** (2007), no. 4, 495–516.

[24] L.C. Evans, *Partial differential equations: Second edition*, American Mathematical Society, 2010.

[25] D.S. Goodsell, *The molecular perspective: Cytochrome c and apoptosis*, The Oncologist **9** (2004), no. 2, 226–227.

[26] S. Grimm and D. Brdiczka, *The permeability transition pore in cell death*, Apoptosis **12** (2007), no. 5, 841–855.

[27] R.A. Haworth and D.R. Hunter, *The Ca^{2+}-induced membrane transition in mitochondria. II. Nature of the Ca^{2+} trigger site*, Archives of Biochemistry and Biophysics **195** (1979), no. 2, 460–467.

[28] D.R. Hunter, R.A Haworth, and J.H. Southard, *Relationship between configuration, function, and permeability in calcium-treated mitochondria*, Journal of Biological Chemistry **251** (1976), no. 16, 5069–5077.

[29] F. Ichas, L. S. Jouaville, and J. P. Mazat, *Mitochondria are excitable organelles capable of generating and conveying electrical and calcium signals*, Cell **89** (1997), no. 7, 1145–1153.

[30] G.E.N. Kass and S. Orrenius, *Calcium signaling and cytotoxicity*, Environmental Health Perspectives **107** (1999), no. 1, 25–35.

[31] T. Kato, *Schrödinger operators with singular potentials*, Israel Journal of Mathematics **13** (1972), no. 1–2, 135–148.

[32] D. Kinderlehrer and G. Stampacchia, *An introduction to variational inequalities and their applications*, Classics in Applied Mathematics, Society for Industrial and Applied Mathematics, 1987.

[33] Y. Kirichok, G. Krapivinsky, and D.E. Clapham, *The mitochondrial calcium uniporter is a highly selective ion channel*, Nature **427** (2004), no. 6972, 360–364.

[34] G. Kroemer, L. Galluzzi, and C. Brenner, *Mitochondrial membrane permeabilization in cell death*, Physiological Reviews **87** (2007), no. 1, 99–163.

[35] J.C. Lagarias, J.A. Reeds, M.H. Wright, and P.E. Wright, *Convergence properties of the Nelder–Mead simplex method in low dimensions*, SIAM Journal on Optimization **9** (1998), no. 1, 112–147.

[36] S. Massari, *Kinetic analysis of the mitochondrial permeability transition*, Journal of Biological Chemistry **271** (1996), no. 50, 31942–31948.

[37] K. Mitra, C. Wunder, B. Roysam, G. Lin, and J. Lippincott-Schwartz, *A hyperfused mitochondrial state achieved at G_1-S regulates cyclin E buildup and entry into S phase*, Proceedings of the National Academy of Sciences **106** (2009), no. 29, 11960–11965.

[38] S. Naghdi, M. Waldeck-Weiermair, I. Fertschai, M. Poteser, W.F. Graier, and R. Malli, *Mitochondrial Ca^{2+} uptake and not mitochondrial motility is required for STIM1-Orai1-dependent store-operated Ca^{2+} entry*, Journal of Cell Science **123** (2010), no. 15, 2553–2564.

[39] D.G. Nicholls and S. Chalmers, *The integration of mitochondrial calcium transport and storage*, Journal of Bioenergetics and Biomembranes **36** (2004), no. 4, 277–281.

[40] M. Ôtani, *Nonmonotone perturbations for nonlinear parabolic equations associated with subdifferential operators, Cauchy problems*, Journal of Differential Equations **46** (1982), no. 2, 268–299.

[41] V. Petronilli, C. Cola, S. Massari, R. Colonna, and P. Bernardi, *Physiological effectors modify voltage sensing by the cyclosporin A-sensitive permeability transition pore of mitochondria*, Journal of Biological Chemistry **268** (1993), no. 29, 21939–21945.

[42] P. Pinton, C. Giorgi, R. Siviero, E. Zecchini, and R. Rizzuto, *Calcium and apoptosis: ER-mitochondria Ca^{2+} transfer in the control of apoptosis*, Oncogene **27** (2008), no. 50, 6407–6418.

[43] A.V. Pokhilko, F.I. Ataullakhanov, and E.L. Holmuhamedov, *Mathematical model of mitochondrial ionic homeostasis: Three modes of Ca^{2+} transport*, Journal of Theoretical Biology **243** (2006), no. 1, 152–169.

[44] M. Renardy and R.C. Rogers, *An introduction to partial differential equations*, vol. 13, Springer, 2004.

[45] R. Rizzuto, S. Marchi, M. Bonora, P. Aguiari, A. Bononi, D. De Stefani, C. Giorgi, S. Leo, A. Rimessi, R. Siviero, E. Zecchini, and P. Pinton, *Ca^{2+} transfer from the ER to mitochondria: When, how and why*, Biochimica et Biophysica Acta (BBA)-Bioenergetics **1787** (2009), no. 11, 1342–1351.

[46] R. Rizzuto and T. Pozzan, *Microdomains of intracellular Ca^{2+}: Molecular determinants and functional consequences*, Physiological Reviews **86** (2006), no. 1, 369–408.

[47] R.T. Rockafellar, *On the maximal monotonicity of subdifferential mappings*, Pacific Journal of Mathematics **33** (1970), no. 1, 209–216.

[48] D. Ron, *Translational control in the endoplasmic reticulum stress response*, Journal of Clinical Investigation **110** (2002), no. 10, 1383–1388.

[49] S. Schulz, S. Schmitt, R. Wimmer, M. Aichler, S. Eisenhofer, J. Lichtmannegger, C. Eberhagen, R. Artmann, F. Toókos, A. Walch, D. Krappmann, C. Brenner, C. Rust, and H. Zischka, *Progressive stages of mitochondrial destruction caused by cell toxic bile salts*, Biochimica et Biophysica Acta (BBA)-Biomembranes **1828** (2013), no. 9, 2121–2133.

[50] V.A. Selivanov, F. Ichas, E.L. Holmuhamedov, L.S. Jouaville, Y.V. Evtodienko, and J.P. Mazat, *A model of mitochondrial Ca^{2+}-induced Ca^{2+} release simulating the Ca^{2+} oscillations and spikes generated by mitochondria*, Biophysical Chemistry **72** (1998), no. 1–2, 111–121.

[51] J. Simon, *Compact sets in the space $L^p(0, T; B)$*, Annali di Matematica Pura ed Applicata **146** (1986), no. 1, 65–96.

[52] R. Temam, *Infinite dimensional dynamical systems in mechanics and physics*, vol. 2, Springer, 1997.

[53] H. Triebel, *Interpolation theory, function spaces, differential operators*, J.A. Barth, 1995.

[54] J.L. Vázquez, *The porous medium equation: Mathematical theory*, Clarendon Press, 2007.

[55] D. Werner, *Funktionalanalysis*, Springer, 2011.

[56] E. Zeidler, *Functional analysis and its applications I: Fixed-point theorems*, Springer, 1985.

[57] E. Zeidler, *Functional analysis and its applications II/B: Nonlinear monotone operators*, Springer, 1990.

[58] H. Zischka, N. Larochette, F. Hoffmann, D. Hamöller, N. Jägemann, J. Lichtmannegger, L. Jennen, J. Müller-Höcker, F. Roggel, M. Göttlicher, A. M. Vollmar, and G. Kroemer, *Electrophoretic analysis of the mitochondrial outer membrane rupture induced by permeability transition*, Analytical Chemistry **80** (2008), no. 13, 5051–5058.